NASA CR-145147

SCAR ARROW-WING ACTIVE FLUTTER SUPPRESSION SYSTEM

By

C. K. Gordon and O. E. Visor

Prepared under Contract No. NAS 1-14205

By

BOEING WICHITA COMPANY

A Division of The Boeing Company o Wichita, Kansas o 67210

For

NASA

National Aeronautics and Space Administration

1. Report No.	2. Government Accession No.	3. Recipient's Catalog No.
NASA CR-145147		

4. Title and Subtitle	5. Report Date
SCAR Arrow Wing Active Flutter Suppression System	April 1977
	6. Performing Organization Code

7. Author(s)	8. Performing Organization Report No.
C. K. Gordon O. E. Visor	D3-11139-1
	10. Work Unit No.

9. Performing Organization Name and Address	11. Contract or Grant No.
The Boeing Company 3801 S. Oliver Wichita, Kansas 67210	NAS1-14205
	13. Type of Report and Period Covered
12. Sponsoring Agency Name and Address	Final report January 1976 through December 1976
NASA Langley Research Center Hampton, Virginia 23665	14. Sponsoring Agency Code

15. Supplementary Notes

16. Abstract

The potential performance and direct operating cost benefits of an active flutter suppression system (FSS) for the NASA arrow-wing supersonic cruise configuration were determined. A FSS was designed to increase the flutter speed of the baseline airplane 20 percent. A comparison was made of the performance and direct operating cost (DOC) between the FSS equipped aircraft and a previously defined configuration with structural modifications to provide the same flutter speed.

Control system synthesis and evaluation indicated that a FSS could provide the increase in flutter speed without degrading airplane reliability, safety, handling qualities or ride quality, and without increasing repeated loads or hydraulic and electrical power capacity requirements.

Mechanization studies indicated that the FSS could be implemented with a weight penalty of 159.2 kg (351 lb) compared to the structural weight of 4309 kg (9500 lb) to obtain the same flutter speed. A notable improvement in DOC was obtained with the FSS configured vehicle with the major contributing factor being reduced fuel consumption associated with the reduced vehicle weight. Improvements with the FSS are 2.55 percent in operating empty weight, 2.36 percent in price and typical values of 2.14 percent in block fuel and 1.77 percent in DOC based on a 5555 km (3000 n. mi.) trip and 1976 international fuel prices. Cost improvements with the FSS became more pronounced with fuel price increases.

17. Key Words (Suggested by Author(s))	18. Distribution Statement
Active Control Technology Arrow-wing Flutter Suppression System (FSS) Supersonic Cruise Aircraft Research	Unlimited

19. Security Classif. (of this report)	20. Security Classif. (of this page)	21. No. of Pages	22. Price*
Unclassified			

* For sale by the National Technical Information Service, Springfield, Virginia 22161

TABLE OF CONTENTS

TABLE OF CONTENTS (CONT)

LIST OF FIGURES

LIST OF FIGURES (CONT)

LIST OF TABLES

NOMENCLATURE

SYMBOL		UNITS
A	Root mean square/unit gust	varies
ACT	Active Control Technology	-
ATA	Air Transport Association	
BL	Buttock Line	m or in
BS	Body Station	m or in
CCV	Control Configured Vehicle	-
db	Decibel	-
deg	Degree	-
DOC	Direct Operating Cost	-
FAR	Federal Aviation Regulations	-
FSS	Flutter Suppression System	-
ft	Feet	-
g	Acceleration, gravity normalized	-
gpm, (gal/min)	Gallons per minute	-
HSAS	Hard Stability Augmentation System	-
Hz	Hertz	cycles/sec
j	Square root of -1 ($\sqrt{-1}$)	-
K	Flutter suppression system gain	varies
KEAS	Knots equivalent airspeed	nautical miles/hr.
kg	Kilograms	-
km	Kilometers	-
L	Random gust scale length	m or ft
lb	Pounds	-
m	Meters	-
M	Mach number	-
N	Newtons	-
n.mi	Nautical miles	-
OWE	Operational Weight Empty	kg or lb
P	Probability of occurrence	-
PSD	Power Spectral Density	varies
q	Dynamic pressure	varies
g(s)	Airplane generalized mode displacement	-
rad	Radians	-

NOMENCLATURE

SYMBOL		UNITS
RMS	Root Mean Square	varies
s,sec	Second	-
S	Laplace operator	-
SAS	Stability Augmentation System	-
SCAR	Supersonic Cruise Airplane Research	-
SLST	Sea Level Static Thrust	N or lb
U_o	True Airspeed, nominal condition	m/sec or ft/sec
V_C	Design cruise speed	varies
V_D	Design dive speed	varies
V_H	Maximum horizontal airspeed (military designation)	varies
W_g	Vertical gust velocity	varies
Y_d	Design limit value of variable Y	-
δ	Control surface deflection	rad or deg
Δ	Incremental change	varies
ζ	Damping ratio for characteristic roots $S = a \pm jb, \quad \zeta = -a/\sqrt{a^2 + b^2}$	varies
η_d	Ratio of design limit value to RMS value	-
$\dot{\theta}$	Airplane pitch rate	rad/sec or deg/sec
σ_y	RMS value of variable Y	varies
ω	Frequency	rad/sec
ω_n	Natural frequency - for characteristic roots $S = a \pm jb, \omega_n = \sqrt{a^2 + b^2}$	rad/sec

1.0 SUMMARY

This study was performed under NASA Contract NAS1-14205 with the objective of evaluating the economic and performance benefits of applying active flutter control to the SCAR Arrow Wing configuration. These benefits were evaluated in terms of difference in direct operating cost (Δ DOC), Δ payload, and Δ range. Direct comparisons were made between a configuration with an active flutter control system and a passive flutter configuration for which flutter was corrected by stiffening the structure.

This study considered a limited application of an active flutter suppression system (FSS), in that the FSS is employed to provide only the flutter margin above the design dive speed, V_D. A strength design configuration of the SCAR arrow wing supersonic cruise airplane was defined in a previous NASA study under Contract NAS1-12287 (Reference 1). The strength design configuration fluttered at a low airspeed at the critical Mach number of 0.9. Structural modifications were identified involving a relatively small weight penalty, but which achieve a large increase in flutter speed, although the flutter boundary design goal was not realized. The flutter speed of this modified configuration was selected as V_D for this program, and the addition of a FSS provides the twenty percent flutter margin.

Only approximately 318 kg (700 lb) of structural mass is required to increase the flutter speed to V_D. The airplane configuration with this first increment of structural modification to raise the flutter speed to V_D is called the "baseline" configuration in this document. It was established under Contract NAS1-12287 that an additional 4309 kg (9500 lb) of mass is required to modify the structure from the baseline configuration to increase the flutter speed to 1.2 V_D. This study, then, compares the economics and performance of the active and passive flutter control methods of modifying the baseline airplane to increase the flutter speed from V_D to 1.2 V_D.

Criteria were developed for preliminary synthesis of a flutter suppression system that would produce reasonable design requirements, and ultimately, realistic cost and performance comparisons. The primary flutter criteria are that (1) the airframe must be flutter free for all airspeeds up to 1.2 V_D, and (2) all flutter critical structural modes must have at least 1 1/2 percent equivalent viscous (three percent equivalent structural) damping at airspeeds up to V_D. Phase and gain stability criteria were adopted which are essentially in agreement with MIL-F-9490 requirements. Design random turbulence criteria were developed from the strength design

envelope described in MIL-A-8861A. The airplane must be stable and controllable, and the damping criterion described above must be satisfied in the presence of the design turbulence at airspeeds up to V_D. Criteria were also specified to assure FSS/airplane compatibility regarding ride quality, repeated loads, and handling qualities. The general requirement regarding safety/reliability is that the probability of flutter be no greater than 10^{-8}.

Flutter control system synthesis and hardware mechanization studies were conducted to define a system design concept with sufficient detail to conduct realistic economic analyses of the FSS configuration. The preliminary system definition developed utilizes wing trailing edge aileron-type control surfaces, activated by accelerometers located in the wing and aft fuselage.

The effectiveness of the system is shown in Figure 1-1 by a graph of the critical flutter mode damping ratio as a function of airspeed, at the constant design Mach number of 0.9. The graph shows that the baseline configuration flutters at V_D, and has less than the required 1 1/2 percent damping ratio at airspeeds less than V_D. Addition of the FSS increases the flutter speed beyond 1.2 V_D and satisfies the minimum damping criterion for all airspeeds.

Synthesis results indicate that flutter suppression system gain scheduling will be required as a function of both dynamic pressure and Mach number in order to satisfy stability criteria throughout the flight regime.

Performance analyses confirmed that the flutter suppression system satisfied compatibility criteria regarding airplane ride quality, repeated loads, and handling qualities.

Mechanization studies developed specific FSS and airplane system requirements and defined hardware configurations for the mechanization of the FSS. The control surface size was selected as required to satisfy FSS stability criteria in the presence of the design random turbulence, with realistic rate and position limits. This was accomplished by including describing functions (linear transfer function approximations) of control surface rate and position saturation in the linear root locus analyses. The control surface area required on each wing is 1.35 m^2 (14.5 ft^2) with a control surface position limit of .33 rad (19 deg) and a surface rate limit of 2.1 rad/sec (120 deg/sec.)

A tanden actuator was selected for the FSS surface to implement the required single-fail-operate capability. A triple actuator/supply arrangement was proposed, to be consistent with the primary control surface actuation, and was configured to protect against flutter/buzz when two hydraulic systems fail. The required area of each

tandem piston is 0.00092 m^2 (1.43 in^2). The required stroke is 0.069 m (2.7 in), assuming a crank length of 0.10 m (4.0 in). The maximum required flow for the FSS from each of the three hydraulic systems (including both wings) is 0.0003 m^3/sec (4.8 gal/min).

The capacity of the baseline airplane hydraulic systems was designed by the requirements for the landing flare phase of operation in severe turbulence. At the critical flutter design condition, from .0039 to .0045 m^3/sec (61 to 71 gal/min) of hydraulic flow is available from each of the four systems above the design requirements for the baseline airplane. Therefore, no additional hydraulic capacity or hydraulic cooling is required for FSS operation.

Triple redundant sensors and feedback filter electronics were required to accomplish the single-fail-operate capability. It was assumed that active flutter control law computations could be incorporated into the baseline airplane flight control system (with added cost and weight for wire bundles and additional computer interface). A preliminary appraisal indicated that the baseline electrical power capacity would accommodate the FSS.

The weight increments involved in incorporation of the FSS were estimated as indicated below:

o actuation and hydraulic plumbing	86.2 kg (190 lb)
o sensors and electrical systems	73.0 kg (161 lb)
Total FSS	159.2 kg (351 lb)

The FSS configuration operating mass, empty, is 4150 kg (9150 lb) less than the passive configuration. If the FSS and passive configurations have equal payloads and the FSS weight saving is absorbed as additional fuel, the FSS configuration will have 344 km (186 n. mi) greater maximum range. Or for a given range the FSS configuration can carry 4150 kg (9150 lb) greater payload with the same amount of fuel. For equal payloads and range, the lighter FSS configuration requires less fuel, as discussed in the following paragraphs.

The difference in DOC between the two airplane configurations was determined using the Air Transport Association (ATA) standard formula for estimating comparative DOC's, Reference 2, utilizing 1976 coefficients. Procurement and maintenance costs of the FSS were estimated separately. Figure 1-2 summarizes the savings of the FSS configuration in terms of percentage of the passive configuration; viz., 2.55 percent in OEW, 2.36 percent in price, 2.14 percent in block fuel, and 1.77 percent in total DOC. Block fuel

and DOC savings shown in Figure 1-2 are calculated for a trip distance of 5555 km (3000 n. mi), and a fuel price of 10.83¢/liter (41¢/gallon). Increases in fuel prices will increase the Δ DOC. For instance, if the fuel price is increased to 15.85¢/liter (60¢/gallon), the Δ DOC increases by 31.6 percent, to 2.33 percent of the total passive configuration DOC.

It was found that, for this class of airplane, the difference in maintenance between the two configurations is an insignificant component of the Δ DOC. The maintenance DOC of the active flutter system itself is only 0.25 percent of the total airplane maintenance, including the engines. And it was estimated that 75 percent of the FSS maintenance cost would be offset by the cost of maintaining 4309 kg (9500 lb) of added structure on the passive configuration.

Figure 1-3 shows a summary comparison of DOC components, in percent of total passive configuration DOC, for a given fuel price and distance. This shows a reduction of 1.77 percent from the total passive airplane DOC, most of which is realized from reduced fuel costs. Although this appears to be a small percentage, commercial transport marketing personnel have indicated that it is quite significant and that it would justify consideration of the FSS concept in a transport design.

The application of active flutter mode control in the design of the SCAR arrow-wing configuration is predicted to offer substantial benefits in the form of increased payload, increased range, and cost savings.

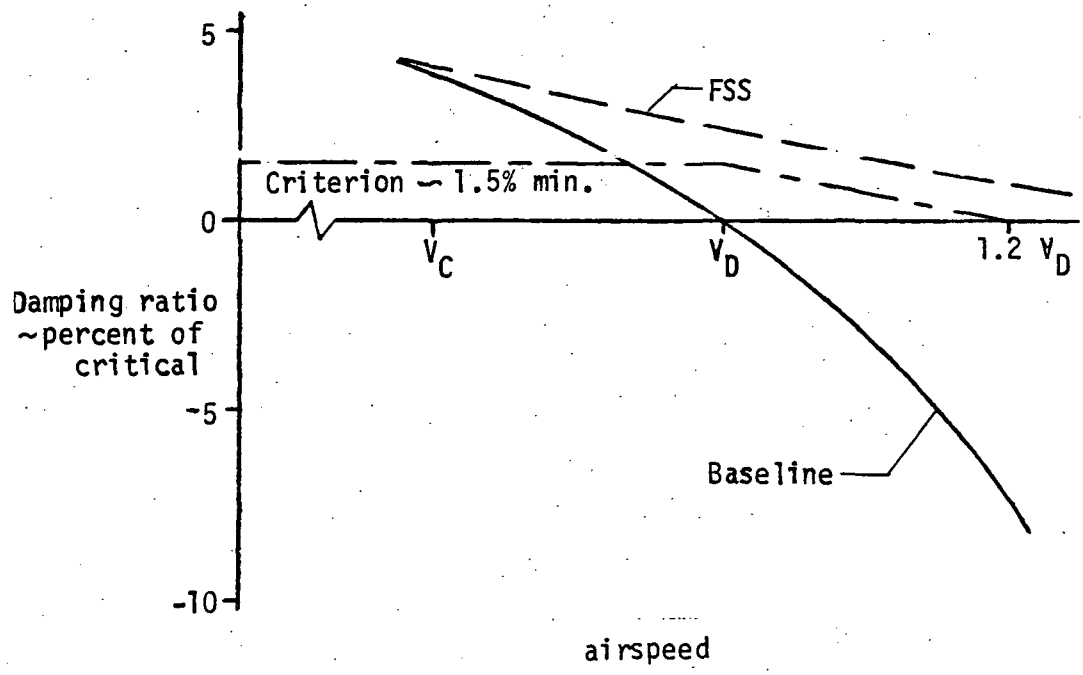

Figure 1-1: FLUTTER MODE DAMPING AT MACH 0.9

- Trip distance = 5555 km (3000 n. mi.)
- Fuel Price of 10.83¢/liter (41¢/gal.)

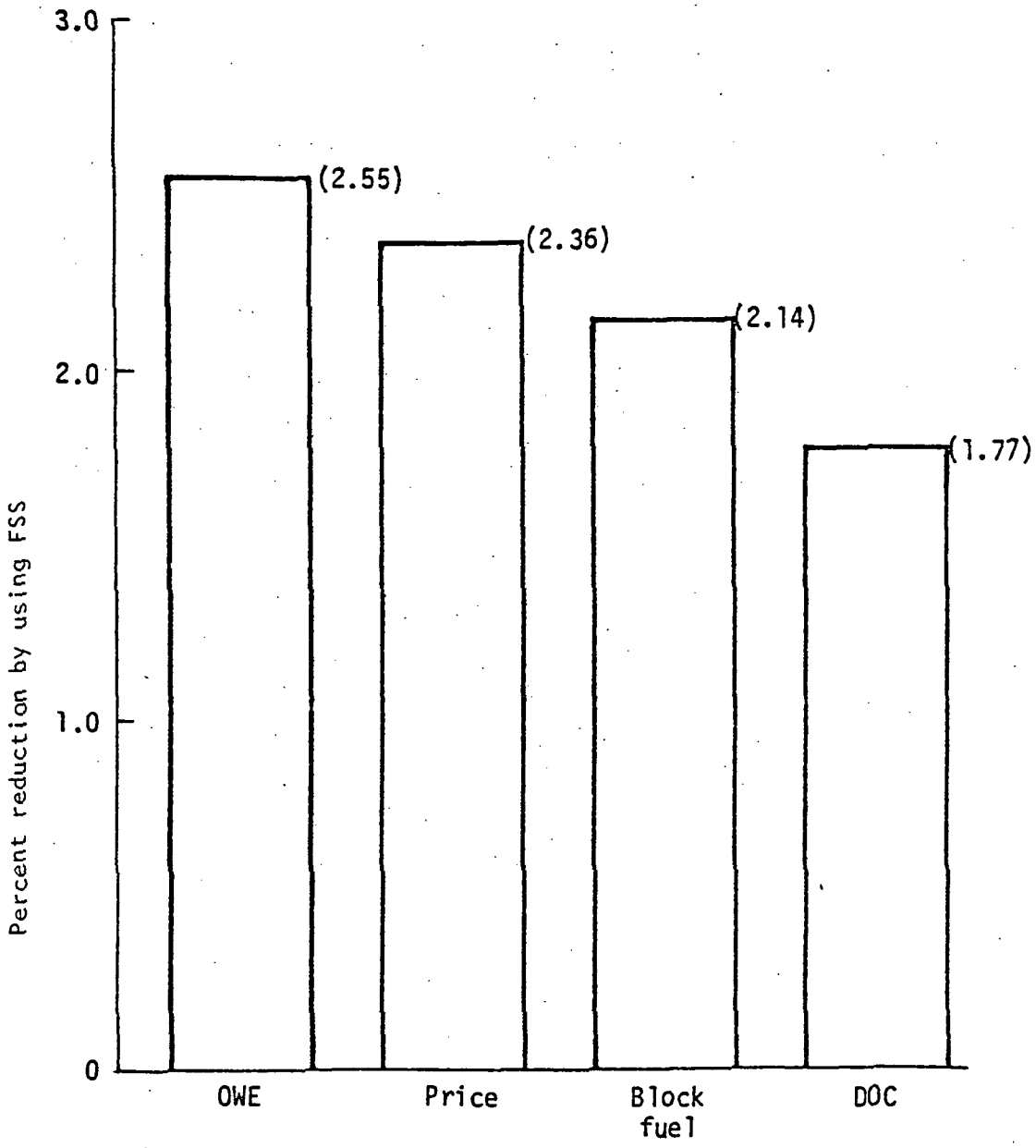

Figure 1-2: WEIGHT, PRICE, BLOCK FUEL AND DIRECT OPERATING COST COMPARISON

- o Trip distance 5555 km (3000 n. mi.)
- o Fuel price 10.83¢/liter (41¢/gal.)

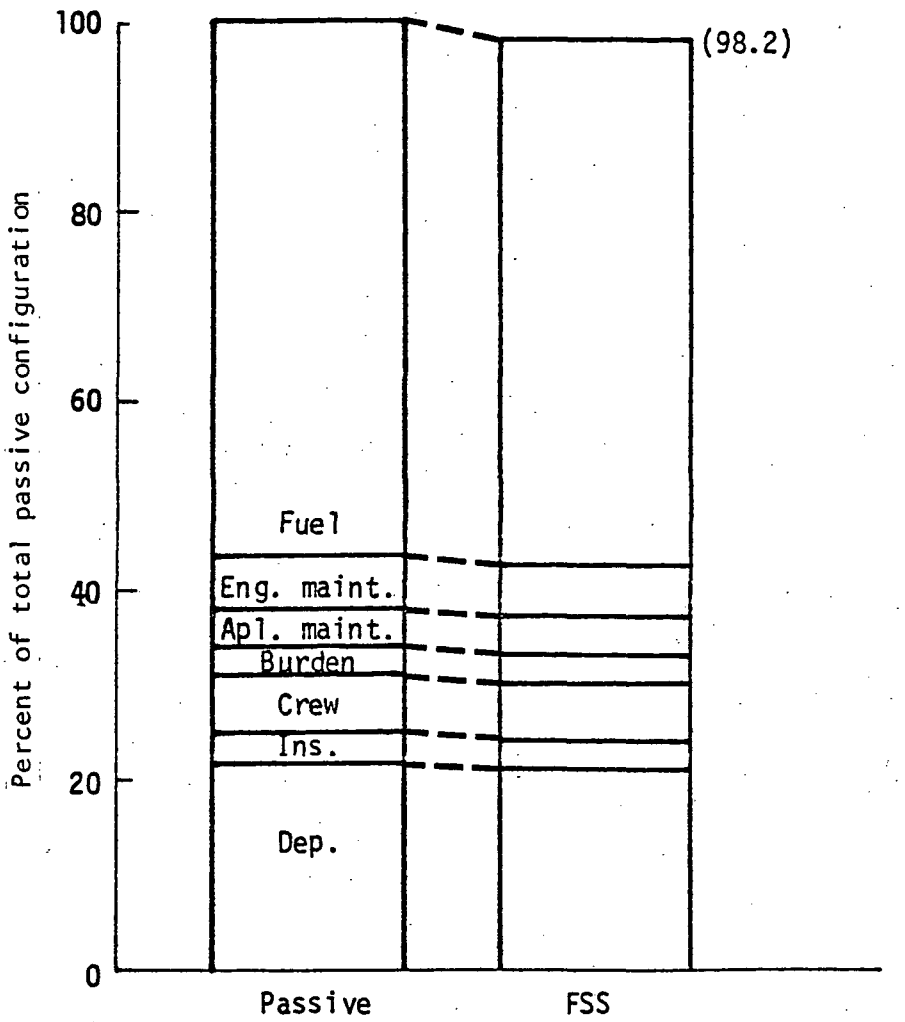

Figure 1-3: COMPARISON OF DIRECT OPERATING COST COMPONENTS

2.0 INTRODUCTION

Airplane designers are currently considering increased incorporation of active controls in the design of new technology commercial aircraft to improve performance. This document describes research conducted under NASA Contract NAS1-14205, which studied the potential benefits of active flutter control when applied in the design of a supersonic cruise airplane. The technical feasibility of active flutter suppression has been demonstrated. The next logical step toward incorporation of active flutter suppression in the design of commercial transports is to assess the performance and economic benefits, which is the objective of this study.

Recent studies have indicated that an active flutter control system, or flutter suppression system (FSS), might provide flutter margins with smaller weight penalty than required for a conventional passive flutter design (increased stiffness and mass balance) and thus improving performance and cost. However, there are weights and costs involved in providing the control surfaces, actuators, electronics, electrical and hydraulic power and cooling required for a FSS. A detailed comparison of weight, performance and cost between passive and active flutter configurations is required to assess the net benefits of a FSS.

The specific purpose of this current study was to compare the weight, performance and cost of a passive flutter configuration and an active flutter control configuration of the arrow wing supersonic cruise airplane defined in a previous study under Contract NAS1-12287 (Reference 1).

The initial SCAR airplane configuration was developed based on strength requirements. The strength design was quite deficient regarding flutter, having a flutter speed far below the original design goal at the critical Mach number of 0.9. Structural design modifications to the strength design were identified that requires only 318 kg (700 lb) of additional mass, to increase the flutter speed to what was considered to be a reasonable design dive speed. This configuration is designated the baseline configuration for this study, and its flutter speed is selected as V_D.

The current study considered a limited application of active flutter control which achieves the flutter margin above V_D, as illustrated in Figure 2-1. The active flutter control configuration is defined as the baseline airplane plus a FSS to increase the flutter speed from V_D to 1.2 V_D. The passive flutter configuration is defined as the baseline airplane plus additional structural modifications required to increase the flutter speed from V_D to 1.2 V_D. The structural modifications required for the passive configuration require 4309 kg (9500 lb) of additional mass above the baseline configuration.

This study compares the performance and economics of the active and passive flutter control methods of modifying the baseline airplane to increase the flutter speed from V_D to 1.2 V_D. The strength design, baseline, and passive flutter configurations were identified from work accomplished in the previous NASA contract.

The arrow-wing configuration is shown in Figure 2-2, and the geometric and baseline operating weight characteristics are listed in Table 2-I.

TABLE 2-I

GEOMETRIC PROPERTIES AND WEIGHT OF BASELINE ARROW-WING CONFIGURATION

Ref wing area, m^2 (ft^2)	914.91(9 848)
Gross wing area, m^2 (ft^2)	1044.60(11 244)
Body length, m (ft)	92.46(303.3)
Horizontal tail area, m^2 (ft^2)	55.74(600)
Vertical tail area, m^2 (ft^2)	41.71(449)
Vertical tail area (wing mounted), m^2 (ft^2)	162 825(358 970)
Payload, kg (lb)	22 183(48 906)
Maximum taxi mass, kg (lb)	340 194(750 000)
Total operating empty mass, kg (lb)	158 189(348 770)

Specific tasks accomplished under the current contract are:

- Mathematical description of the flexible baseline airplane with candidate control surfaces
- Synthesis of a flutter suppression system
- Preliminary design (mechanization) of the flutter suppression system -- to a depth required to accomplish a meaningful comparison of the weight, performance, and direct operating costs (DOC) of the passive and active flutter configurations

- Evaluation of the impact of the FSS on airplane ride quality, repeated loads, and handling qualities

- Evaluation and comparison of performance and DOC between passive and active flutter configurations.

Configuration 969-512B

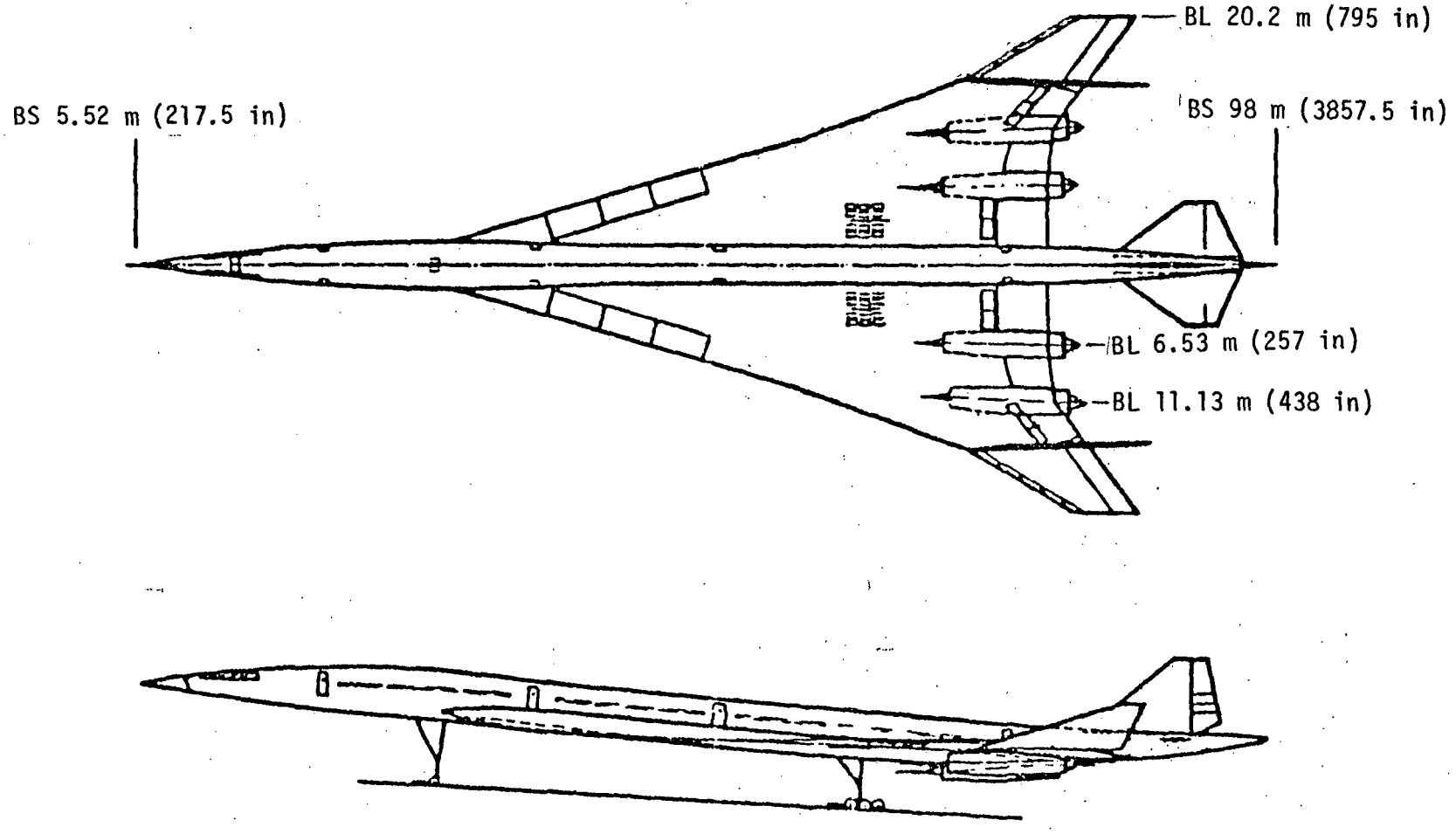

Figure 2-1: NASA ARROW-WING SUPERSONIC CRUISE CONFIGURATION

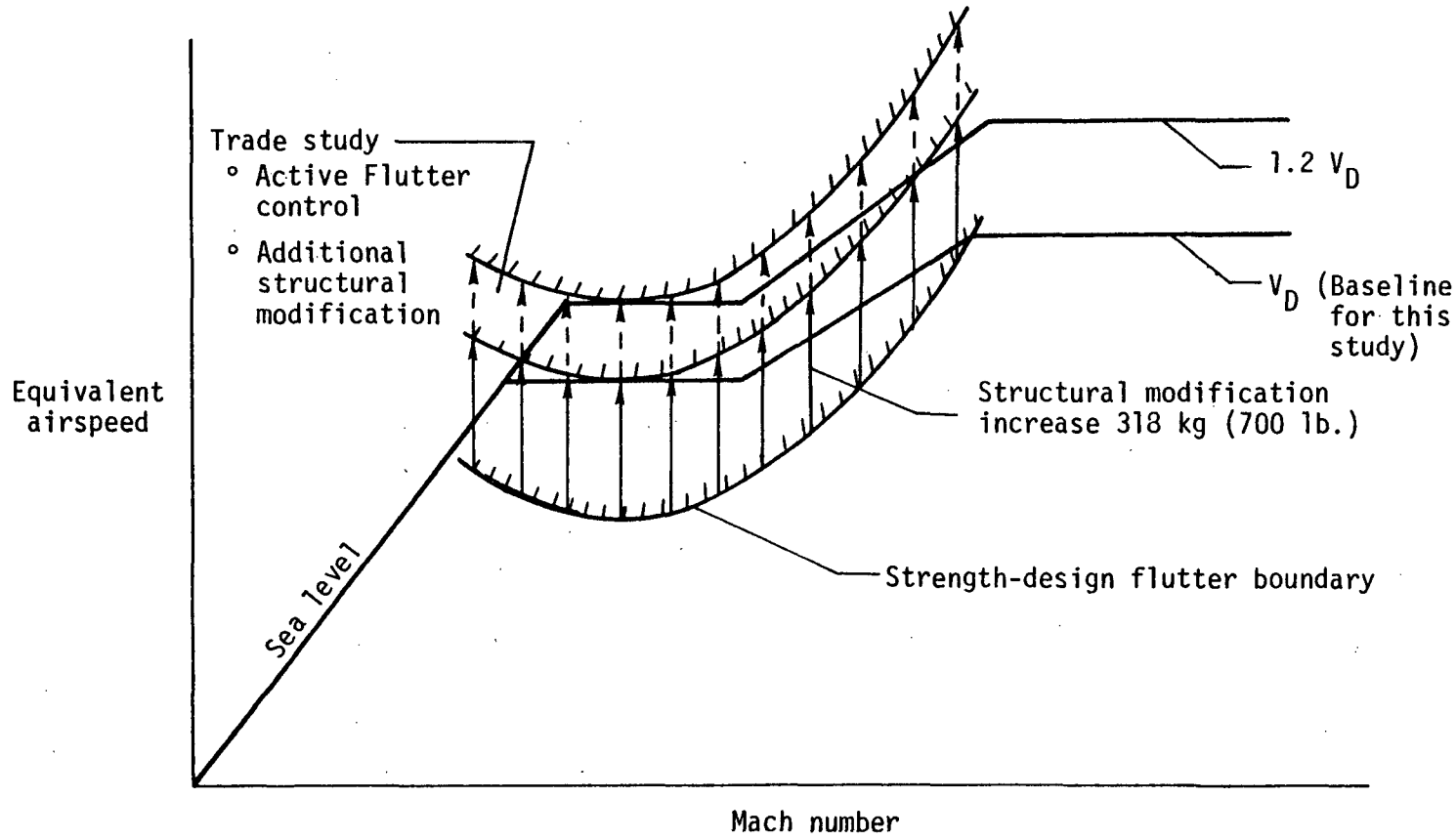

Figure 2-2: LIMITED APPLICATION FLUTTER SUPPRESSION SYSTEM

3.0 SYSTEM DESIGN CRITERIA

Design criteria were adopted based on contemporary design practices and existing Federal Aviation Regulations (FAR) and military specifications.

3.1 Flutter Criteria

3.1.1 Flutter margin. - The airframe must be flutter free for all airspeeds up to 120 percent of the design dive speed (1.2 V_D).

3.1.2 Minimum damping ratio. - At the design dive speed, V_D, at least 1 1/2 percent equivalent viscous (3 percent equivalent structural) damping must exist for all flutter critical structural modes. This criterion applies only to flutter critical modes. Lower damping may exist for modes that do not reach zero damping or do not rapidly approach zero damping at airspeeds below 1.2 V_D.

3.1.3 Phase and gain stability margins. - Phase and gain margins were adopted which are essentially in agreement with MIL-F-9490 requirements. Gain margins of ± 6 db and phase margins of $\pm .785$ rad (45 deg) were required for all aeroelastic modes at airspeeds up to V_D. No gain and phase margins are required simultaneously with the flutter speed margin of 1.2 V_D.

3.2 System Saturation Criteria (Design Random Turbulence)

Design random turbulence criteria were developed from the strength design envelope analysis described in Paragraph 3.22.2.1.2 of MIL-A-8861A, which specifies strength and rigidity requirements for airplane flight loads. Minimum values for the ratio Y_d/A are specified as a function of altitude. In this equation Y_d is a selected design limit load response, and A is the unit response or ratio of the RMS of Y to the RMS of gust velocity ($A = \sigma_Y/\sigma_{W_g}$). If η_d is defined to be the ratio of the expected peak response to the RMS response ($\eta_d = Y_d/\sigma_Y$), then the minimum values of Y_d/A may be interpreted as minimum values for peak gusts, expressed by the product $\sigma_{W_g} \cdot \eta_d$, where η_d is also the ratio between the expected peak gust velocity to RMS gust velocity. That is:

$$\frac{Y_d}{A} = \frac{\sigma_Y \cdot \eta_d}{\sigma_Y / \sigma_{W_g}} = \sigma_{W_g} \cdot \eta_d$$

The design random turbulence, σ_{W_g}, was used to determine FSS control surface size and hydraulic flow requirements. The value of σ_{W_g} was derived from the minimum values of $\sigma_{W_g} \cdot \eta_d$ in MIL-A-8861A. For this preliminary design, η_d was assumed to be two to produce a conservative σ_{W_g} for sizing the surface and hydraulic system.

The $\sigma_{W_g} \cdot \eta_d$ products specified in MIL-A-8861A, as described above, are for an airplane velocity of V_H (the maximum horizontal flight airspeed). These design peak intensities (or the derived σ_{W_g}) may be reduced to 50 percent of the specified values at the design speed, V_D, similar to the discrete gust requirements for strength design in both MIL-A-8861A and FAR Part 25. Figure 3-1 shows the resulting design random turbulence criteria at V_D as a function of altitude. The RMS turbulence criterion for the design condition in this preliminary design (V_D at M = 0.9) is 4.3 m/sec (14 ft/sec).

3.3 Compatibility Criteria

3.3.1 Ride quality. - The RMS accelerations along the fuselage of the FSS airplane will not be greater than five percent above the comparable RMS accelerations of the baseline airplane.

3.3.2 Repeated loads. - To show compatibility regarding wing loads and fatigue, RMS accelerations along the FSS airplane wing will not be greater than five percent above the comparable RMS accelerations of the baseline airplane.

3.3.3 Handling qualities. - In general, the FSS shall not significantly degrade the handling qualities of the airplane with Hard Stability Augmentation System (HSAS). The undamped natural frequency of the short period will not be changed more than 0.2 radians/second (on the complex plane). The minimum safe handling qualities of the HSAS will be maintained, vis., the short period damping ratio shall not be less than 0.15 in any configuration or flight condition. The phugoid mode was not simulated in these analyses, since the FSS and the phugoid mode should have practically no effect upon each other. Therefore, no phugoid mode criteria are applicable to this study.

3.4 Flight Safety and Reliability

The general requirement regarding safety/reliability is that the probability of flutter be no greater than the probability of primary structural failure, for which a generally accepted value is 10^{-8}.

Two circumstances must occur simultaneously in order for flutter to occur: (1) the airplane must be above the design dive speed, since the minimum flutter speed of the baseline airplane has been increased to V_D by passive methods, and (2) there must be a loss of the FSS function.

Since events 1 and 2 are independent, the general requirement is, numerically: $P(1) \cdot P(2) \leq 10^{-8}$. For system design purposes, a probability of 10^{-4} was chosen for each event. Admittedly, this choice is somewhat arbitrary for the probability of being beyond the design dive speed, but it is believed to be a realistic value. Design of a flutter suppression system with a probability of loss of function less than 10^{-4} is well within the state of the art.

3.5 Flutter Suppression System Mechanization

The primary design criterion regarding implementation is that the probability of loss of the FSS function be 10^{-4} or less. The following discussion includes assumed ground rules for this preliminary design, as well as basic decisions regarding design requirements in order to meet the functional reliability criterion.

3.5.1 System Failure philosophy and redundancy.

In order to satisfy the safety/reliability criterion that the probability of loss of the FSS function be 10^{-4} or less, the design requirement was established that the system will be fail-operational. That is, the FSS will remain completely operational following a first failure. This led to a design requirement that the FSS will be triple redundant.

3.5.2 Implementation criteria/ground rules.

The FSS actuators, control surfaces, and feedback sensors will be dedicated hardware. The actuators and control surface hingelines will be mounted on firm wing structure, rather than mounted as an aft segment of an existing primary manual control surface.

The hydraulic system flow rate for the control system will be based on the most critical of (a) engines idling descent, all engines operational, airplane upset control requirements plus active control flutter suppression system flow requirements, or (b) engines idling descent, one system out, active flutter suppression system flow requirements only.

The FSS actuators will be sized to provide full hinge moment authority with one hydraulic system failed.

Specific details of the preliminary design implementation are discussed in Section 7.0.

3.5.3 Operational ground rules. - Following the first failure in the FSS, an alternate flight envelope placard will be enforced. The alternate envelope will be developed so that the flutter critical mode of the baseline airplane has a damping ratio of at least 1.5 percent at flight conditions below the alternate placard, and the flutter speed of the baseline airplane is at least twenty percent above the alternate placard. The placard is required after the first failure, since a second failure would cause loss of the FSS function.

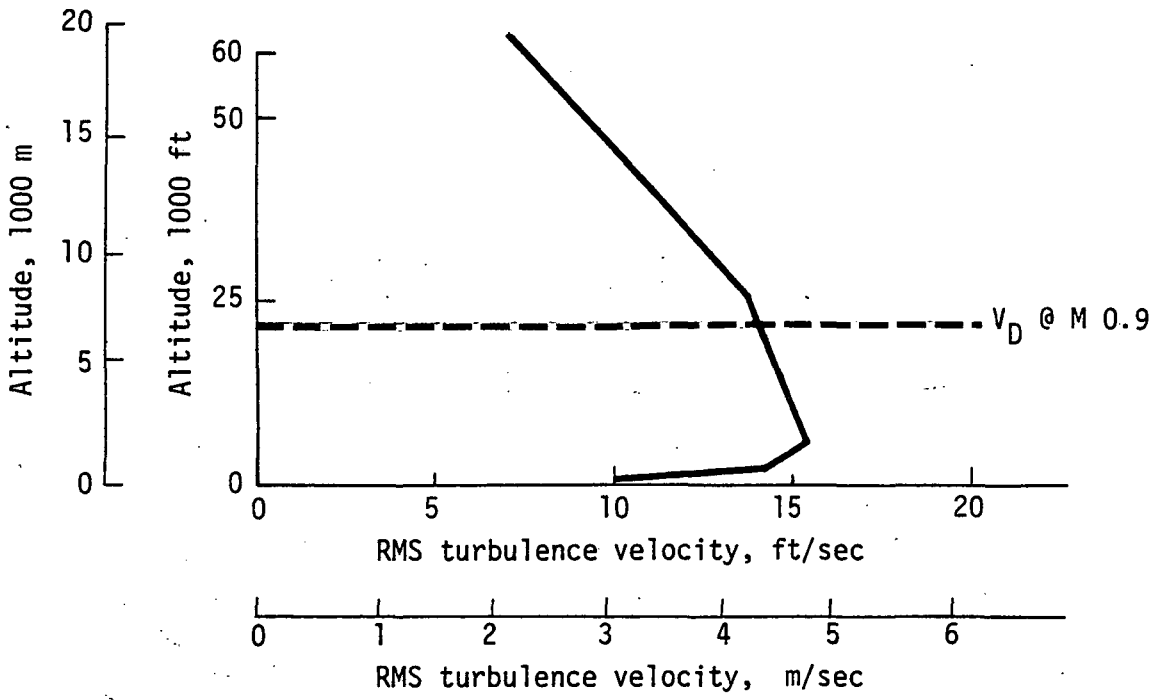

Figure 3-1: DESIGN RANDOM TURBULENCE CRITERIA

4.0 MATHEMATICAL MODEL

4.1 Structural Model

The rigid body and elastic modes used to form the generalized equations of motion for the SCAR arrow-wing were obtained via an ATLAS model of the baseline airplane. The equations were formed using two rigid body modes (vertical displacement and pitch rotation) and 18 elastic modes with natural frequencies ranging from .98 to 8.39 Hertz. The elastic modes are shown graphically in Appendix A.

The rigid body and elastic degrees of freedom were augmented with five additional degrees of freedom representing control surface rotations. The control degrees of freedom represent three wing trailing edge surfaces, one wing leading edge surface and the stabilizer/ elevator. The locations and chord lengths of the candidate FSS wing control surfaces are given in Table 4-1. The stabilizer/elevator was included so that the basic longitudinal Hard Stability Augmentation System (HSAS) could be modeled.

TABLE 4-1

WING CONTROL SURFACE LOCATIONS AND SIZES

Control Surface	Buttock Line Location at		Chord Length m(in)
	Inboard Edge, m(in)	Outboard Edge, m(in)	
Inboard trailing edge	8.00 (315)	9.53 (375)	1.11 (43.7)
Middle trailing edge	12.45 (490)	13.72 (540)	1.00 (39.2)
Outboard trailing edge	16.00 (630)	17.27 (680)	.84 (33)
Outboard leading edge	16.00 (630)	17.27 (680)	.81 (32)

4.2 Aerodynamic Forces

Unsteady aerodynamic forces on the wing, wing fin and horizontal stabilizer were generated using a three-dimensional plate-doublet finite-element solution. The theory accounts for Mach number and finite span effects and includes aerodynamic interference between airplane components. The unknown pressure distribution is determined for each airplane mode by considering pressure to be constant over a given aerodynamic panel and solving for the pressure based on a specific reduced frequency and Mach number. The primary surfaces and control surfaces are modeled with a mesh of trapezoidal elements arranged so that each control surface has at least two elements in the streamwise and chordwise directions. The aerodynamic panels are shown in Appendix A.

4.3 Equations of Motion

Initial equations of motion were formed using complex oscillatory aerodynamic coefficients generated for specific values of the reduced frequency parameter, ω/U_o. Final equations of motion were formulated in terms of real matrices through introduction of an "interpolating" or "approximating" function.

The original equations were the standard form:

$$\left(-(j\omega)^2\,[\text{MASS}]+(j\omega)\,[\text{DAMPING}]+[\text{STIFFNESS}]\right)\left\{q(j\omega)\right\}$$
$$+\rho U_o^2\left[A_I\left(\frac{j\omega}{U_o}\right)\right]\left(\left[C_\theta\right]\left\{q(j\omega)\right\}+\frac{j\omega}{U_o}\left[C_Z\right]\left\{q(j\omega)\right\}\right.$$
$$\left.+\frac{1}{U_o}\left[C_W\right]\left\{\frac{W_g}{\bar{V}_g}\,(j\omega)\,(j\bar{\omega})\right\}\right)=0$$

where q is the generalized coordinate and A_I is an aerodynamic influence coefficient matrix which can be evaluated for specific values of ω/U_o. The matrices C_θ, C_Z and C_W prescribe the usual linearized boundary conditions.

If one of the elements of the complex matrix A_I is plotted, as ω takes on selected values from 0 to 56 radians/second, the result appears as the X's in Figure 4-1.

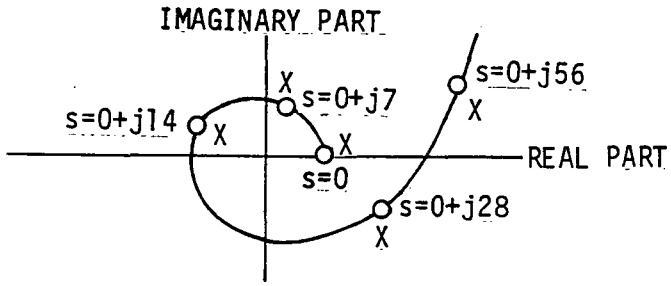

Figure 4-1: TYPICAL COMPLEX COEFFICIENT AS A FUNCTION OF FREQUENCY

The solid line of Figure 4-1 is an approximating function, chosen as a rational polynomial function of the complex variable s. The circles are values of the approximating function at values of s for which the X's are plotted. The approximating function was chosen to permit accurate approximation of the time delays inherent in the unsteady aerodynamics subject to the following restrictions:

- It must have complex conjugate symmetry
- It must have denominator roots in the left half-plane
- It must approximate the value of the complex coefficient when $s = 0 + j\omega$, for those values of ω analyzed.

The approximating function for each element in the aerodynamic influence coefficient matrix was determined after analysis at seven discrete frequencies. When the approximating functions are substituted in the equations of motion for the complex aerodynamic coefficients, a new set of equations results, whose coefficients are coefficients of the approximating function. After rearrangement, the final form of the equations of motion with variable density ρ and velocity U_o and without gust penetration is:

$$\left(s^2\,[\text{MASS}] + s\,[\text{DAMPING}] + [\text{STIFFNESS}]\right)\{q(s)\}$$

$$+\left(s^2\,\rho\,[C_1] + s\rho U_o\,[C_2] + \rho U_o^2\,[C_3] + \rho U_o^2 \sum_{i=1}^{4} [D_i]\,\frac{s}{s + U_o B_i}\right)\{q(s)\}$$

$$+\left(\rho U_o\,[R_o] + \rho U_o \sum_{i=1}^{4} [R_i]\,\frac{s}{s + U_o G_i}\right)\left\{\frac{W_g}{V_g}(s)\right\} = \{0\}$$

The items in the first line of the above equation are structural coefficients; items in the second line are aerodynamic coefficients; items in the third line are gust velocity coefficients, where:

s	= LaPlace variables
ρ	= Air density
U_o	= True airspeed
[MASS]	= Structural mass
[DAMPING]	= Structural damping
[STIFFNESS]	= Structural stiffness
$[C_1],[C_2],[C_3]$	= Aerodynamic parameters
$[D_1],[D_2],[D_3],[D_4]$	= Aerodynamic parameters
$[B_i],[G_i]$	= Lift growth parameters
$[R_0],[R_1],[R_2],[R_3],[R_4]$	= Vertical and lateral gust coefficients
$q(s)$	= Rigid body, structural and control surface freedoms
$W_g(s)$	= Vertical gust
$V_g(s)$	= Lateral gust

Because of the continuity of the aerodynamic coefficients as ω varies (no aerodynamic poles or zeros in the vicinity of the imaginary axis) these equations are considered to be a good approximation of the LaPlace transformed equations. They should not be depended upon for values of s too remote from the imaginary axis (greater than 40 radians/second) or above the highest frequency analyzed (greater than 56 radians/second).

5.0 SYNTHESIS AND SYSTEM PERFORMANCE

The flutter boundary of the arrow-wing configuration with the passive flutter fix as defined during the previous study under contract NAS1-12287 is shown in Figure 5-1. The 1.2 V_D design envelope established from results of the passive flutter fix study is also shown in Figure 5-1. The Mach 0.9 V_D speed of the baseline airplane was determined during the previous study to be 375 KEAS (193 m/sec). The Mach 0.9 V_D speed obtained from equations generated for the present study is 393 KEAS (202 m/sec), an increase of 18 KEAS (9.3 m/sec) above that obtained during the previous study. The FSS synthesis was conducted at the Mach 0.9 condition based on the flutter speed of the present equations, making the 1.2 V_D speed slightly above the design envelope as shown in Figure 5-1.

Mach 1.2 and 2.7 conditions shown in Figure 5.1 were analyzed to assure adequate operation of the system at speeds/Mach conditions above the critical flutter region. Although operation of the FSS is not necessary for flutter stability at speeds/Mach conditions substantially above the Mach 0.9 synthesis condition, a system-on status is desirable for system monitoring and failure detection.

To assure satisfactory FSS operation at all speeds up to 1.2 V_D, synthesis was conducted at corresponding V_c (.8 V_D) and V_D as well as the 1.2 V_D conditions as shown in Figure 5-1.

The synthesis approach was to define a flutter suppression system that would provide flutter mode control at all speeds up to 1.2 V_D at the constant 0.9 Mach number and then to minimize the system complexity required to allow the system to operate at higher altitude, higher speed, non-flutter-critical flight conditions.

The objective of the synthesis was to develop an uncomplicated preliminary design FSS concept to meet the design criteria with a minimum number of sensors and control surfaces. The synthesis philosophy was to define the system without resorting to an extensive optimizing process if possible. This philosophy would possibly yield a system concept which would have some margin for refinement to compensate for additional design constraints which might be imposed during a final design effort, such as a necessary relocation of control surfaces or sensors.

Control surfaces included in the mathematical model for investigation of FSS benefits are shown in Figure 5-2. Control surface dimensions are given in Section 3.0. Initial efforts to identify the control

surfaces with the greatest potential involved a mode controllability assessment utilizing transfer function zero locations. Zero loci as a function of surface and sensor placement were used to identify combinations of control surfaces and sensor locations that would control the flutter mode and minimize adverse coupling with other structural modes. The mode controllability assessment indicated that initial efforts to define a system should concentrate on the two outboard trailing surfaces and the vertical accelerometer sensors shown in Figure 5-2.

Further synthesis to define a surface, sensor and feedback filter combination utilized root locus techniques. All synthesis to define a system included the actuator first order transfer function $40/(S + 40)$ which is considered representative of that used for the size of control surfaces considered.

Root locus synthesis indicated that the middle aileron (shown in Figure 5-2), when used with a vertical accelerometer at BL 434, showed adequate effectiveness to control the flutter mode. However, this concept tended to destabilize a 17 radian/second mode, resulting in insufficient gain margin. To correct this problem with the minimum number of additional components, a sensor was added at the airframe centerline.

The final flutter suppression system definition utilizing the middle aileron and accelerometers at BL 434 and at the aft body centerline is shown in the block diagram of Figure 5-3.

At the Mach 0.9 V_D condition, system phasing at the flutter mode frequency and system gain were determined by a phase lag limit on the flutter mode and a phase lead limit on a six rad/sec mode as shown by the partial root loci of Figure 5-4. Minimum gain limit on the flutter mode and a maximum gain limit on a 25 rad/sec mode determined the gain at the Mach 0.9/1.2 V_D condition as shown by the root loci of Figure 5-5. The gain required at Mach 0.9/1.2 V_D was approximately 20 percent more than that required at Mach 0.9 V_D. At Mach 1.2 and 2.7 flight conditions and at speeds below approximately 0.9 V_D at Mach 0.9 the basic airplane was flutter stable and the FSS was not required. Also, other structural modes become more sensitive to system operation at the higher Mach numbers. Therefore, the system gain was reduced at these conditions to minimize undesirable control authority.

The required gain variations at the various flight conditions dictated gain scheduling as a function of both dynamic pressure and Mach number. The required gains at the evaluation flight conditions are shown in Table 5-1.

TABLE 5-I

FLUTTER SUPPRESSION SYSTEM GAIN VALUES

Mach Number	Gain, Rad/m/Sec^2 (Rad/in/sec^2) At:		
	V_c	V_D	$1.2V_D$
0.9	5.91 (0.15)	11.81 (0.30)	13.78 (0.35)
1.2 and 2.7	1.97 (0.05)	3.94 (0.10)	4.59 (0.117)

Complete root loci for the final system covering the entire airplane structural frequency range are given in Appendix B for V_C, V_D and 1.2 V_D at constant Mach numbers of 0.9, 1.2 and 2.7. Performance of the FSS in terms of its effect on the flutter mode at the critical Mach 0.9 condition is summarized in the damping and frequency plots of Figure 5-6. The FSS produced a negligible effect on the flutter mode at V_C due to gain scheduling. At V_D the FSS provided damping in excess of the 1.5 percent equivalent viscous damping criteria and provided stability at speeds in excess of 1.2 V_D.

A Bode plot of the final system is shown in Figure 5-7. The system was synthesized to attenuate the feedback signal at frequencies above and beyond the flutter frequency to minimize coupling with rigid body and high frequency structural motion and to eliminate steady state acceleration sensor signals.

Synthesis to define the FSS was conducted without the HSAS included in the mathematical model. After HSAS performance was evaluated and found acceptable as discussed in the next section, FSS performance with the HSAS included in the mathematical model was evaluated. Damping and frequency of airplane rigid body and structural modes with the FSS and HSAS are compared to the airplane with HSAS for V_C, V_D and 1.2 V_D at the three evaluation Mach numbers in Appendix "B." Structural mode damping and frequency in Appendix "B" with the FSS and HSAS are almost identical to those indicated for the nominal FSS system only in the root loci plots of Appendix "B." As indicated by this comparison, the HSAS had very little effect on the airplane structural modes; and its inclusion in the mathematical model did not alter the performance of the FSS.

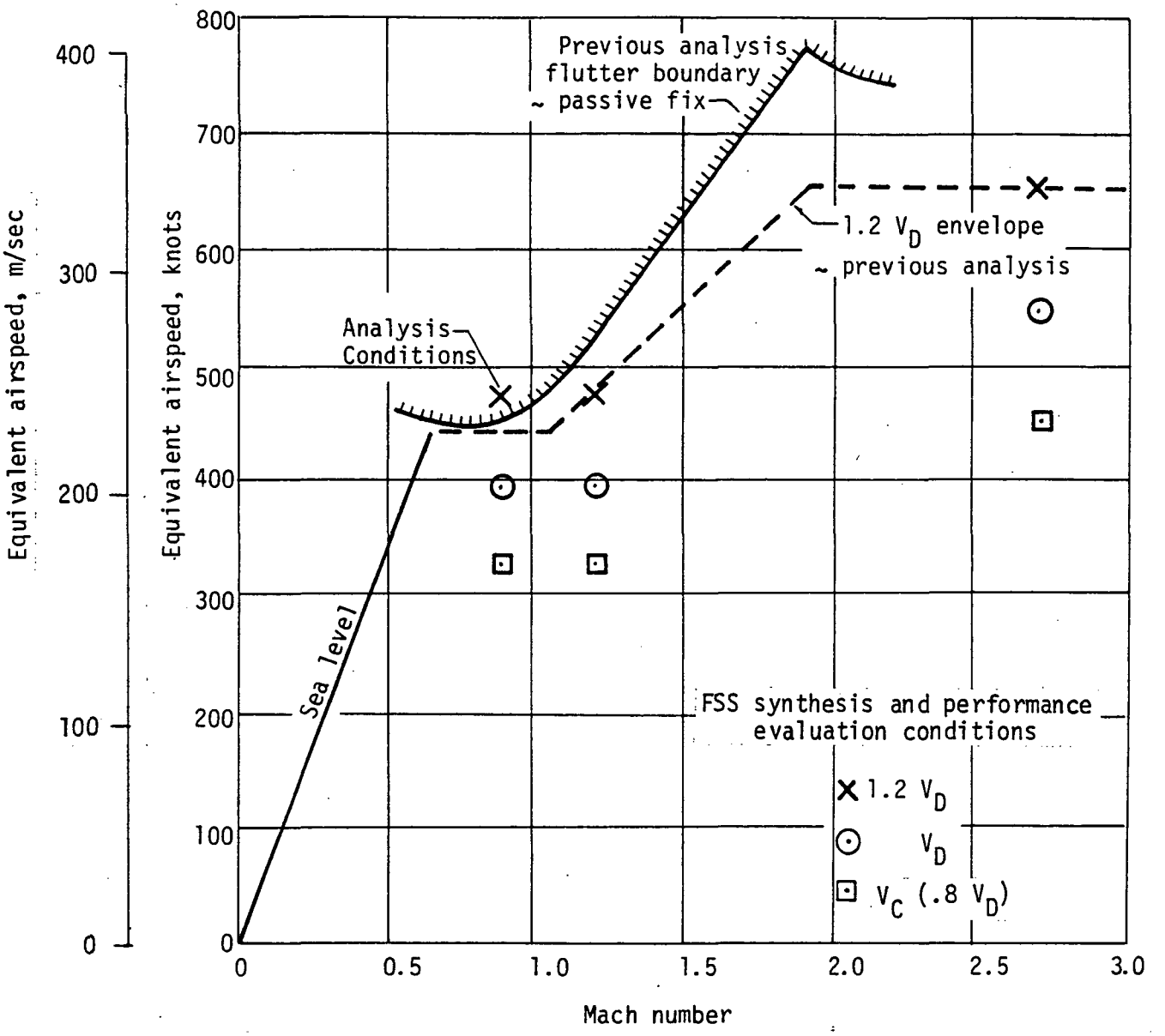

Figure 5-1: FLUTTER BOUNDARY AND SYNTHESIS FLIGHT CONDITIONS

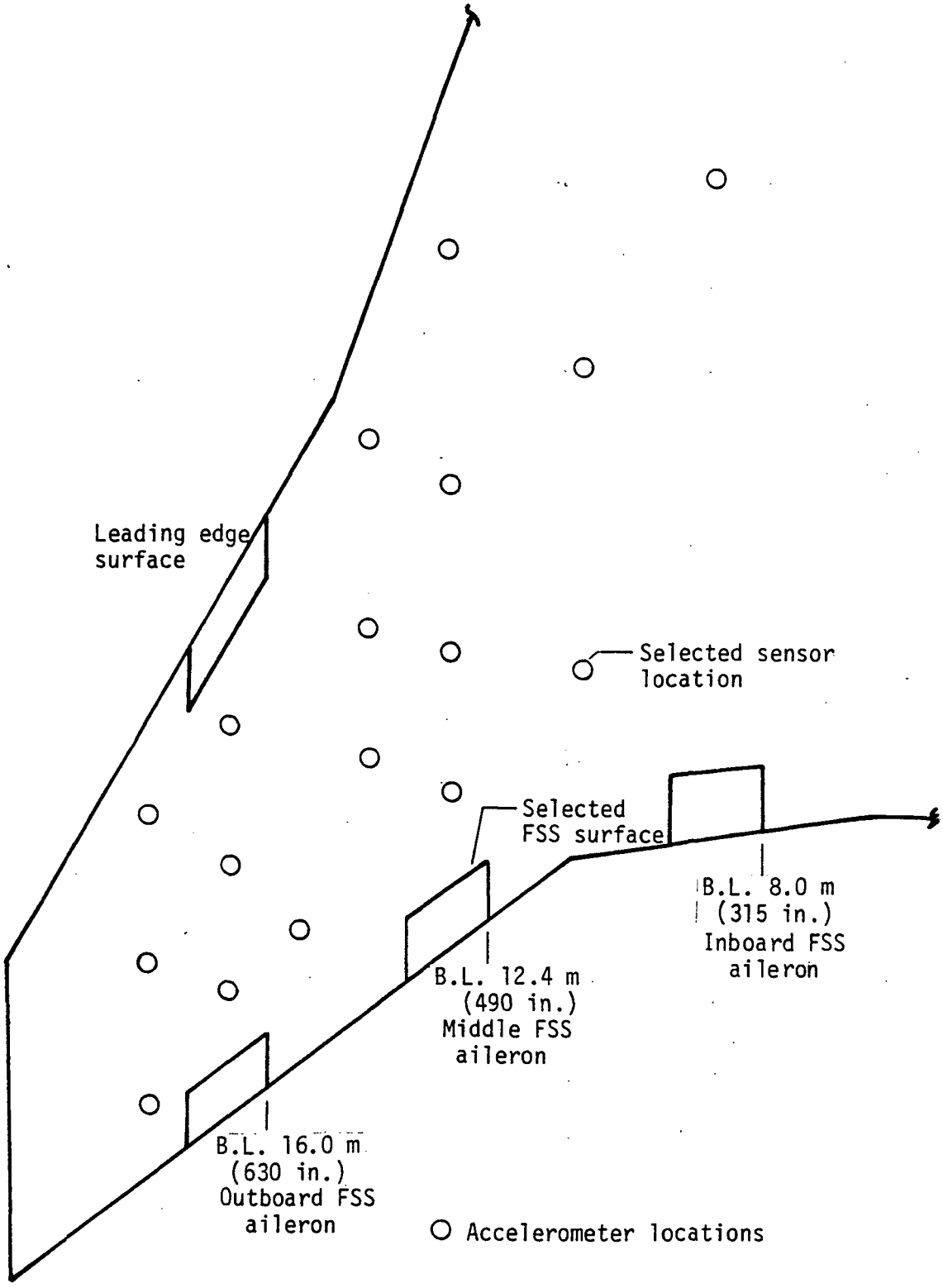

Figure 5-2: CANDIDATE CONTROL SURFACES AND SENSOR LOCATIONS

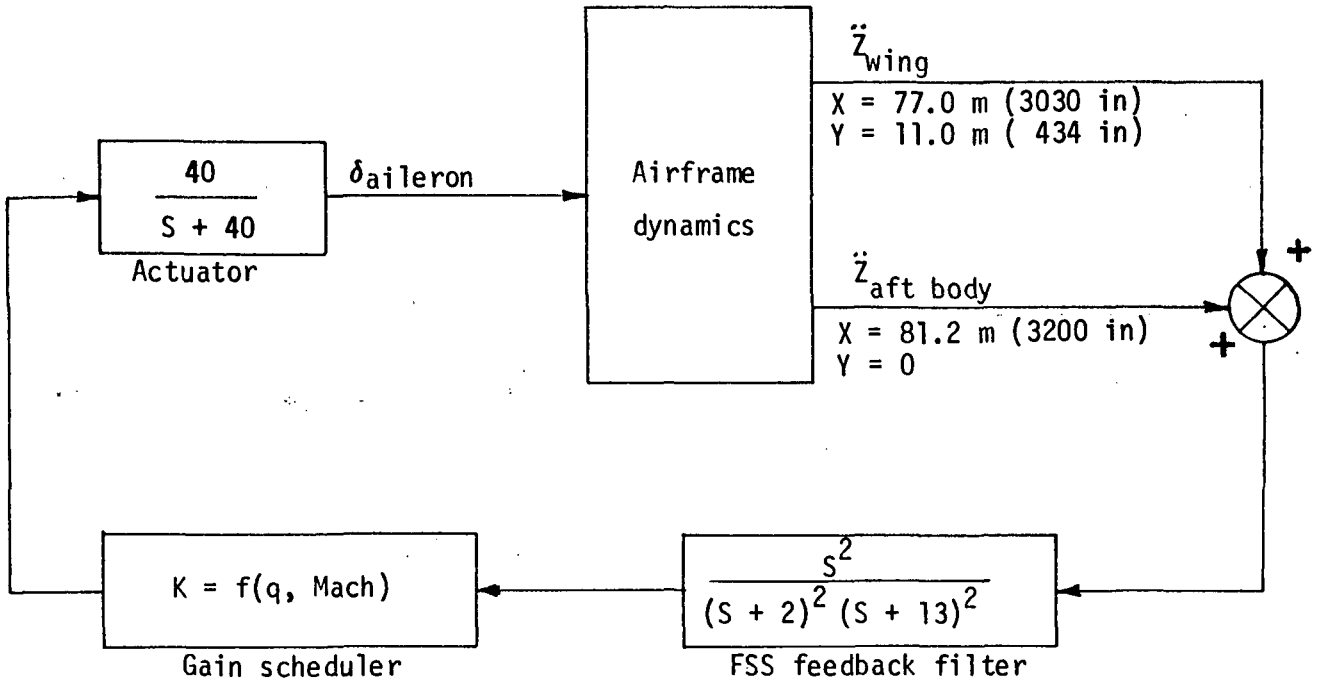

Figure 5-3: FLUTTER SUPPRESSION SYSTEM BLOCK DIAGRAM

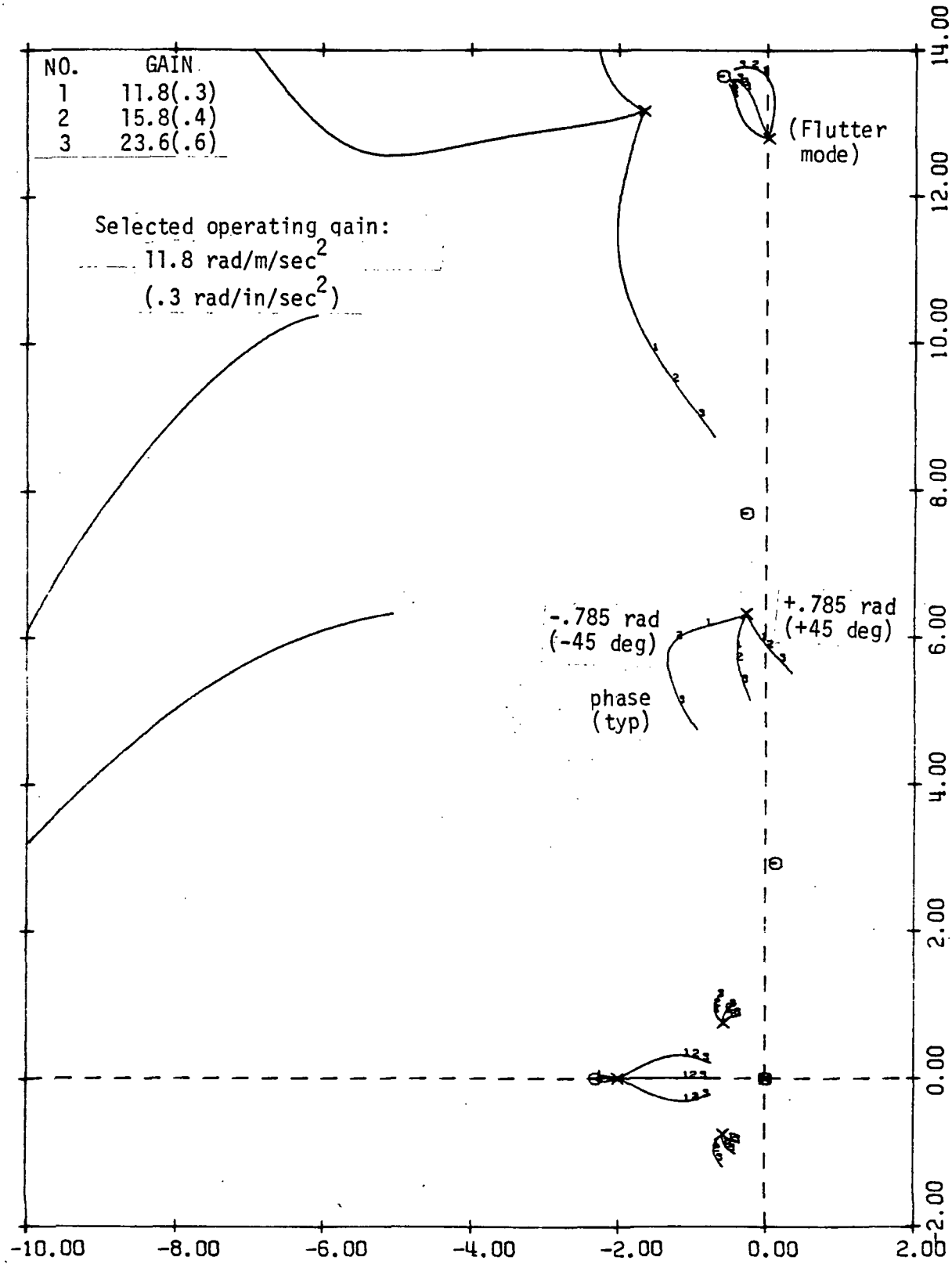

Figure 5-4: PHASE/GAIN ROOT LOCI FOR MACH 0.9 - V_D

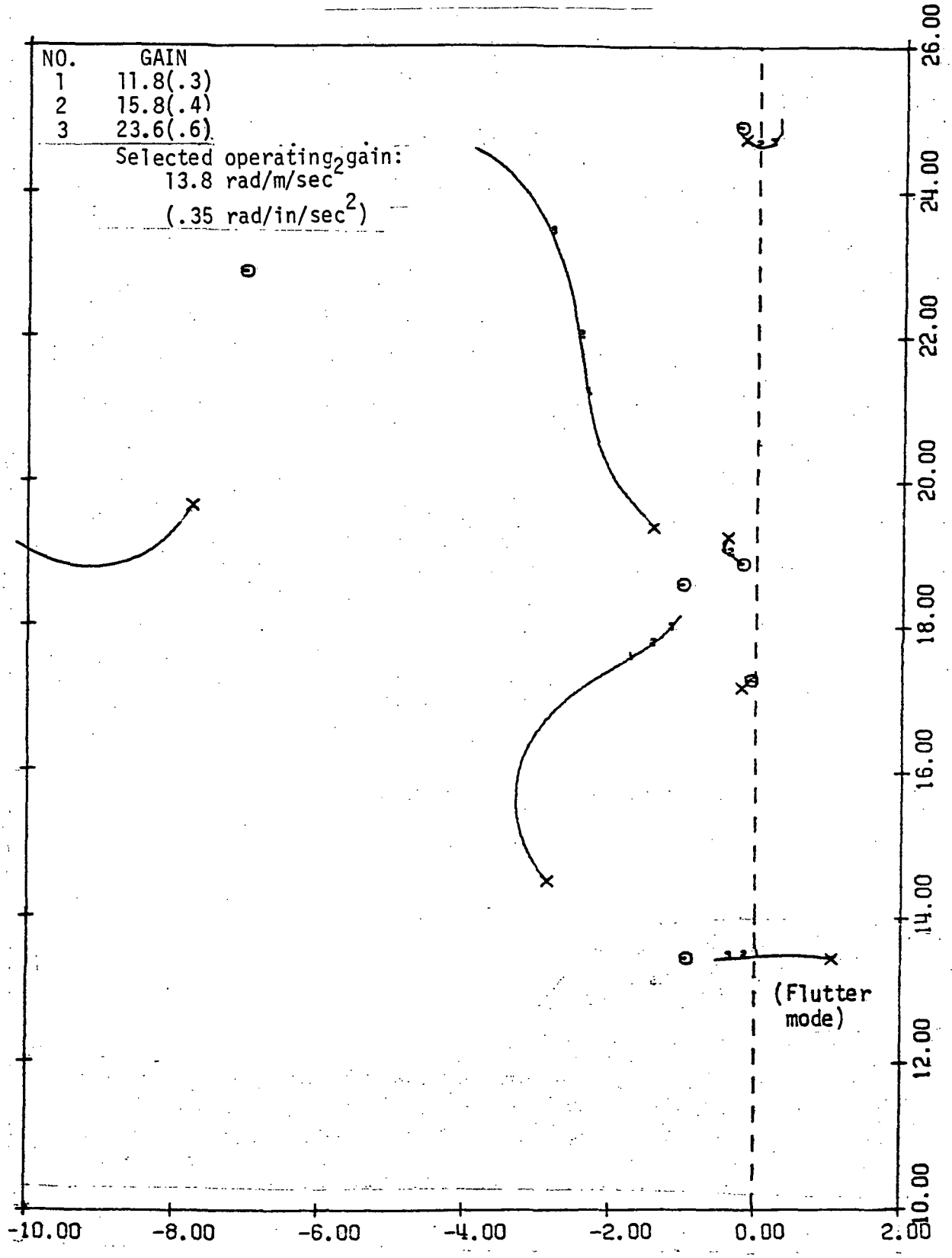

Figure 5-5: GAIN ROOT LOCI FOR MACH 0.9 - 1.2 V_D

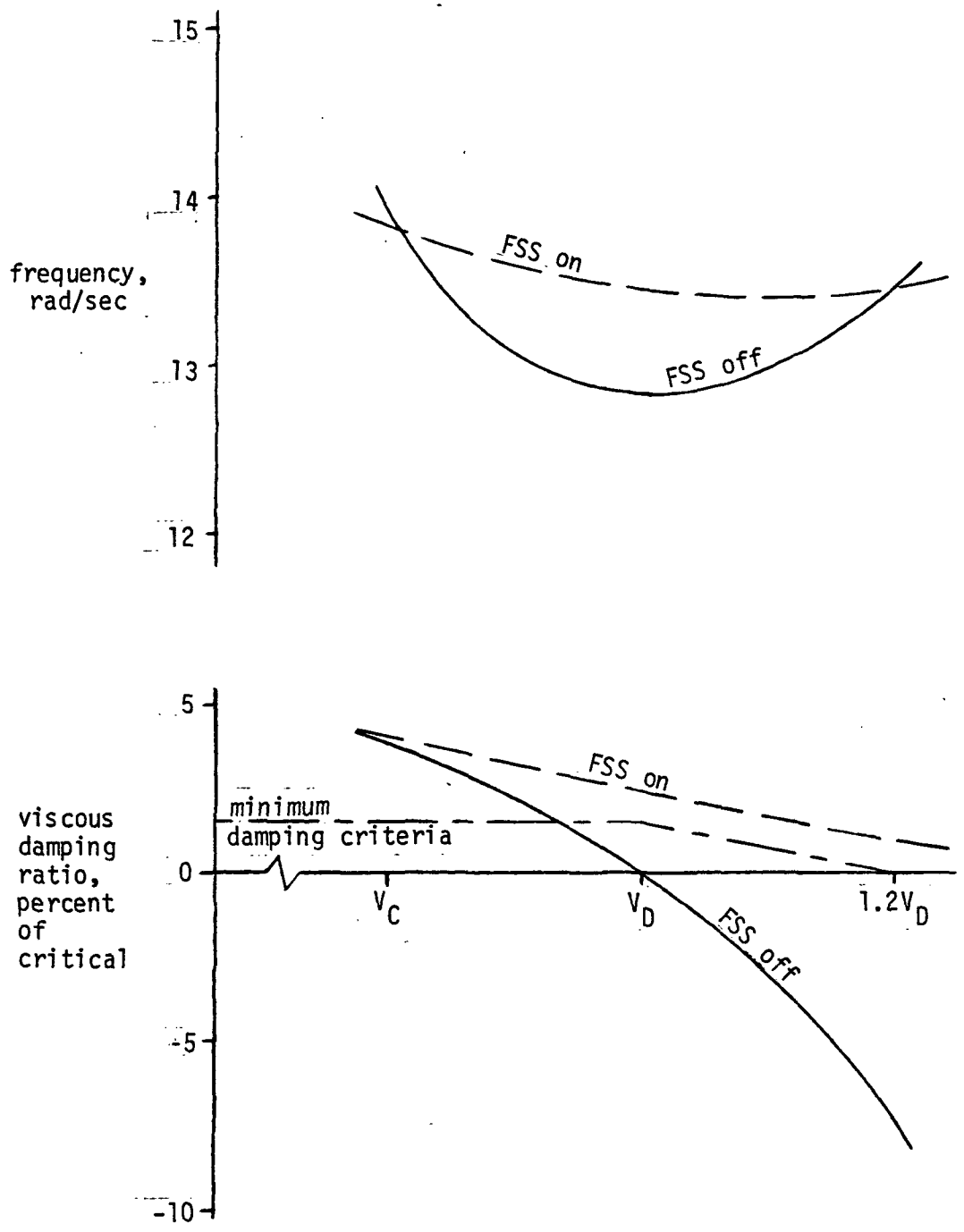

Figure 5-6: EFFECT OF FSS ON FLUTTER MODE DAMPING AND FREQUENCY AT MACH 0.9

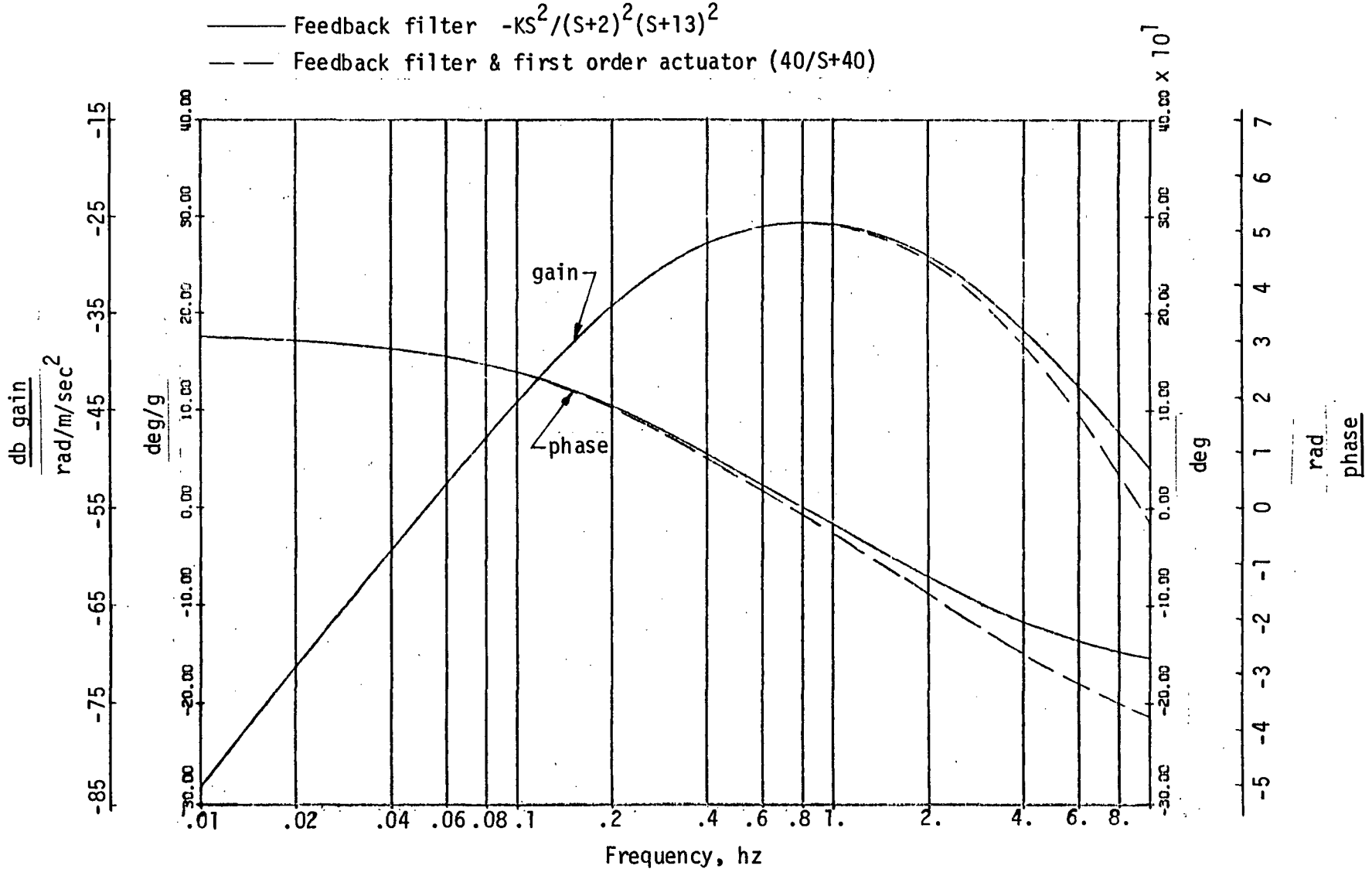

Figure 5-7: FLUTTER SUPPRESSION SYSTEM BODE PLOT

6.0 FSS COMPATIBILITY

The final FSS configuration defined in Figure 5.3 of Section 5.0 was evaluated for its compatibility with airplane ride, repeated loads and handling qualities.

6.1 Handling Qualities Compatibility

Effect of the FSS on handling qualities was evaluated relative to the airplane with a basic stability augmentation system (defined HSAS) which was required to meet minimum-safe stability and control criteria. The HSAS shown in Figure 6.1 was synthesized under the arrow wing structural design concept study, Contract NAS1-12287, Reference 1. The HSAS was synthesized using rigid body airframe equations of motion but included a structural mode filter.

The primary function of the HSAS is to provide stability to divergent phugoid roots at certain flight conditions. Longitudinal airplane motion was not included in the equations developed for the present study because of its negligible effect on flutter characteristics. Without the airplane longitudinal degree of freedom, the HSAS as defined during the previous study meets minimum safe stability and control criteria pertaining to airplane short period characteristics. Also, the HSAS has a negligible effect on airplane structural modes at the flutter evaluation flight condition as shown by the comparison of airplane characteristic roots in Table 6-I. and therefore, was used for the FSS handling qualities evaluation without further synthesis or refinement.

Handling quality effects were evaluated at V_C and V_D for three Mach numbers, 0.9, 1.2 and 2.7.

FSS handling quality criteria considered placement of airplane short period roots relative to that of the airplane-HSAS configuration. Results comparing characteristics with the FSS to that of the airplane-HSAS are shown in Table 6-II. No significant change in frequency occurred at any evaluation flight condition. Maximum reduction in damping is 5.3 percent of critical, occurring at the Mach 0.9 dive condition. No significant change in damping occurred at the other evaluation Mach numbers. At Mach 0.9, the airplane-HSAS has well damped short period characteristics; and consequently, the 5.3 percent change in critical damping at this condition does not produce a minimum damping situation.

The effects of the FSS on short period characteristics are compatible with the handling quality criteria of Section 3.0.

6.2 Ride Quality and Repeated Load Compatibility

Normal acceleration along the fuselage was used to assess the effects of the FSS on ride characteristics, and acceleration along the wing near the rear spar was used as an indicator of the effects on repeated loads.

Ride quality and repeated loads criteria limited any fuselage and wing acceleration increase from FSS activity in turbulence to five percent of baseline values.

Changes in acceleration at the Mach 0.9 climb and Mach 2.7 cruise conditions, which are flutter stable without the FSS, indicate the extent of the influence of the FSS on ride and repeated loads. Plots of RMS fuselage and wing acceleration at the two evaluation flight conditions are shown in Figures 6.2 and 6.3. Typical PSD/cumulative RMS plots are shown in Figure 6.4 for the FSS and baseline airplane.

The FSS produced no significant increase in acceleration anywhere along the fuselage or wing. Some reduction in acceleration occurred on the outboard wing at the Mach 0.9 condition due to damping of the flutter mode. No significant change in the rigid body contribution to acceleration occurred with the FSS.

TABLE 6-I

EFFECTS OF HSAS ON AIRPLANE CHARACTERISTIC ROOTS AT V_D, MACH 0.9

	Free Airplane		Airplane with HSAS	
	Damping ratio, ζ	Frequency rad/sec	Damping ratio, ζ	Frequency rad/sec
Short period	.604	.93	.48	1.06
Structural modes	.043	6.33	.044	6.37
	.000	12.80	.001	12.83
	.123	13.28	.123	13.25
	.019	17.17	.019	17.17
	.231	18.25	.231	18.25
	.018	19.19	.018	19.19
	.032	20.12	.032	20.12
	.014	24.88	.014	24.88
	.085	30.04	.085	30.04
	.017	30.08	.017	30.08
	.145	32.02	.145	32.02
	.008	34.43	.008	34.43
	.010	38.71	.010	38.71
	.011	39.99	.011	39.99
	.016	42.87	.016	42.87
	.011	47.83	.011	47.83

TABLE 6-II

EFFECTS OF FLUTTER SUPPRESSION SYSTEM ON SHORT PERIOD CHARACTERISTICS

Flight Condition	Control System(s)	Short Period Characteristics		Percent critical damping change	Frequency change
		damping, zeta ζ	frequency, ω_n rad/sec		
Mach 0.9 Climb 8992 m (29 500 ft) alt.	HSAS	.407	.96		
	HSAS & FSS	.386	.99	-2.1	+.03
Mach 0.9 Dive 6462 m (21 200 ft) alt.	HSAS	.477	1.06		
	HSAS & FSS	.424	1.13	-5.3	+.07
Mach 1.2 Climb 12 649 m (41 500 ft) alt.	HSAS	.299	1.21		
	HSAS & FSS	.296	1.21	-0.3	.00
Mach 1.2 Dive 10 363 m (34 000 ft) alt.	HSAS	.367	1.33		
	HSAS & FSS	.369	1.33	+0.2	.00
Mach 2.7 Cruise 18 898 m (62 000 ft) alt.	HSAS	.176	1.20		
	HSAS & FSS	.173	1.20	-.03	.00
Mach 2.7 Dive 16 459 m (54 000 ft) alt.	HSAS	.213	1.40		
	HSAS & FSS	.207	1.40	-.06	.00

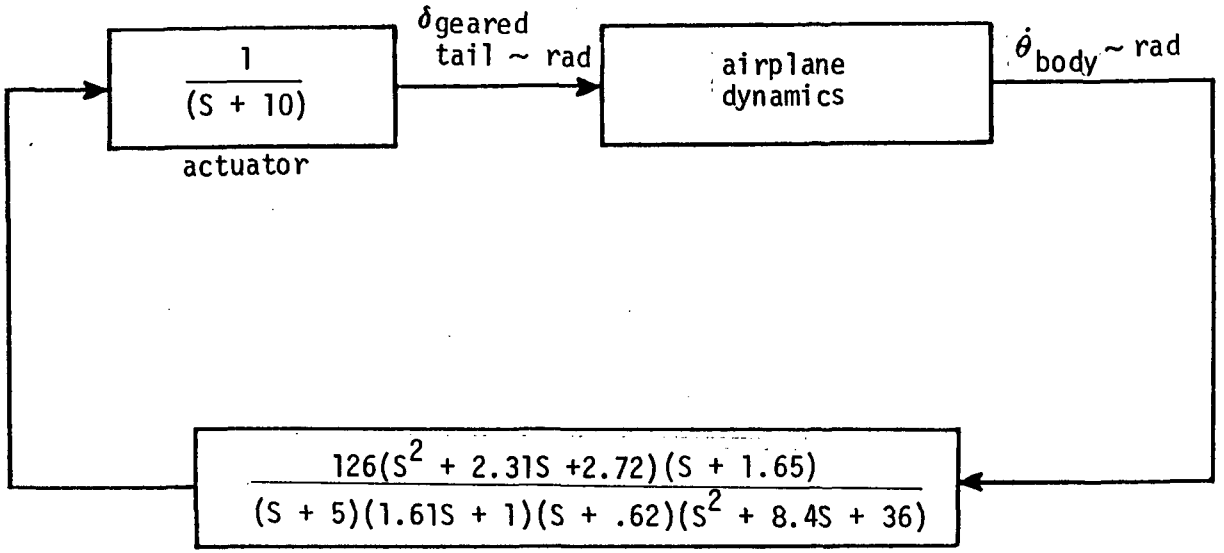

Figure 6-1: HSAS BLOCK DIAGRAM

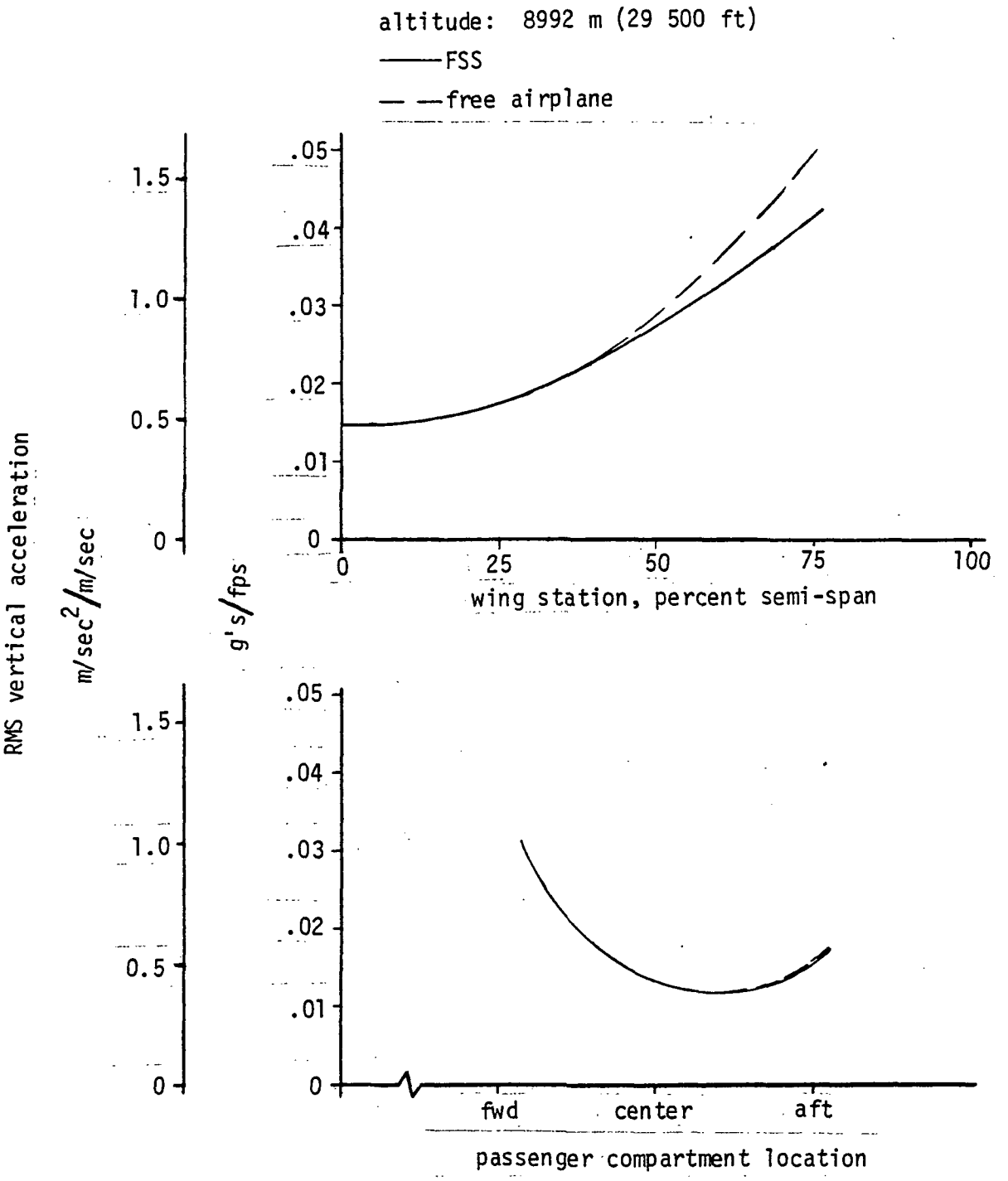

Figure 6-2: RIDE QUALITY AND REPEATED LOAD EVALUATION AT MACH 0.9 -V_C

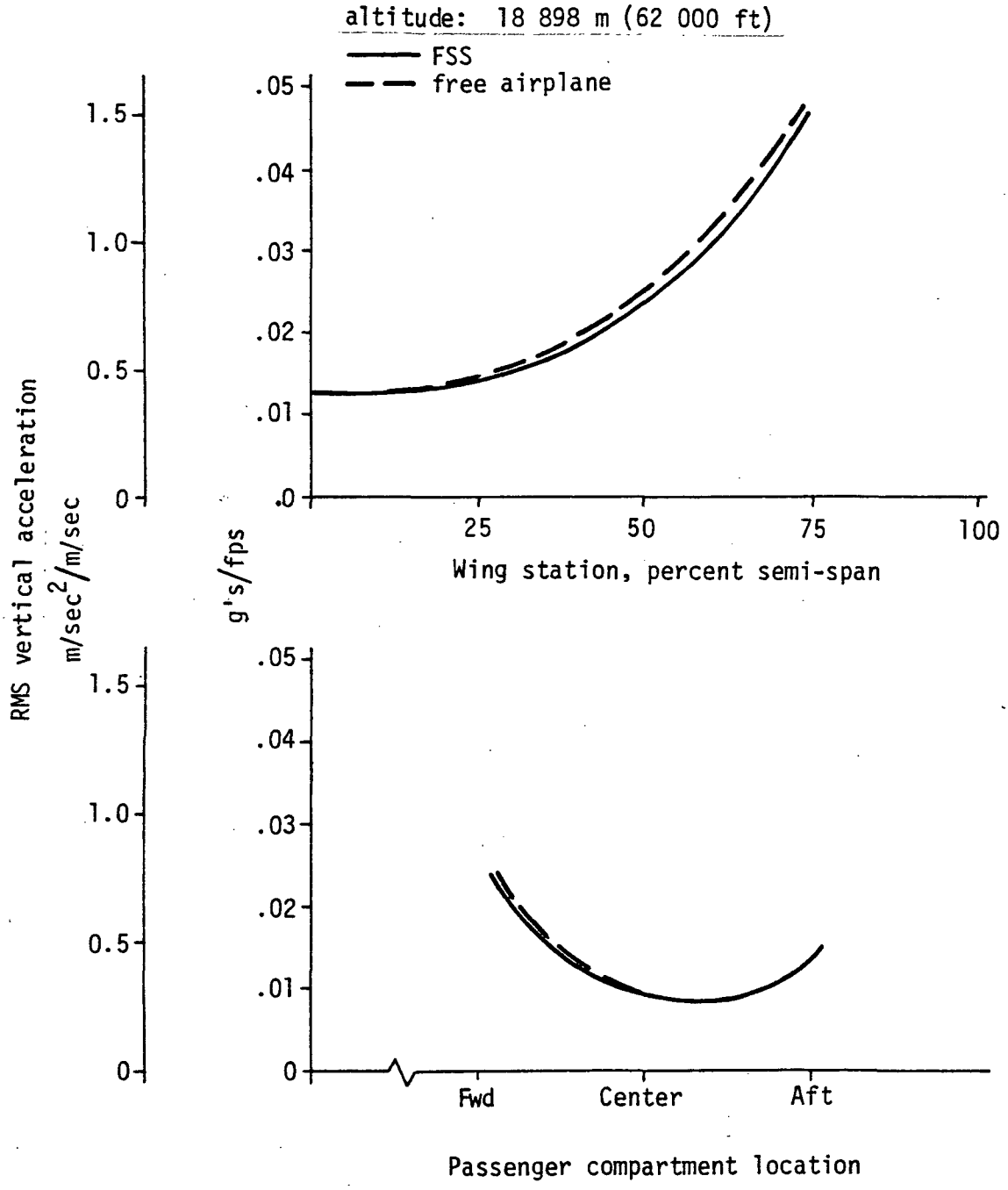

Figure 6-3: RIDE QUALITY AND REPEATED LOAD EVALUATION AT MACH 2.7 - V_C

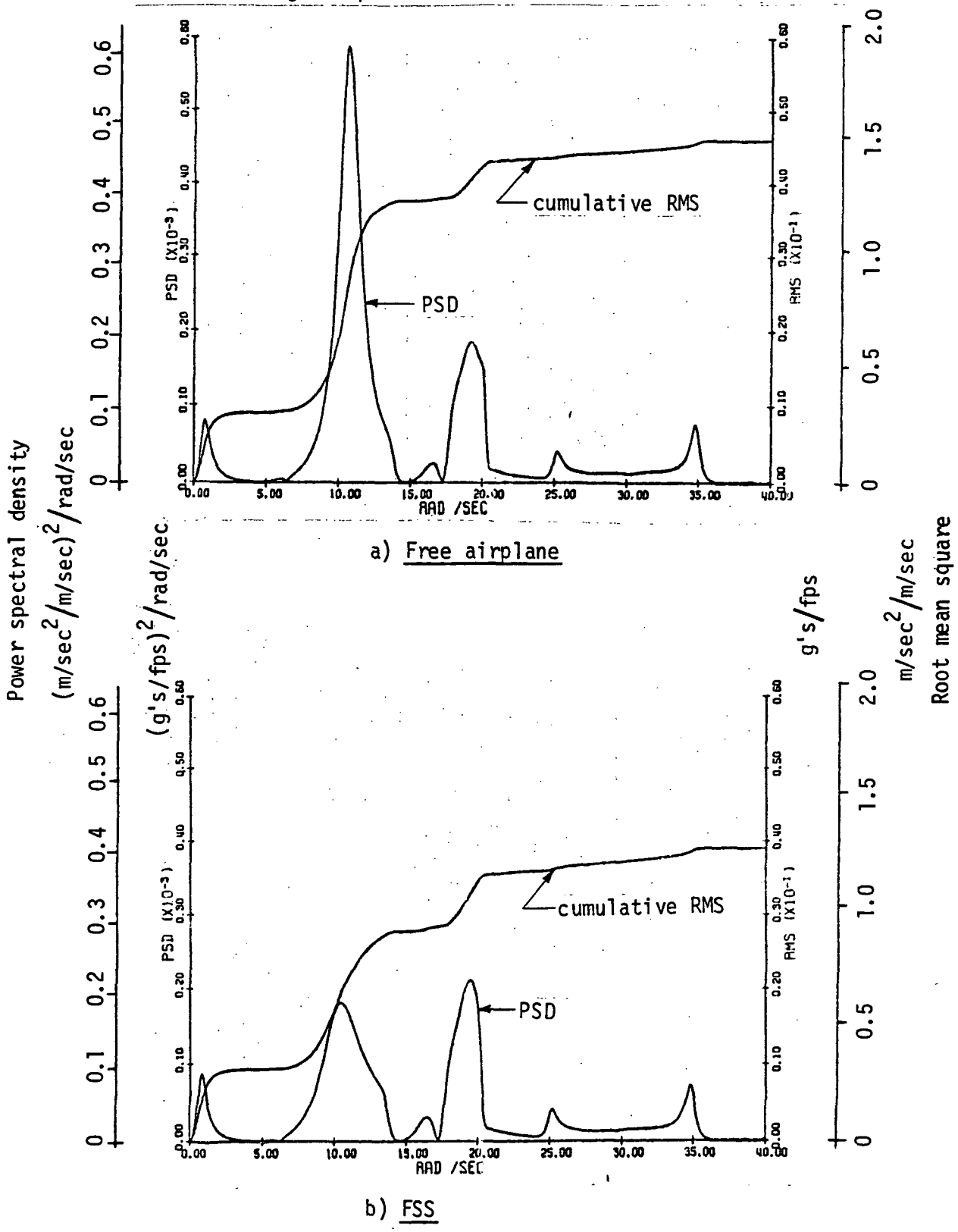

Figure 6-4: PSD-RMS RESPONSE OF OUTBOARD WING VERTICAL ACCELERATION

7.0 FSS MECHANIZATION REQUIREMENTS

FSS mechanization requirements were established to provide a system hardware definition on which to base cost and weight estimates.

The mechanization requirements were based on the assumption that the FSS surface would be dedicated to flutter suppression. The trailing edge surface area identified as the prime location for flutter suppression was allocated to a flaperon in the previous study defining the baseline airplane with a bank of spoilers in front of the FSS surface location. Results of the previous study indicated that some lateral control could be made available; therefore, it was assumed without further analysis to redefine a lateral control concept that a compatible mechanization of the FSS control surfaces could be achieved.

7.1 Actuation Mechanization

Figure 7-1 illustrates the procedure used to establish actuation mechanization requirements, starting with the control law defined during FSS synthesis and culminating with surface and actuator sizes and hydraulic flow requirements.

RMS displacements of the FSS surface size included in the synthesis mathematical model at the various evaluation flight conditions are shown in Table 7-1. PSD and cumulative RMS plots of surface displacement and rate at the Mach 0.9 V_D condition where the surface exhibits its largest activity are shown in Figure 7-2. Linear requirements for the 1.26 m^2 (13.6 ft^2) control surface included in the synthesis model were 0.19 rad (10.8 deg) and 2.27 rad/sec (130 deg/sec) RMS for the 4.27 m/sec (14 ft/sec) RMS design gust at the Mach 0.9 V_D condition. FSS control surface position and rate limits of 0.33 rad (19 deg) and 2.09 rad/sec (120 deg/sec), respectively, were selected as typical for active flutter control, and within the state of the art. Consequently, the requirement for a larger control surface was indicated in order to reduce required displacement and rate. Past experiences with simulations of flutter suppression systems have indicated that some degree of displacement and rate saturation can be tolerated. For this application, saturation was permitted that would allow the system to maintain 1.5 percent critical damping on the flutter mode at the design gust level. To define the required surface size, a describing function analysis of displacement and rate saturation nonlinearities was conducted. Previous results from a describing function analysis performed in parallel with a hybrid simulation of a FSS for the B-52 CCV indicate that using a ratio of two for peak random response to RMS response in the describing function analysis produces reasonable results which were comparable to that obtained from the hybrid simulation. These past studies have indicated that

TABLE 7-I

SUMMARY OF CONTROL SURFACE RMS DISPLACEMENT

Flight Condition	RMS Displacement	
	rad/m/s	deg/ft/sec
V_c - Mach 0.9 8992 m(29 500 ft)	.0149	.261
V_D - Mach 0.9 6462 m(21 200 ft)	.0441	.770
V_c - Mach 1.2 12 649 m (41 500 ft)	.0045	.078
V_d - Mach 1.2 10 363 m(34 000 ft)	.0116	.202
V_c - Mach 2.7 18 898 m(62 000 ft)	.0027	.048
V_D - Mach 2.7 16 459 m(54 000 ft)	.0077	.135

saturations on peaks greater than two sigma are of such short duration to have no effect on flutter characteristics.

The describing function of displacement saturation appears as a reduction in system gain for harmonic motion. Rate saturation which can be represented as a displacement limit in the forward loop of a first order representation of the actuator appears as a reduction in break frequency of the first order model. Rate saturation produces both a system gain attenuation and phase shift.

Describing functions of displacement and rate limits were included in root locus analyses to predict flutter mode damping as a function of gust level and surface area. A plot of flutter mode damping at the design gust level as a function of control surface area with the displacement and rate limit describing functions is shown in Figure 7-3. Required surface area to maintain 1.5 percent critical damping is 1.35 m^2 (14.5 ft^2). Reduced phase margin lag resulting from saturation at the design gust level is shown in Figure 7-4. Phase margin lag with the system at maximum saturation is 0.56 rad (32 deg) compared to 0.91 rad (52 deg) for the unsaturated system.

Actuation size was determined from surface deflection requirements and hinge moment at the Mach 0.9 V_D design condition. A triple tandem actuator similar to that described in Reference 4 was selected to satisfy the fail-operational requirement and to be compatible with the general SCAR requirement that control surface buzz/flutter not occur following two hydraulic system failures. The actuator was sized assuming that full hinge moment capability was required with one hydraulic system out. A piston area of 9.2×10^{-4} m^2 (1.43 in^2) and a stroke of 0.0676 m (2.66 in) was required assuming a 0.1016 m (4.0 in) actuator moment arm.

Hydraulic flow rate was based on the average surface rate for maximum gust intensity at the Mach 0.9 V_D design condition. Average surface rate at the design condition was 1.62 rad/sec (93 deg/sec), yielding an average hydraulic flow rate requirement of $3.05 \times 10^{-4} m^3$/sec (4.84 gpm) per hydraulic system.

The SCAR airplane proposed hydraulic system utilizes four independent hydraulic power systems. Each hydraulic system has two 0.0082 m^3/sec (130 gpm) engine driven pumps. A typical hydraulic system load analysis flight profile is shown in Figure 7-5. As indicated in Figure 7-5, the landing "flare" maneuver in severe turbulence sizes the hydraulic systems.

For flutter suppression application, the most adverse condition is the side gust recovery plus tail gust during descent. Figure 7-6 compares the required FSS flow to the available flow of each of the four hydraulic systems at the Mach 0.9 V_D condition. As shown by this comparison, the

demands of the FSS on the hydraulic system are well below the surplus capacity available; consequently, no hydraulic system capacity increase is required due to addition of the FSS. Since the FSS required flow is minimal compared to total hydraulic flow, hydraulic cooling capability is assumed to be adequate also without adding an incremental capacity for FSS operation.

7.2 Electronics and Sensor Mechanization

Redundancy for a single fail operate capability dictated triple redundant accelerometer units. Three accelerometer units are required, one in each wing and one in the aft fuselage. These units are assumed to be conventional linear force balanced accelerometers with analog single fail operate capability in use in existing aircraft.

Digital computation of the FSS control law was assumed with the capability to incorporate the control law computation, parameter scheduling and redundancy management into the existing digital electrical flight control system. A simplified diagram showing the mechanization redundancy of the FSS electronics and sensors is shown in Figure 7-7.

7.3 FSS Weight Estimates

The weights of system elements shown in Table 7-II were estimated based on mechanization definitions. Total weight penalty for FSS mechanization was estimated to be 159.2 kg (351 lb).

TABLE 7-11

FSS WEIGHT ESTIMATE SUMMARY

	Weight kg (lbm)	
	Component	Total
Actuator system		
Actuators	45.4 (100)	
Hydraulic plumbing increment	11.3 (25)	
Surface weight increment	29.5 (65)	
Total actuation system		86.2 (190)
Electronics and sensors		
Accelerometer units and mounts (three units)	16.3 (36)	
Electronic unit increment	11.3 (25)	
Wire bundles, breakers, etc.	45.4 (100)	
Total electronics and sensors		73.0 (161)
Total System		159.2 (351)

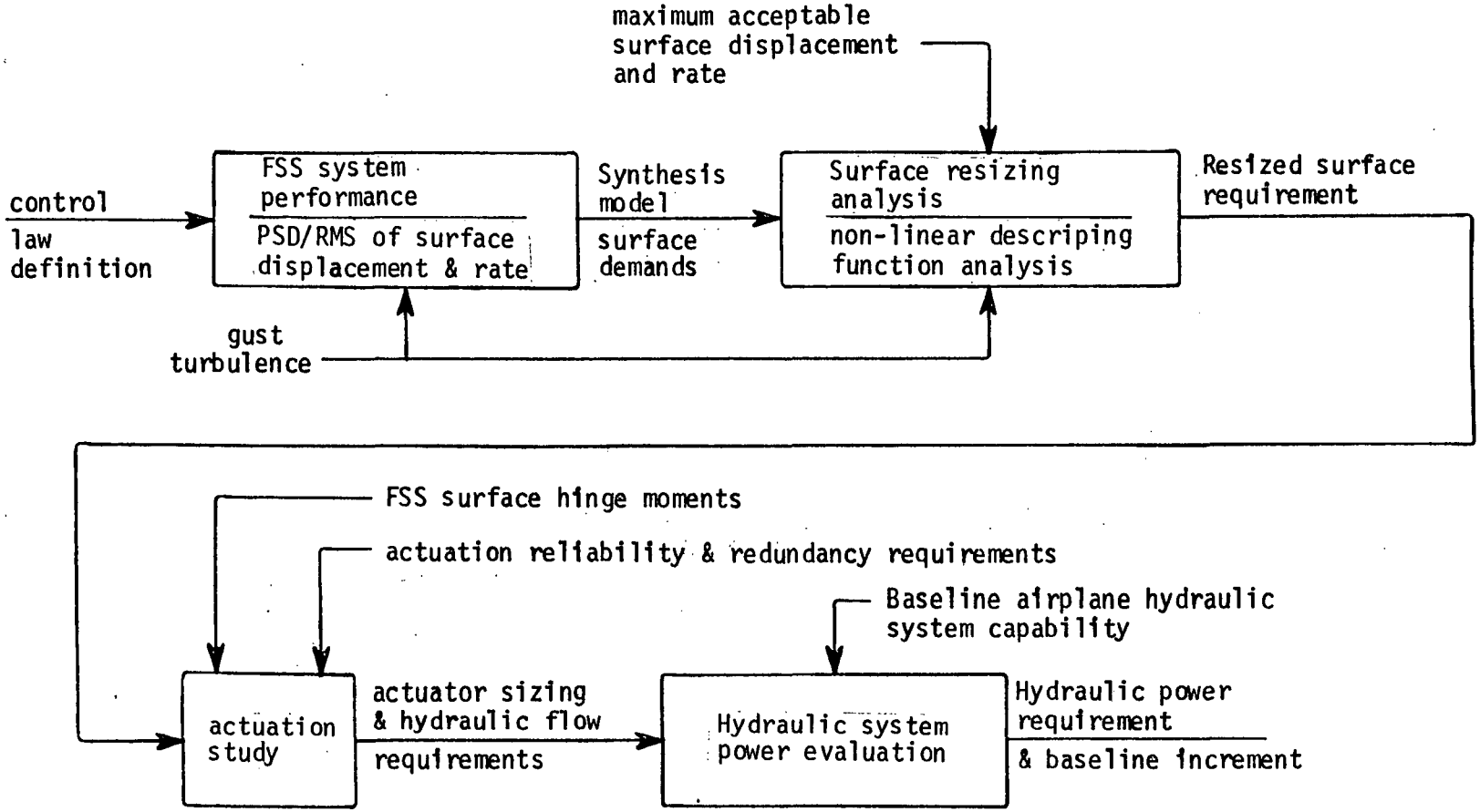

Figure 7-1: CONTROL SURFACE, ACTUATION AND HYDRAULIC SYSTEM MECHANIZATION REQUIREMENTS APPROACH

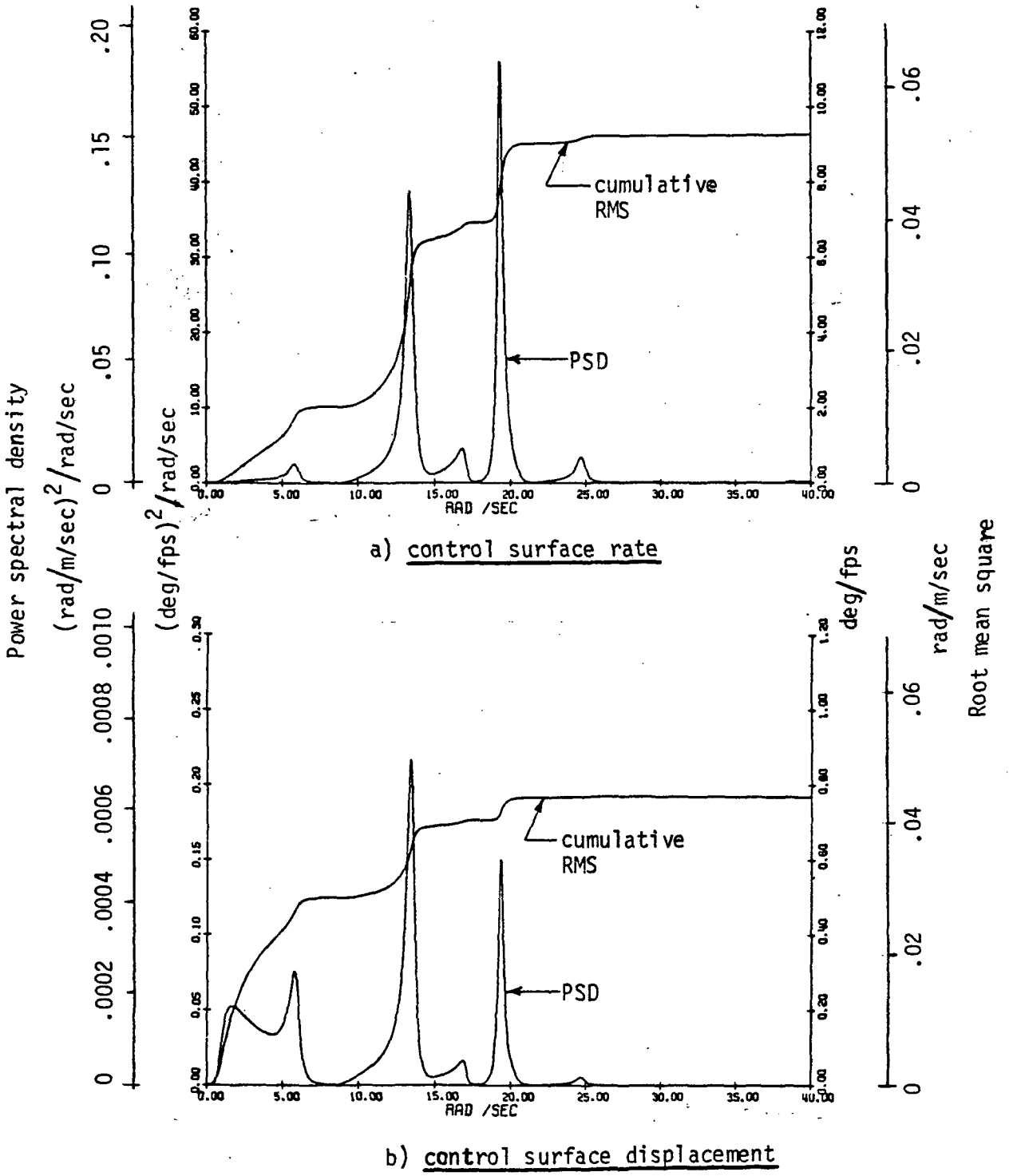

Figure 7-2: PSD-RMS CONTROL SURFACE DISPLACEMENT & RATE FOR V_D - MACH 0.9

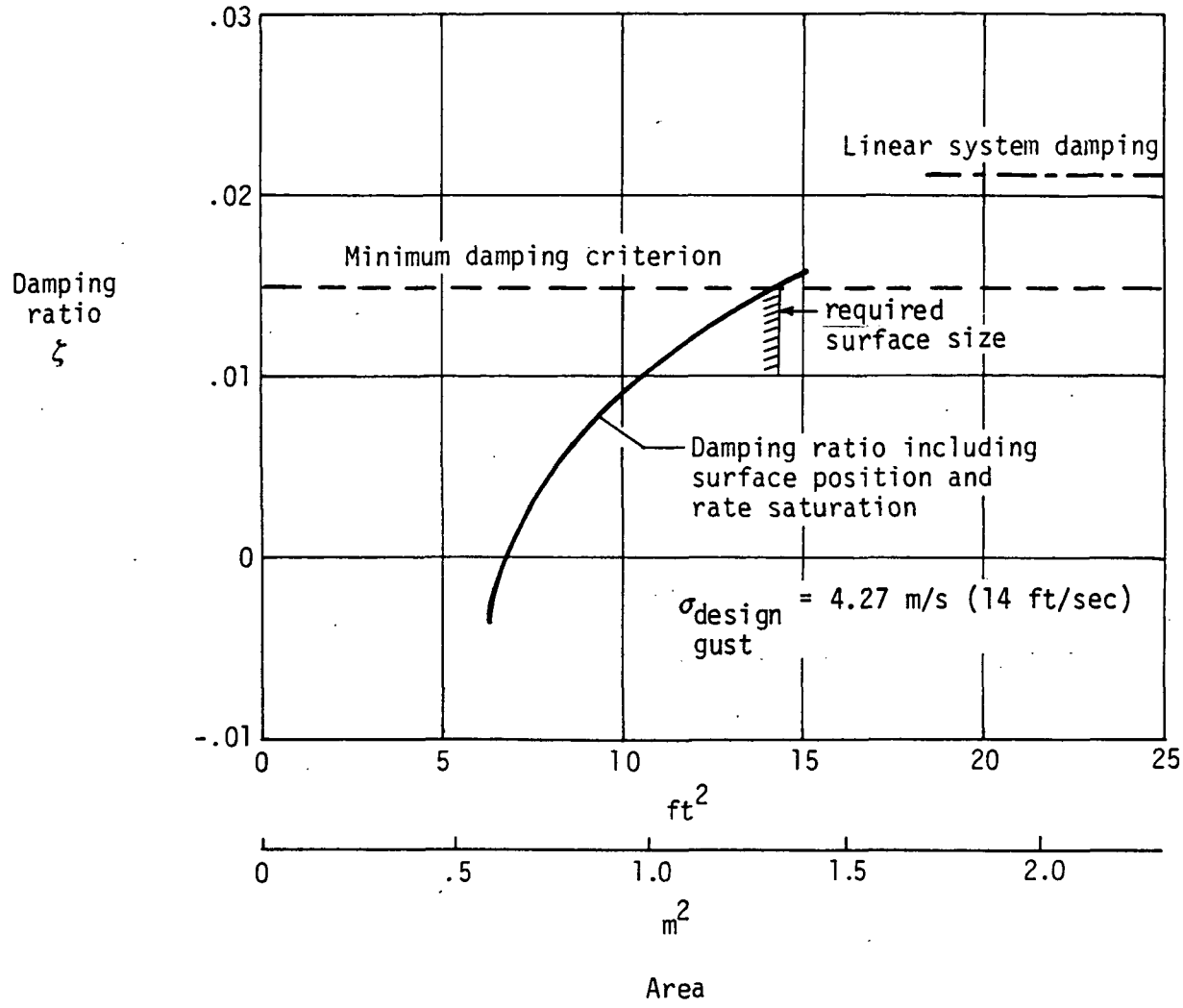

Figure 7-3: EFFECT OF SURFACE AREA ON FLUTTER MODE DAMPING IN DESIGN RANDOM TURBULENCE

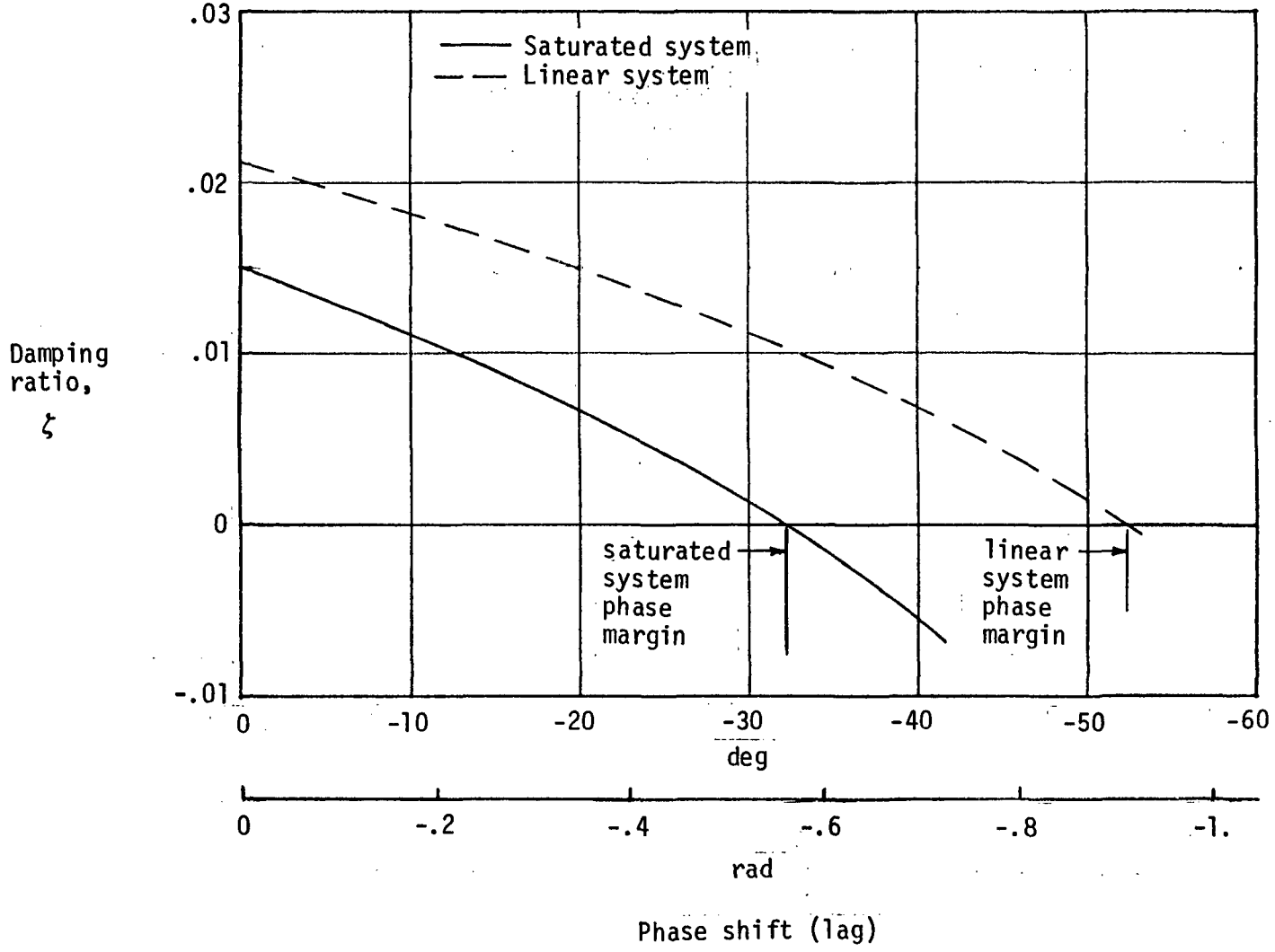

Figure 7-4: FLUTTER MODE DAMPING RATIO OF SATURATED SYSTEM WITH PHASE LAG

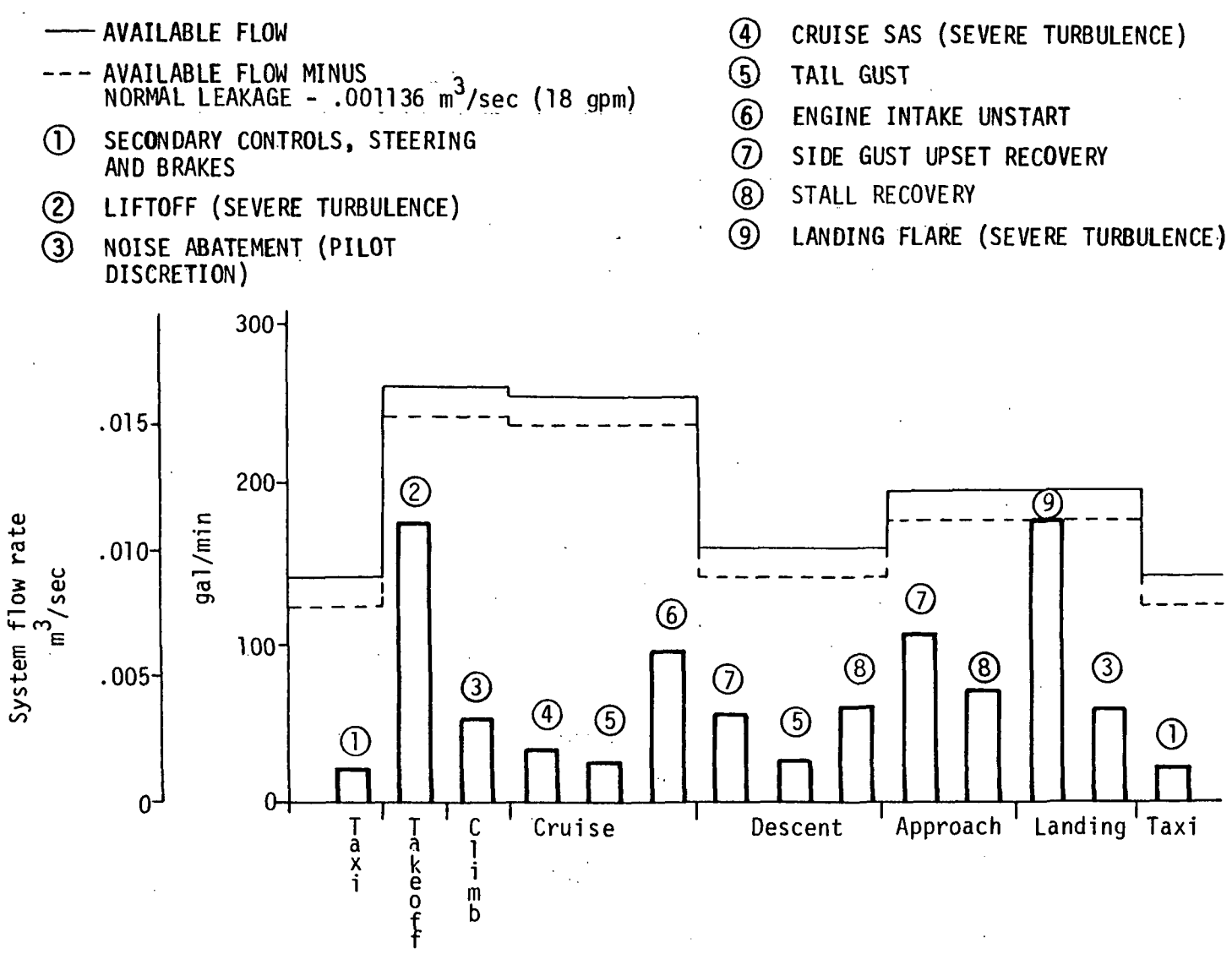

Figure 7-5: TYPICAL HYDRAULIC SYSTEM LOAD/FLIGHT PROFILE

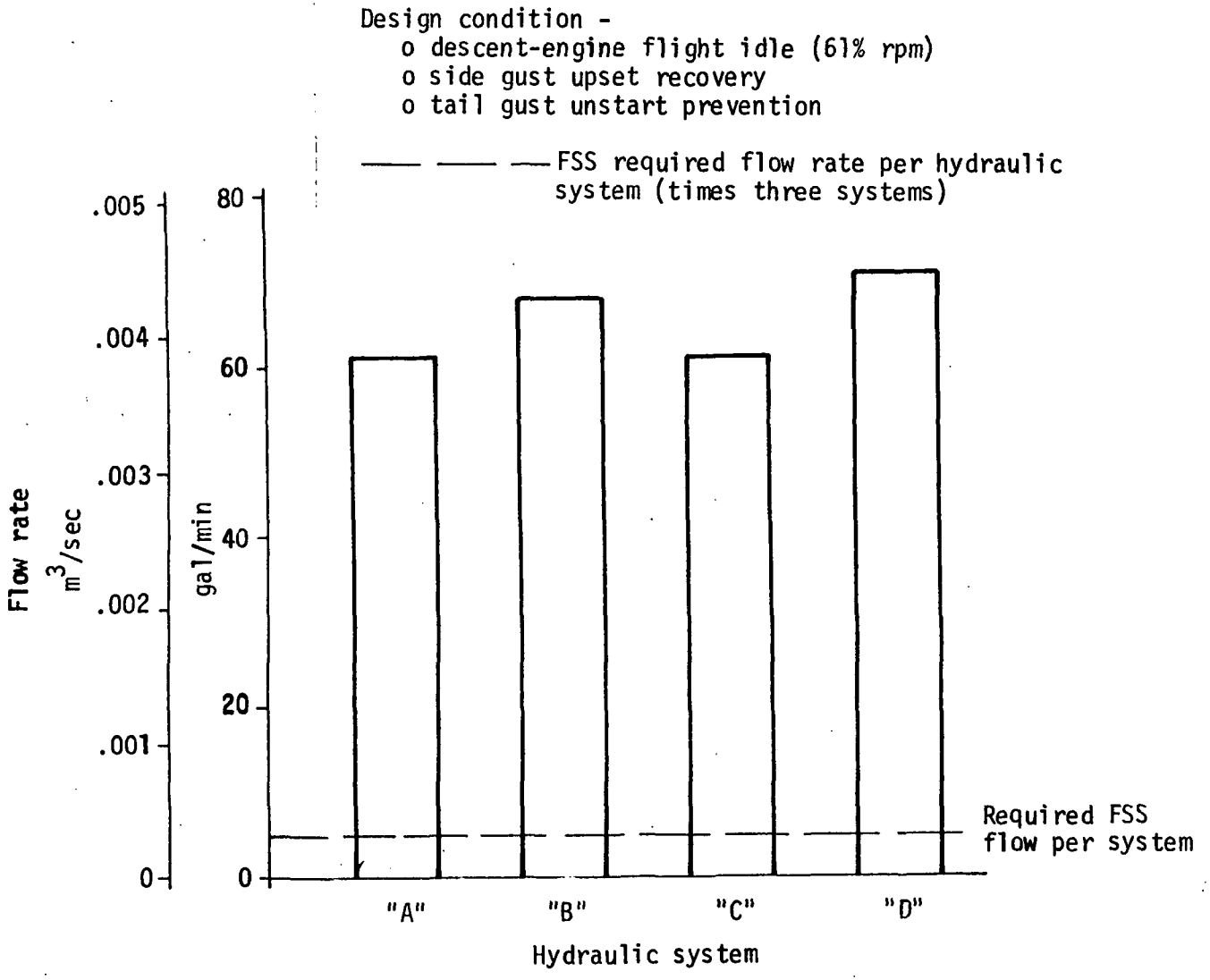

Figure 7-6: HYDRAULIC FLOW REQUIREMENT COMPARISON TO AVAILABLE SURPLUS FLOW

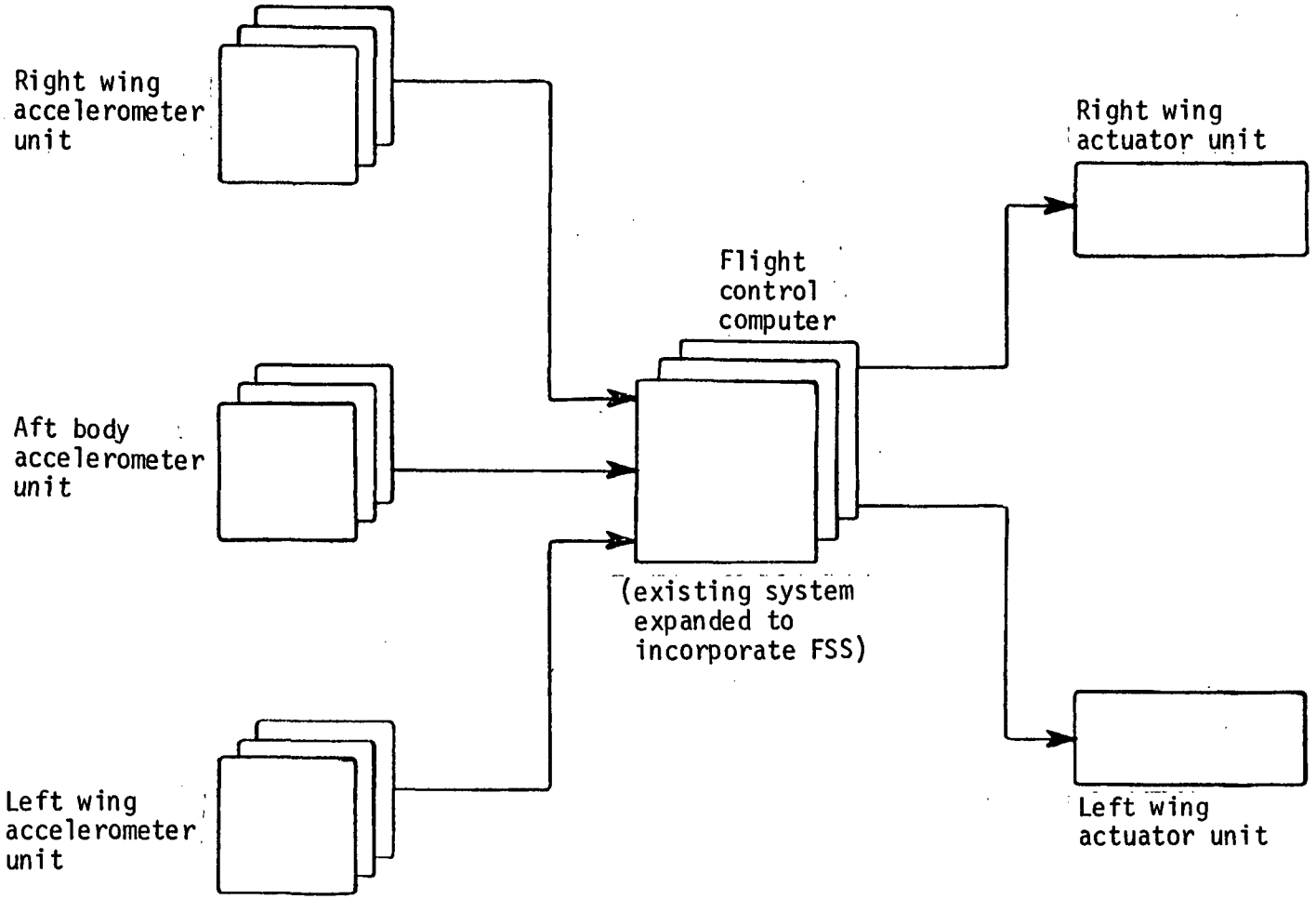

Figure 7-7: ELECTRONIC AND SENSORS MECHANIZATION DIAGRAM

8.0 COMPARISON OF PERFORMANCE AND COST BETWEEN FSS AND PASSIVE FLUTTER CONFIGURATIONS

8.1 Performance Comparison

The weight required to increase the flutter speed of the baseline airplane from V_D to 1.2 V_D by structural modification is 4309 Kg (9500 lb), as determined in the previous NASA study under Contract NAS1-12287. The weight required to increase the flutter speed from V_D to 1.2 V_D by adding a FSS to the baseline airplane is 159 Kg (350 lb). The weight savings realized by using the FSS is 4150 Kg (9150 lb), which is approximately 2.6 percent of the OEW of the baseline airplane.

The advantage of this weight saving, in terms of performance, can be either in increased range or increased payload. The impact on cost is discussed in Paragraph 8.2. If the FSS and passive configurations carry equal payloads, and the FSS weight savings is absorbed as additional fuel, the FSS configuration will have 344 Km (186 n. mi) greater maximum range. For a given range, the FSS configuration can carry 4150 Kg (9150 lb) greater payload with the same amount of fuel. Of course, combinations of increased range and increased payload between these two extremes are available with the FSS configuration. For equal payloads and range, the FSS configuration requires less fuel because of the lighter structure, resulting in lower fuel costs, as discussed in the following paragraphs.

8.2 Cost Comparison

The introduction of active control system components in place of structural material in the design of a transport airplane affects the original cost, maintenance, and operating cost of the airplane as well as the empty weight. A study was conducted to compare the direct operating costs (DOC) between the passive and active flutter configuration airplanes, in order to provide visibility of these factors. This is the ultimate purpose of the program, and all of the tasks previously described are for the purpose of generating inputs that will provide reasonable performance and cost comparisons.

8.2.1 Method of cost analysis. - The difference in DOC between the two airplane configurations was determined using the Air Transport Association (ATA) standard method of estimating comparative DOC of turbine powered transport airplanes, which is discussed in Reference 2. The method involves an equation for calculating DOC, with equation coefficients developed to reflect the costs of the

TABLE 8-I

AIRPLANE CHARACTERISTICS FOR ECONOMIC ANALYSIS

AIRPLANE CHARACTERISTIC	AIRPLANE CONFIGURATION	
	Passive	FSS
Cruise Mach Number	2.7	---- (Same)
Number of Crew Members	3	----
Number of first class seats	0	----
Number of tourist seats	234	----
Number of engines	4	----
Thrust per engine - SLST, N (lb)	235 756 (53 000)	
Maximum take-off Gross Mass, Kg (lb)	339 287 (748 000)	
Total Operating Empty Mass, Kg (lb)	162 509 (358 270)	158 358 (349 120)
Structure Mass, Including Nacelles, Kg (lb)	101 804 (224 440)	97 495 (214 940)
Total Propulsion Systems Mass, Kg (lb)	25 739 (56 740)	----
Total System & Equipment Mass, Kg (lb)	27 728 (61 130)	27 887 (61 480)
Payload Mass, Kg (lb)	22 183 (48 906)	----
Block Time	Reference	----
Block Fuel	Reference	$*\Delta$ = -2.1%**
Price per Engine 1976 dollars	Reference	----
Total Airplane Price 1976 dollars	Reference	$*\Delta$ = -2.4%

$$* \Delta = \frac{\text{Passive - FSS}}{\text{Passive}}$$

**Calculated for a range of 5555 km (3000 n. mi.)

crew, fuel and oil, insurance, maintenance, and depreciation. The objective of the ATA equation is to provide a means for comparing the operating economics of competitive airplanes under a standard set of conditions. Coefficients developed to reflect costs typical for the year 1976 were used in this study.

Figure 8-1 illustrates the method of comparing DOC for this study. DOC for the passive flutter configuration was calculated wholly by the ATA formula. Procurement and maintenance costs of the FSS were estimated separately by comparison with contemporary systems of similar complexity.

The only difference between the two airplanes is the type of flutter improvement. Table 8-I lists the major airplane characteristics used in the DOC calculations. The maximum take-off gross weight and payload are kept constant between the two airplanes. The passive flutter correction required 4309 Kg (9500 lb) of additional structure, so that the passive configuration structure is heavier than the FSS configuration by that amount. The FSS component mass, described in Section 7, is 159 Kg (350 lb), making the equipment and systems mass of the FSS airplane greater than for the FSS airplane by the difference betwen the masses cited above; i.e., 4150 Kg (9150 lb).

8.2.2 Cost analysis results. - The lighter structure of the FSS airplane resulted in a net decrease in price of 2.4 percent from the passive airplane, and a decrease in block fuel; e.g., 2.1 percent at a range of 5555 Km (3000 n. mi).

Figure 8-2 shows a comparison of total DOC as of function of trip distance. DOC with the FSS is less than for the passive flutter correction for all distances shown, ranging from 1.95 percent for 1852 Km (1000 n. mi.) to 1.73 percent for 7407 Km (4000 n. mi.). Figure 8-3 graphically recapitulates the savings of the FSS configuration in operating weight, price, block fuel, and DOC. Block fuel and DOC savings shown in Figure 8-3 are calculated for a trip distance of 5555 Km (3000 n. mi.), and a fuel price of 10.83 /liter (41¢/gallon).

The effect of fuel price on Δ DOC is shown in Figure 8-4. Increasing the fuel price from 10.83¢/liter (41¢/gallon) to 15.85¢/liter (60¢/gallon) increases the DOC savings of the FSS by 31.6 percent. The DOC of the FSS airplane would then be 2.33 percent (1.77 x 1.316) less than the passive airplane for a trip distance of 5555 Km (3000 n. mi.). This figure also shows the dominance of fuel costs in the difference between DOC's.

For this class of airplane, it was found that the difference in maintenance between the two configurations is an insignificant component of ΔDOC. It was estimated that the maintenance DOC for 4309 Kg (9500 lb) of extra structure in the passive flutter configuration offsets 75 percent of the maintenance DOC of the FSS. In fact, without this tradeoff in maintenance between added structure and added systems, the maintenance DOC of the active flutter system was only 0.67 percent of the airplane maintenance DOC excluding engine maintenance, and only 0.25 percent including engines.

Figure 8-5 shows component DOC in percent of total DOC for the passive flutter configuration, as a function of trip distance, with a fuel cost of 10.83¢/liter (41¢/gallon). Fuel is by far the greatest single item of DOC, reaching 58 percent of the total at a range of 7407 Km (4000 n. mi.) The various items contribute almost constant percentages of the total for trip distances above 3703 Km (2000 n. mi.), and do not change by great amounts for distances down to 1852 Km (1000 n. mi.) It is this dominance of the fuel cost in the total DOC that gives the lighter FSS configuration the advantage in DOC.

A summary comparison of DOC components is shown in Figure 8-6, in percent of total passive configuration DOC, for a given fuel price and trip distance. This shows a reduction of 1.77 percent from the total passive airplane DOC, most of which is realized from reduced fuel costs.

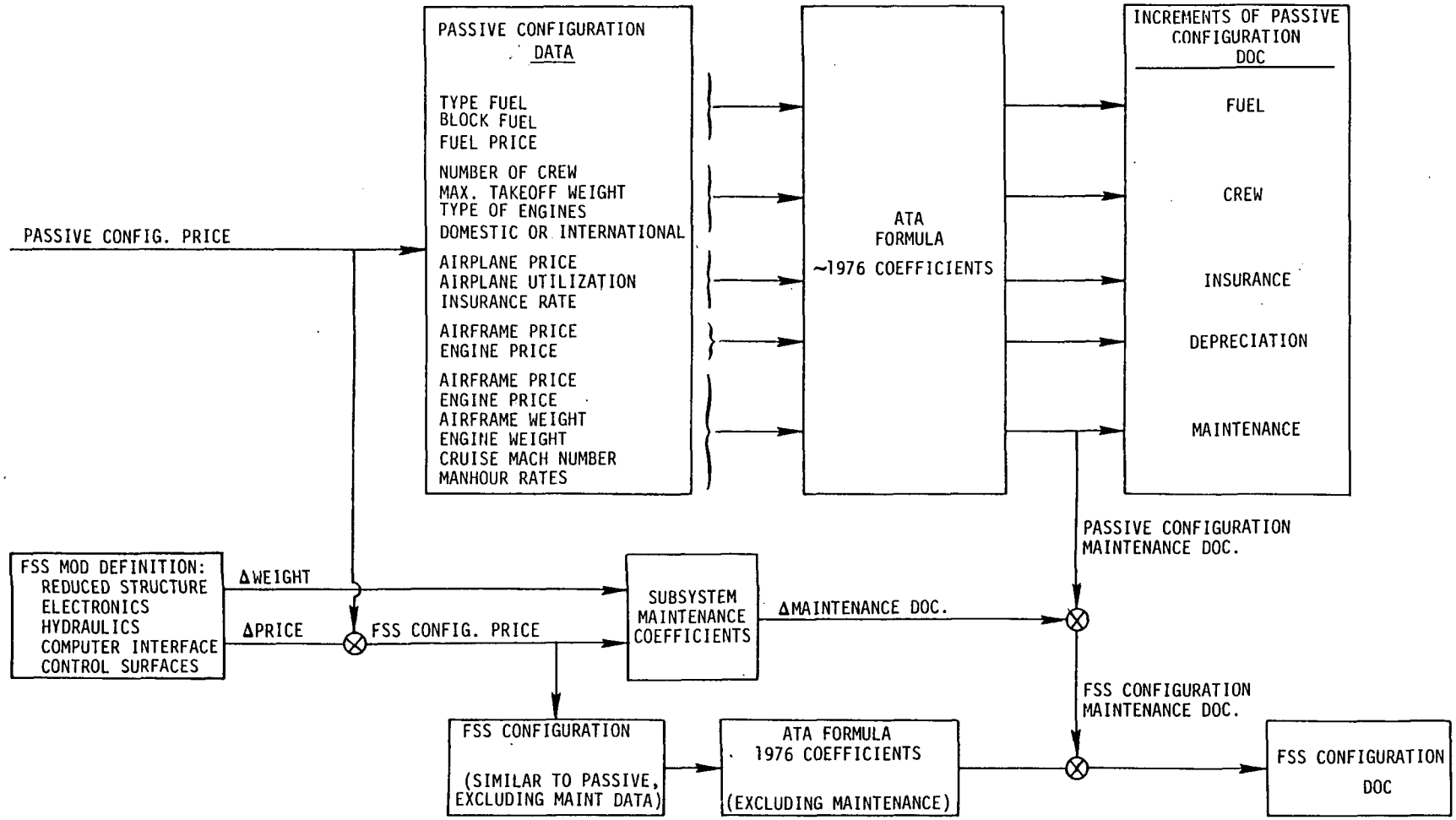

Figure 8-1: METHOD OF COMPARING DIRECT OPERATING COST

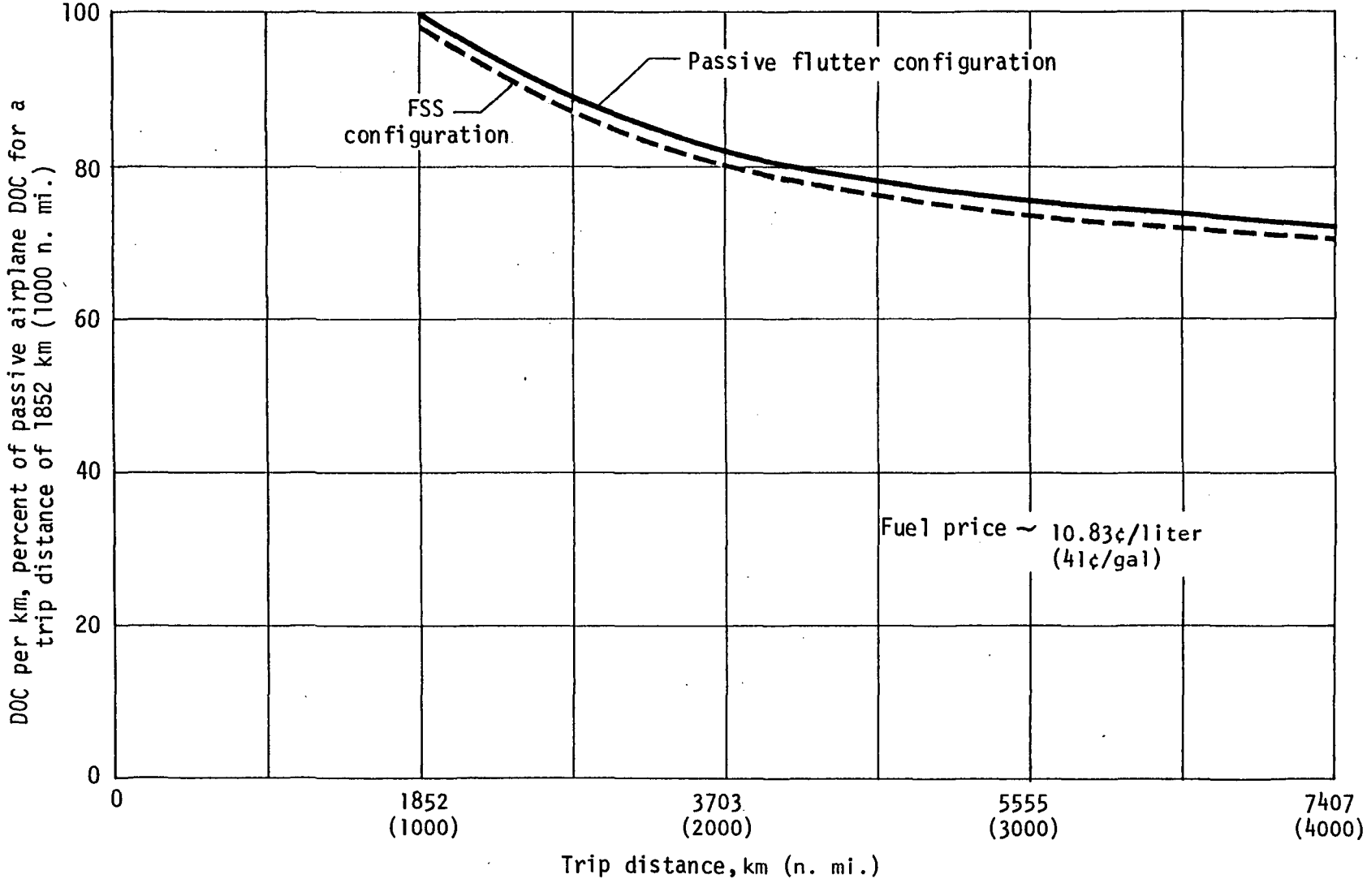

Figure 8-2: DIRECT OPERATING COST COMPARISON

- Trip distance = 5555 km (3000 n. mi.)
- Fuel price of 10.83¢/liter (41¢/gal)

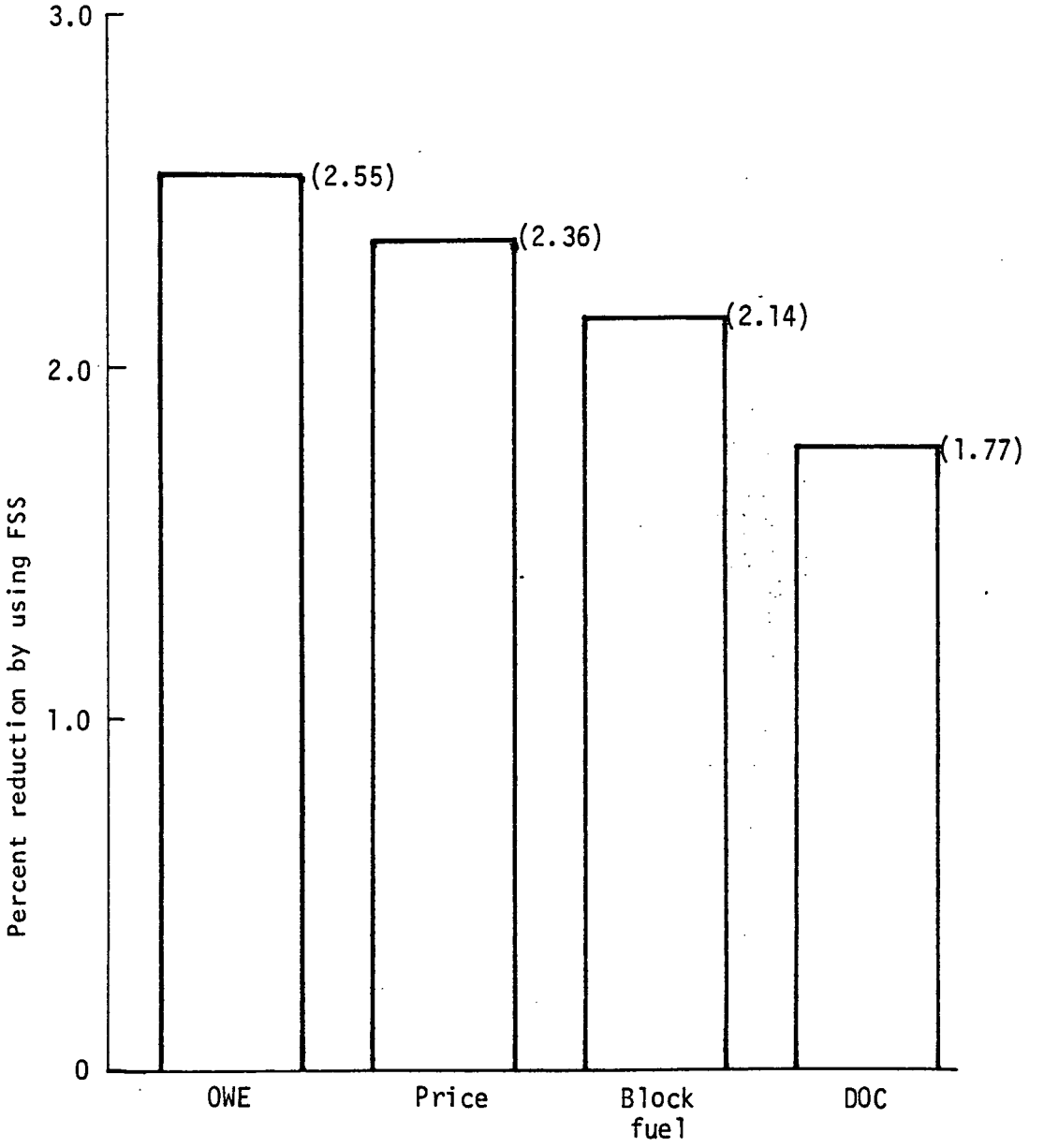

Figure 8-3: WEIGHT, PRICE, BLOCK FUEL AND DIRECT OPERATING COST COMPARISON

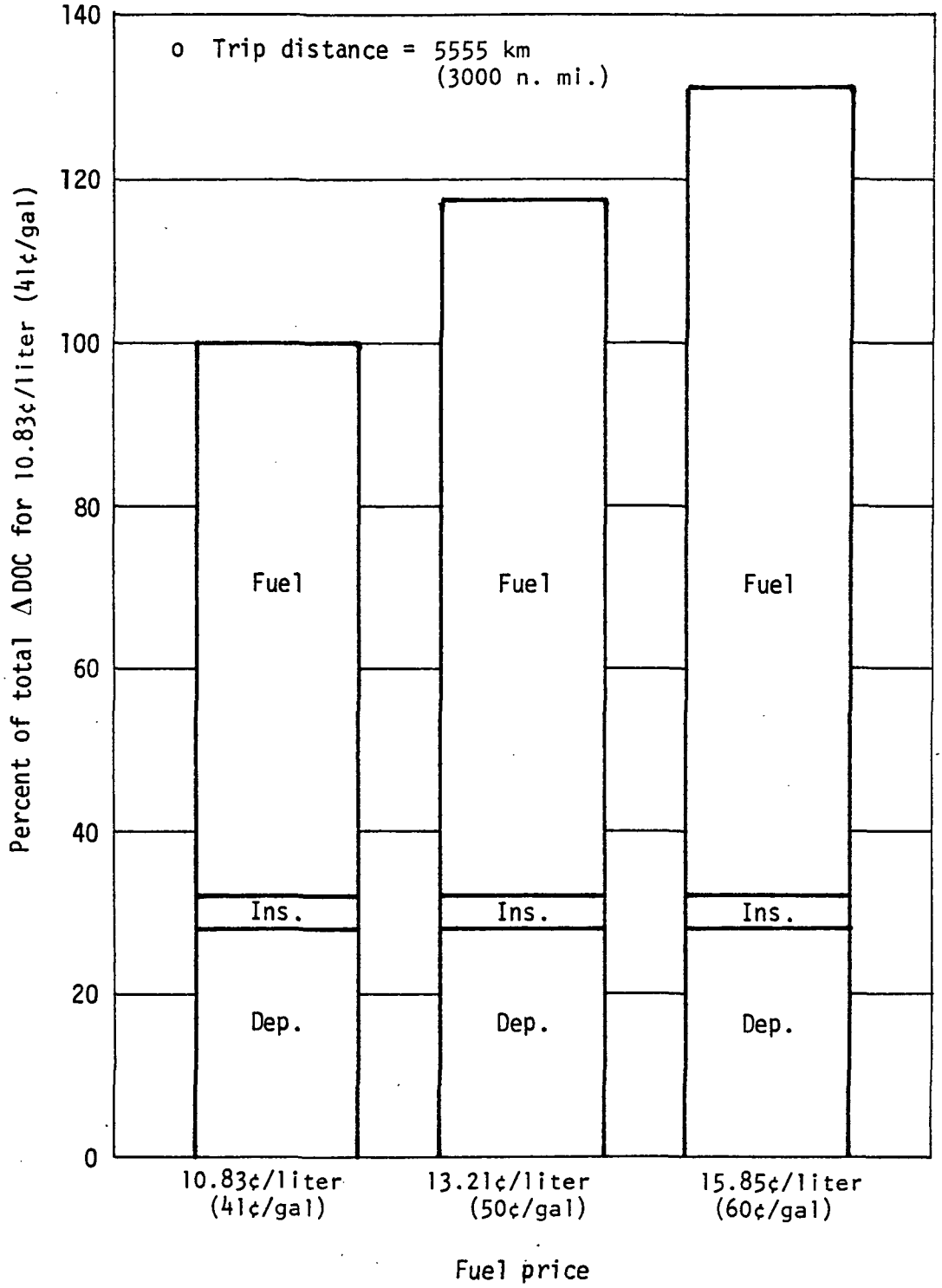

Figure 8-4: EFFECT OF FUEL PRICE ON Δ DOC

- Fuel price 10.83¢/liter (41¢/gal)
- Passive flutter configuration

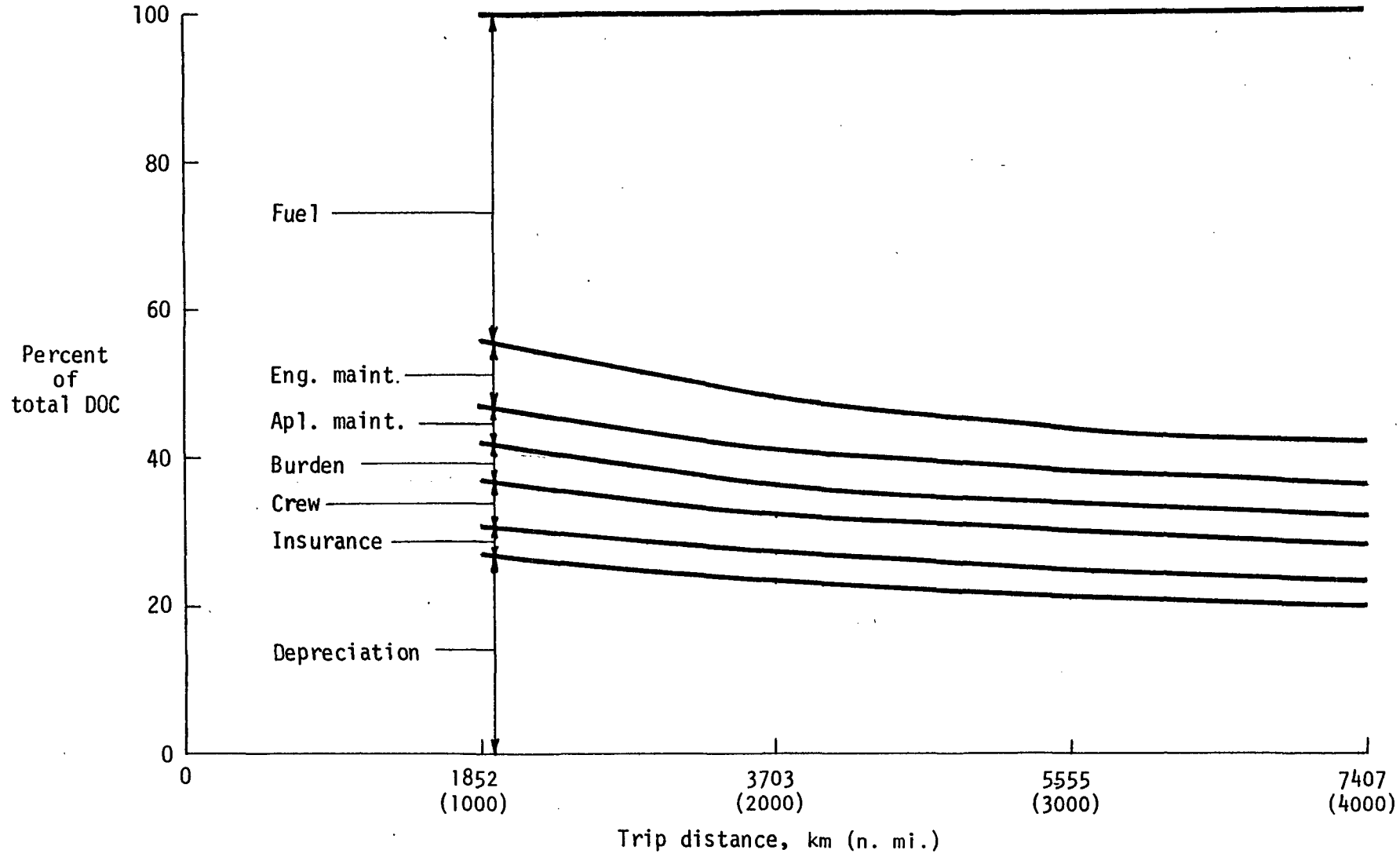

Figure 8-5: EFFECT OF TRIP DISTANCE ON DOC COMPONENTS

- o Trip distance 5555 km (3000 n. mi.)
- o Fuel price 10.83¢/liter (41¢/gal)

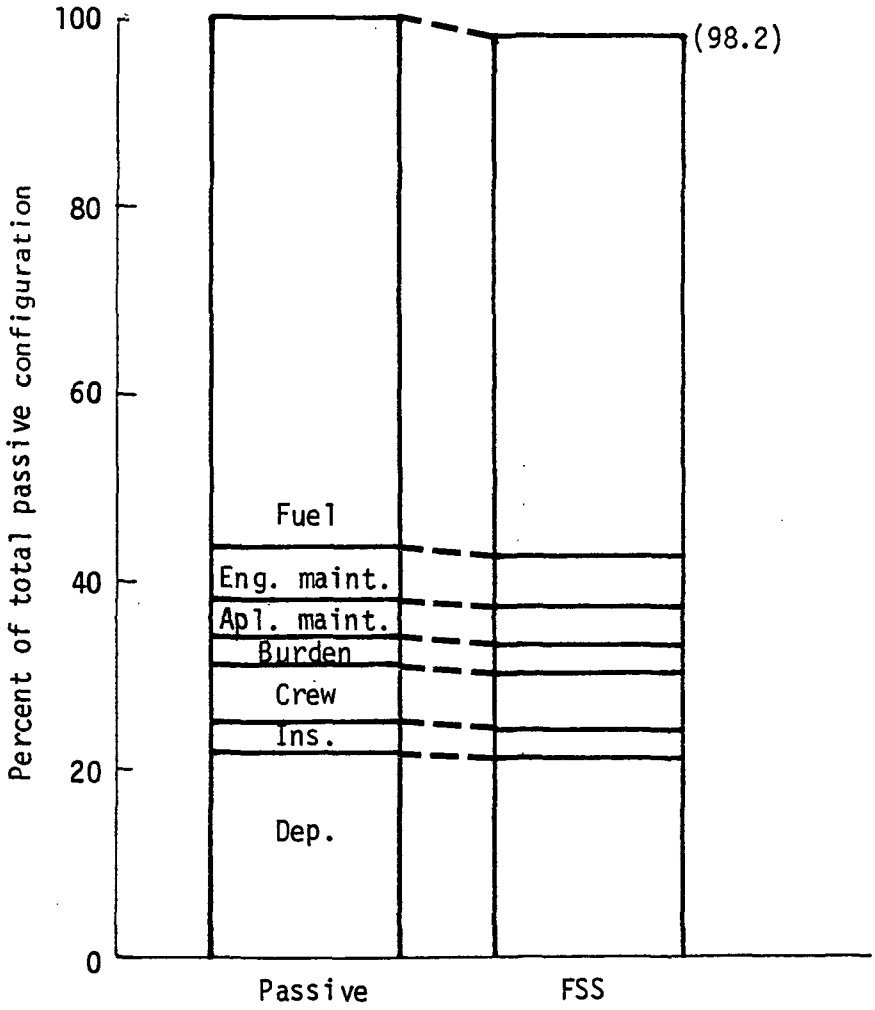

Figure 8-6: COMPARISON OF DIRECT OPERATING COST COMPONENTS

9.0 CONCLUSIONS AND RECOMMENDATIONS

9.1 Conclusions

The major conclusions produced from this study are listed below.

1. Application of active flutter mode control in the design of the SCAR configuration is predicted to offer substantial increases in payload or range, and savings in direct operating costs.

2. Conclusion #1 can be generalized to state that when the weight panelty for passive flutter correction on a large transport airplane is significant (it was approximately 4.5 percent in this case), active flutter control should be considered in the design.

3. The difference in maintenance between the passive and active flutter configurations is an insignificant part of the total ΔDOC.

4. The major saving in DOC from incorporation of a FSS is a result of reduced fuel consumption, given equal payload and range.

5. It is felt that, in general, as in this specific case, active flutter control will not increase the maximum hydraulic power requirement, since the maximum power is designed by requirements for a flight phase in which flutter suppression is not needed.

9.2 Recommendations

The following recommendations are proposed based on the positive results of this study.

1. Design requirements for application of a flutter suppression system should be fully defined to satisfy the requirements for reliability, safety and certification of a commercial transport airplane.

2. Follow-on studies should be conducted to determine potential weight, performance, and cost benefits of other active control technology (ACT) concepts, combined ACT concepts, and ultimately, of a supersonic cruise airplane with fly-by-wire controls fully equipped with ACT concepts.

10.0 REFERENCES

1. Turner, M. J. and Grande, D. L., "Study of Structural Design Concepts for an Arrow Wing Supersonic Transport Configuration," Boeing Document D6-42438-3, February 1976

2. "Standard Method of Estimating Comparative Direct Operating Cost of Turbine Powered Transport Airplanes," Air Transport Association, 1967

3. "Stability and Control, Flight Control, and Hydraulic System Design Criteria, SST," Boeing Document D6-6800-5, August 1970

4. Wiggins, D. A. "Hydraulic Controls for Active Flutter Suppression and Load Alleviation," AGARD Conference Proceedings No. 175, 1975.

APPENDIX A

STRUCTURAL AND AERODYNAMIC REPRESENTATION

OF THE SCAR ARROW-WING CONFIGURATION

This appendix contains graphical representation of 18 symmetric vibration modes and the aerodynamic panel representation of the SCAR arrow-wing configuration.

The structural vibration modes used in the generalized equations of motion are shown in Figures A-1 through A-18. Each of the elastic modes is shown in front, side and top views of the right side of the airplane. The modes are symmetric with respect to the airplane centerline. Each line plotted represents the motion of a streamwise set of points on a surface (wing or wing fin). The single point that appears to the right in each view represents the horizontal stabilizer which was assumed to be rigid for these analyses. For ease of determining structural motion the point representing the horizontal stabilizer has been plotted as if it were at the same waterline as the wing. The displacements shown in the model plots represent only those perpendicular to the surface. Therefore, the wing fin (three horizontal lines) does not show any vertical displacement in the front and side views.

The aerodynamic panels used to represent the primary surfaces and the control surfaces in the three-dimensional plate doublet finite element solution for aerodynamic forces are shown in Figure A-19. The control surfaces defined for possible use in the FSS are shown by the four shaded areas on the right wing. Generalized motion of the panels shown were used to generate unsteady aerodynamic force coefficients for the airplane.

Freq. = 0.98 Hz

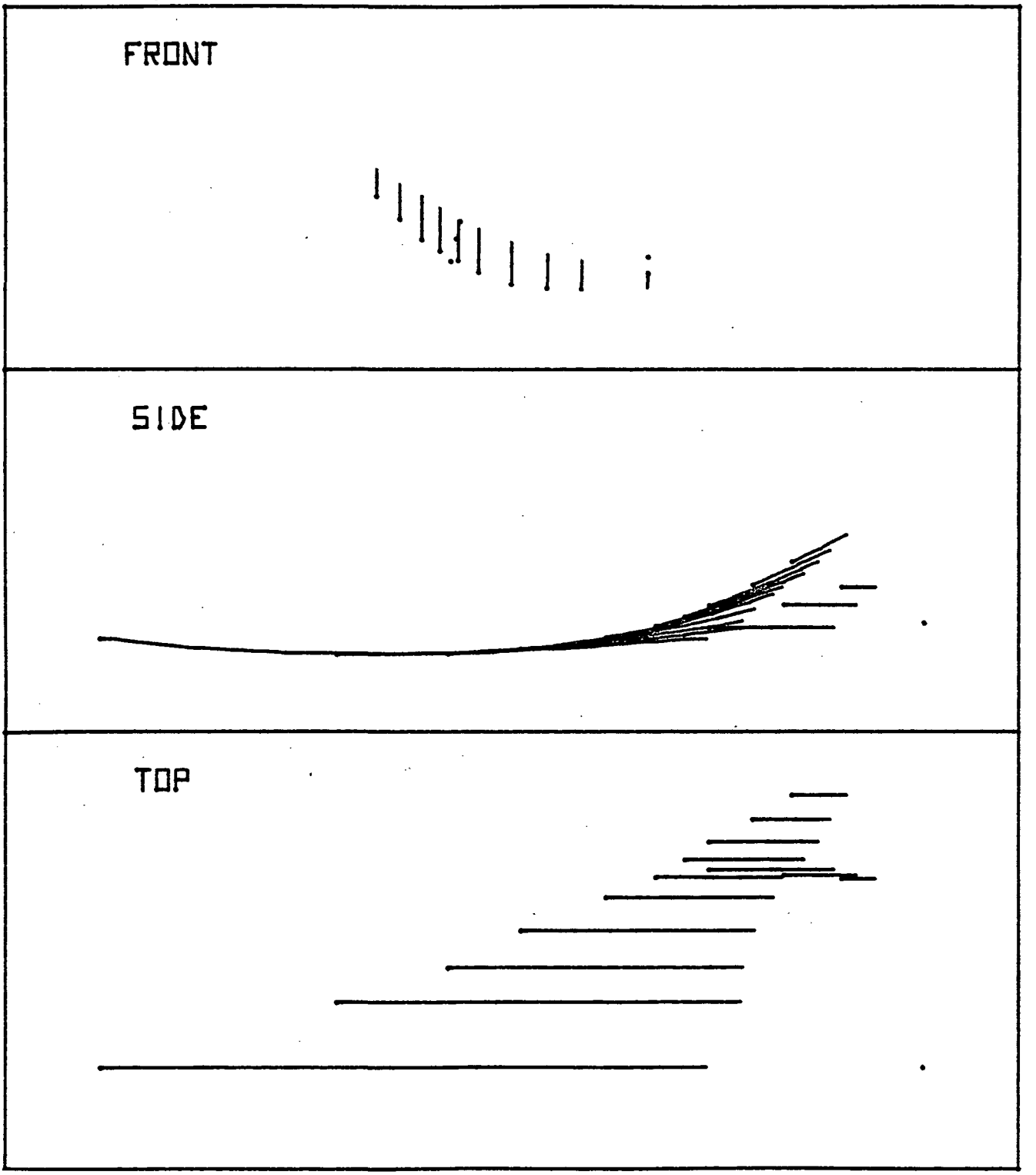

Figure A-1: 1st ELASTIC MODE SHAPE

Freq. = 1.19 Hz

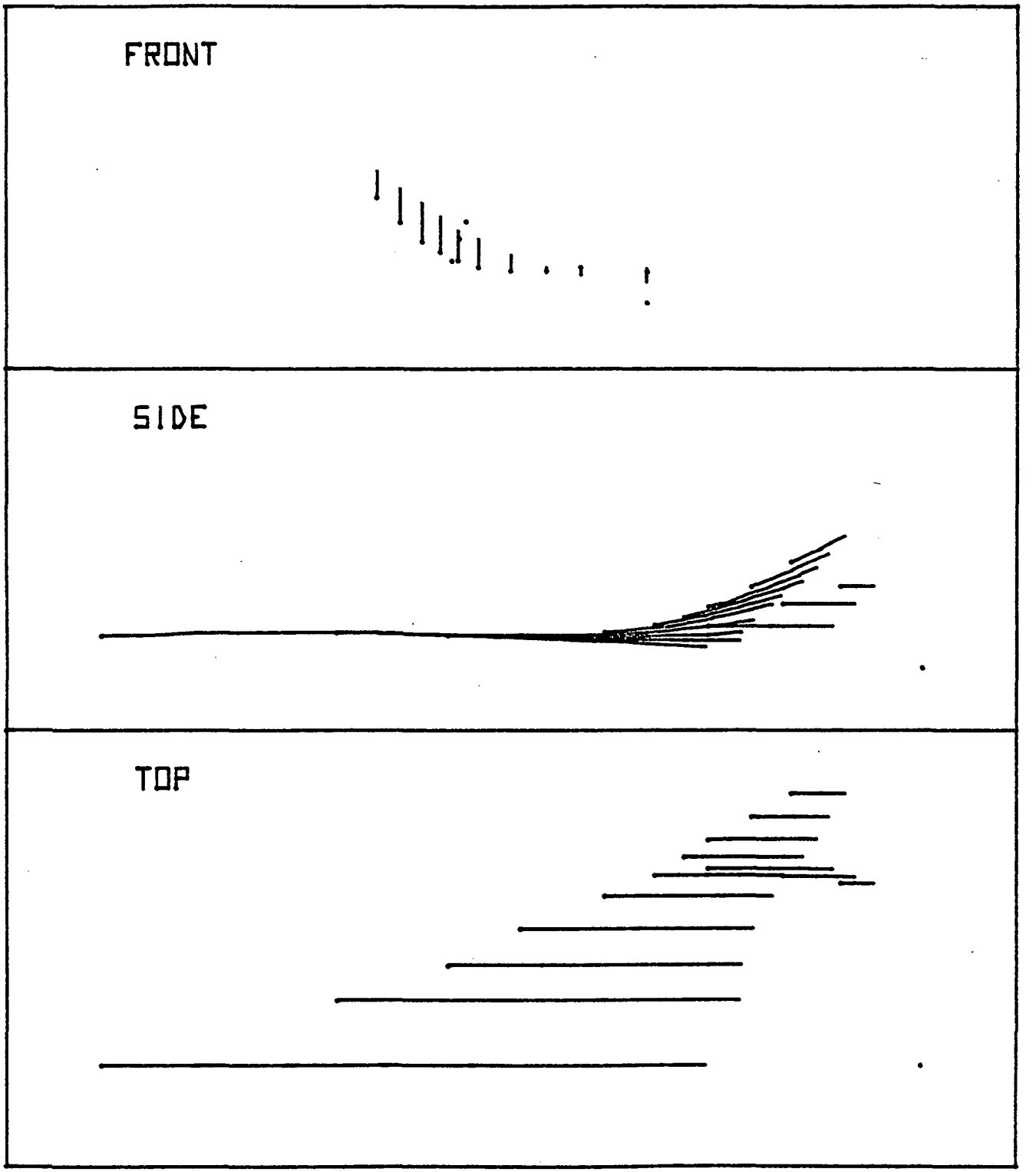

Figure A-2: 2nd ELASTIC MODE SHAPE

Freq. = 2.16 Hz

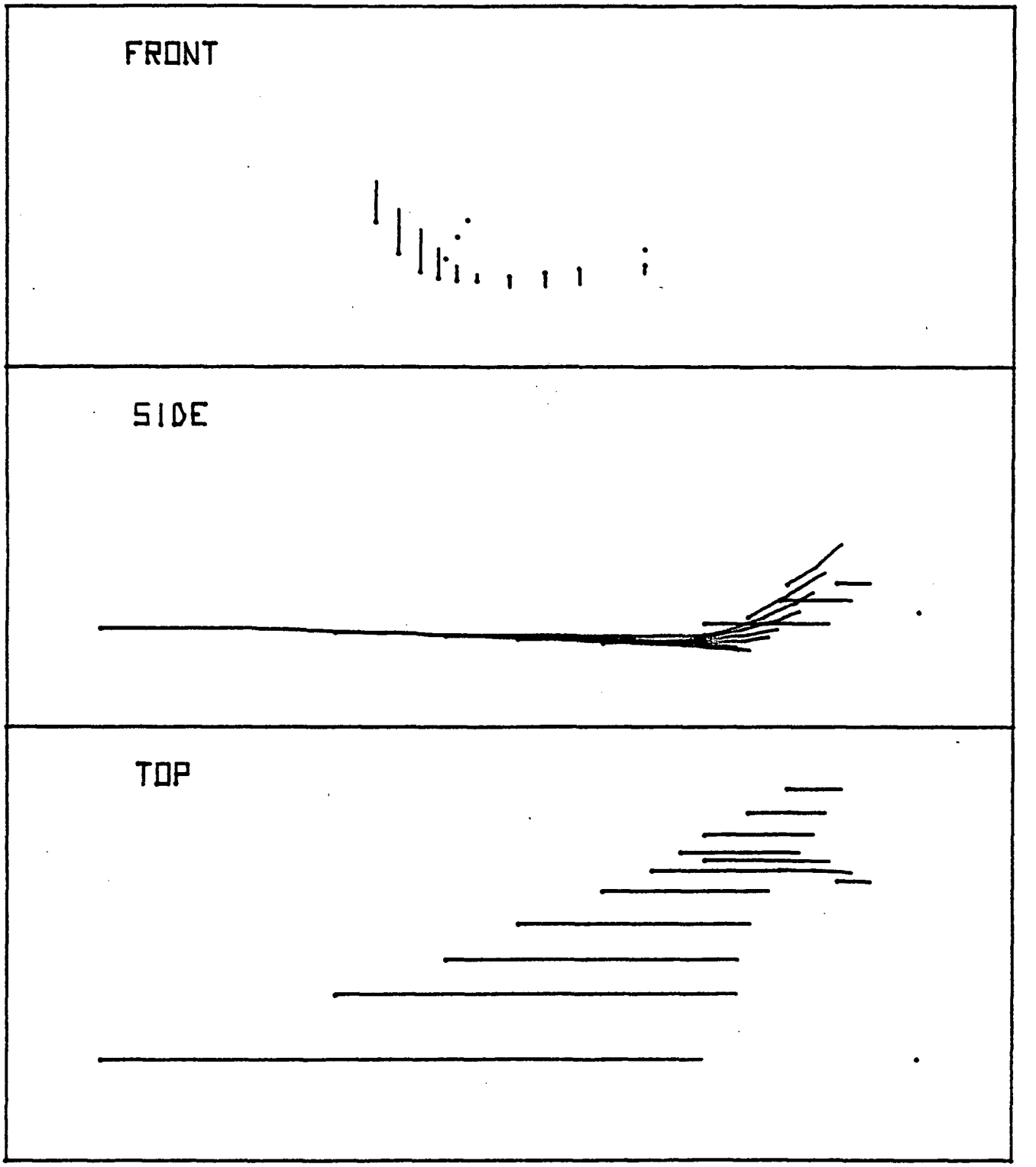

Figure A-3: 3rd ELASTIC MODE SHAPE

Freq. = 2.40 Hz

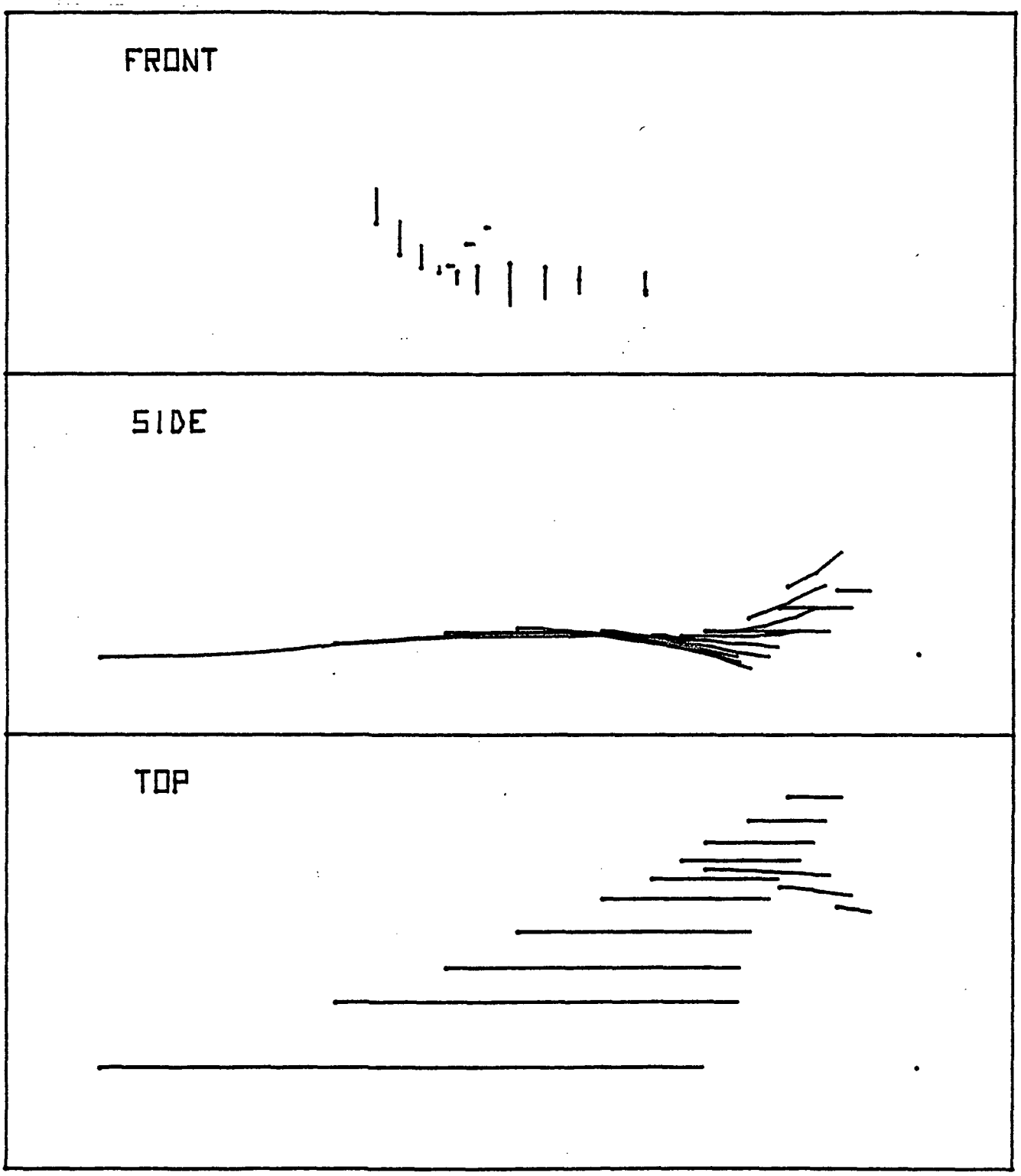

Figure A-4: 4^{th} ELASTIC MODE SHAPE

Freq. = 2.77 Hz

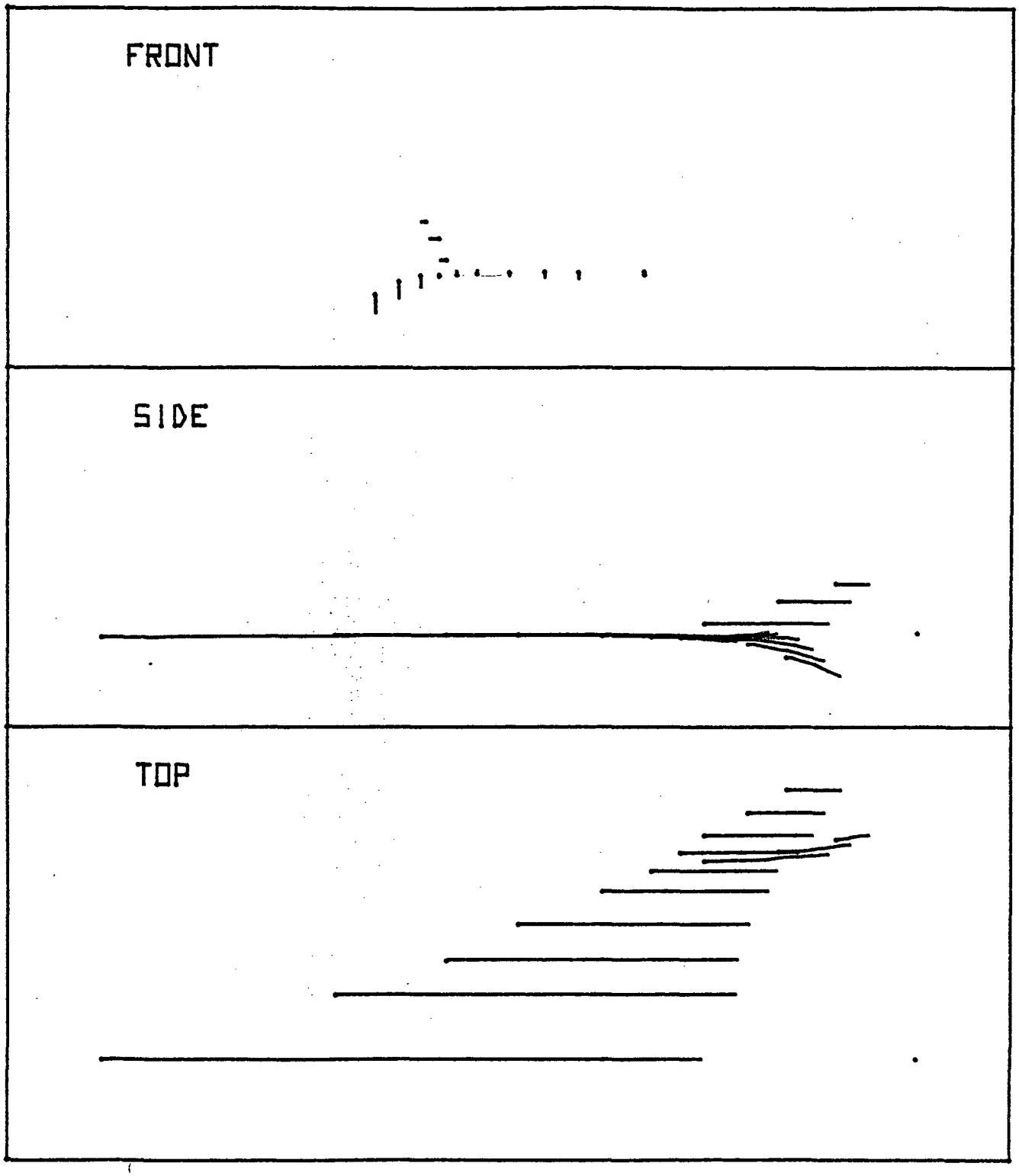

Figure A-5: 5th ELASTIC MODE SHAPE

Freq. = 3.12 Hz

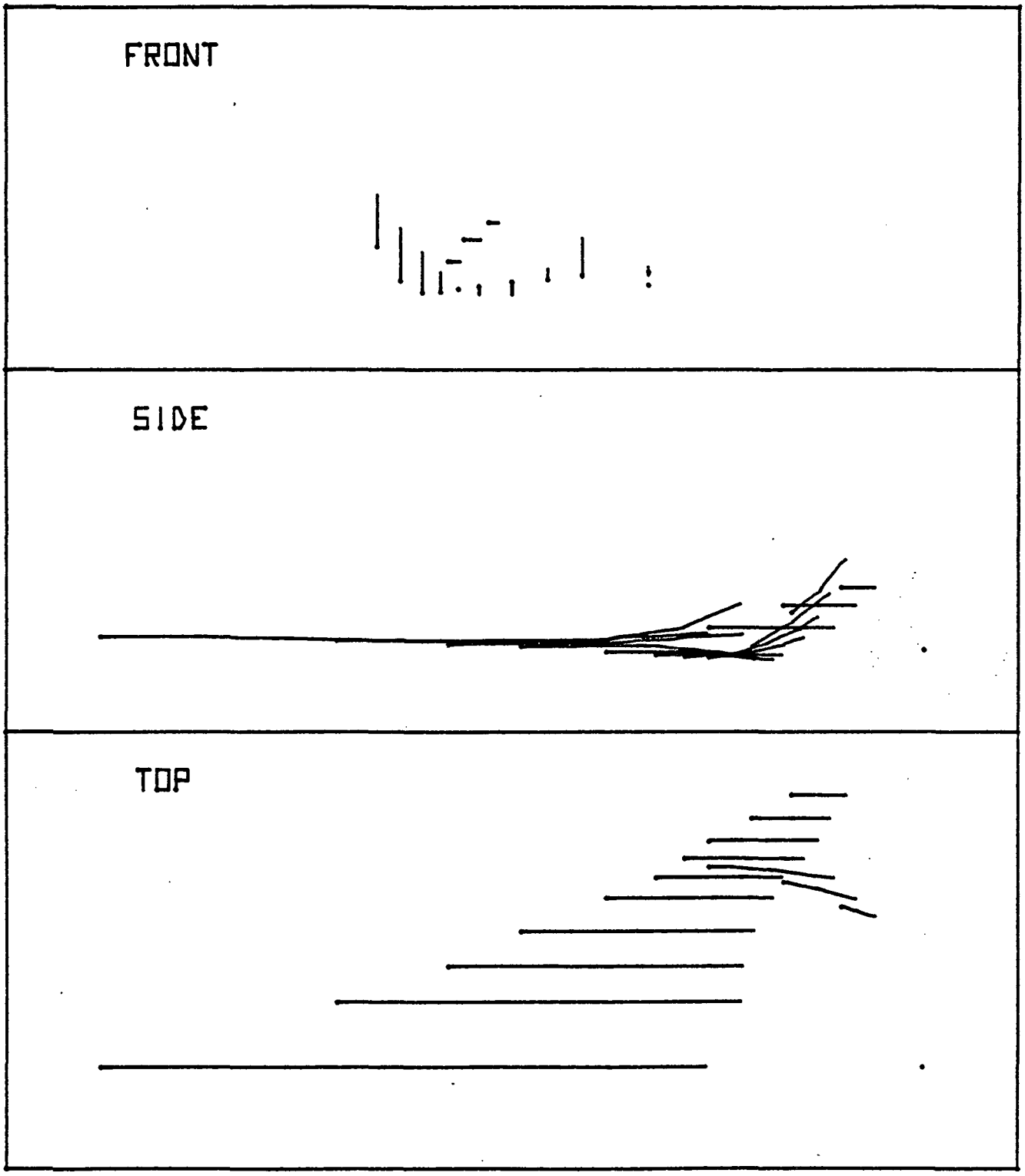

Figure A-6: 6th ELASTIC MODE SHAPE

Freq. = 3.39 Hz

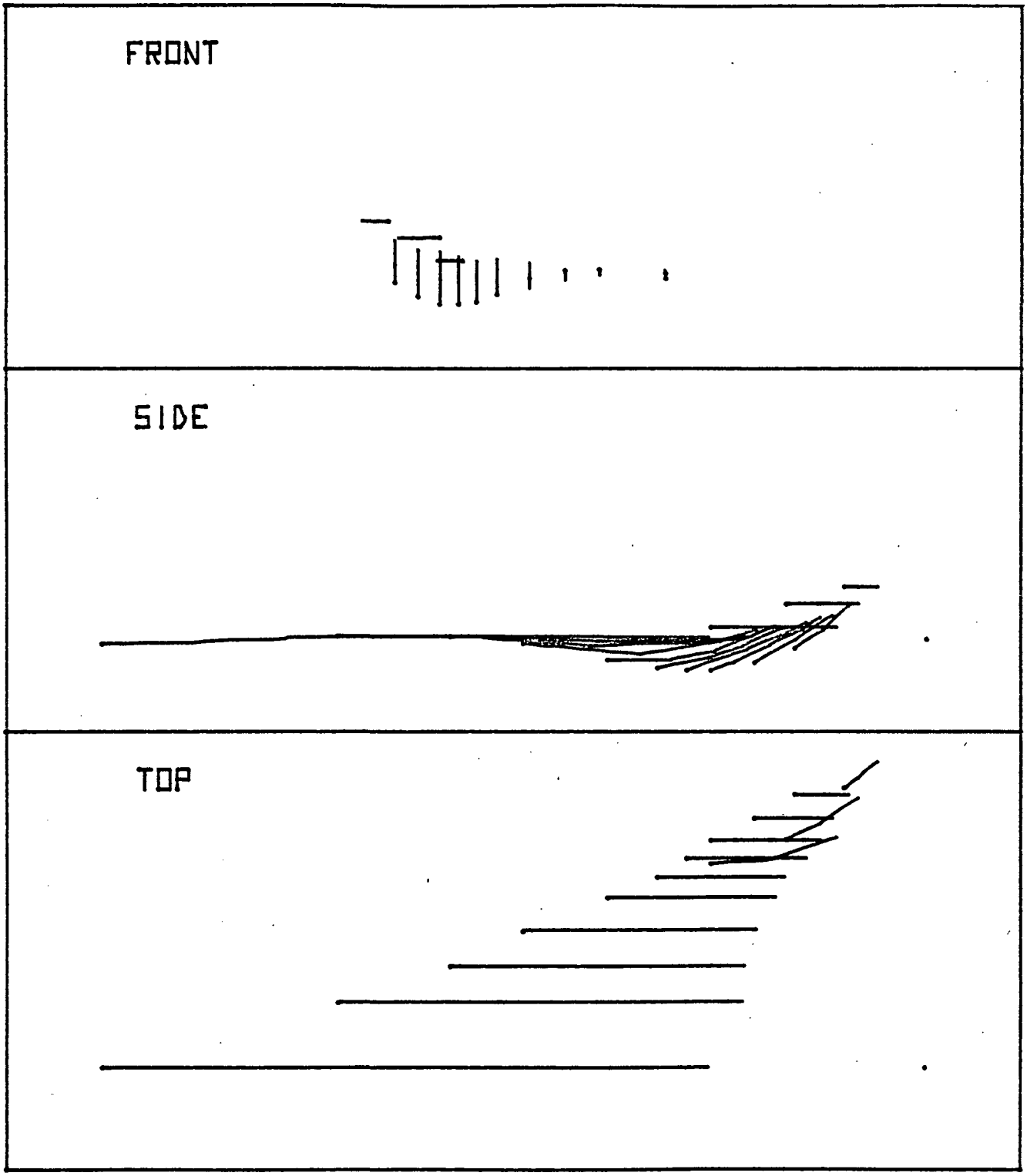

Figure A-7: 7^{th} ELASTIC MODE SHAPE

Freq. = 3.80 Hz

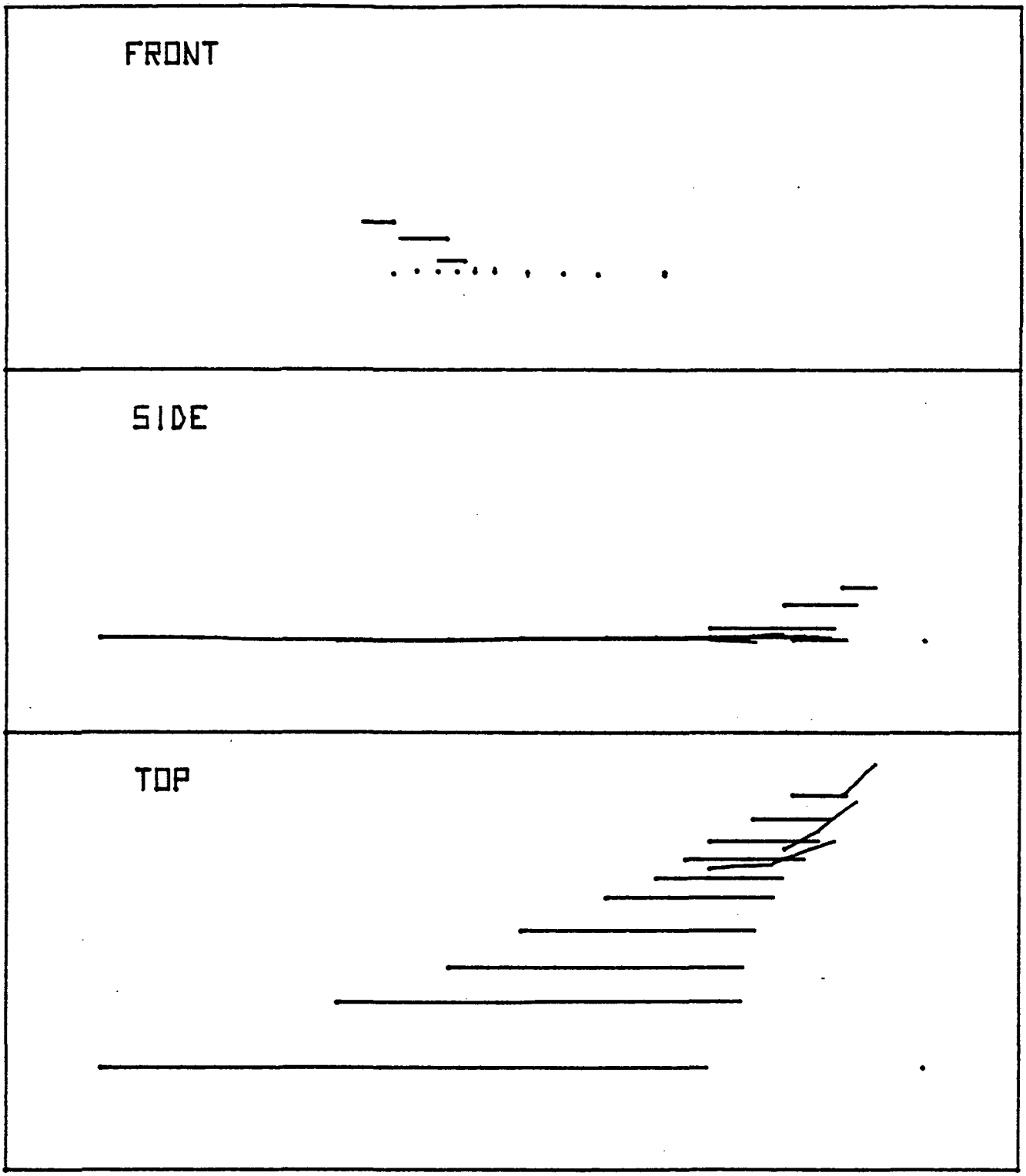

Figure A-8: 8th ELASTIC MODE SHAPE

Freq. = 4.11 Hz

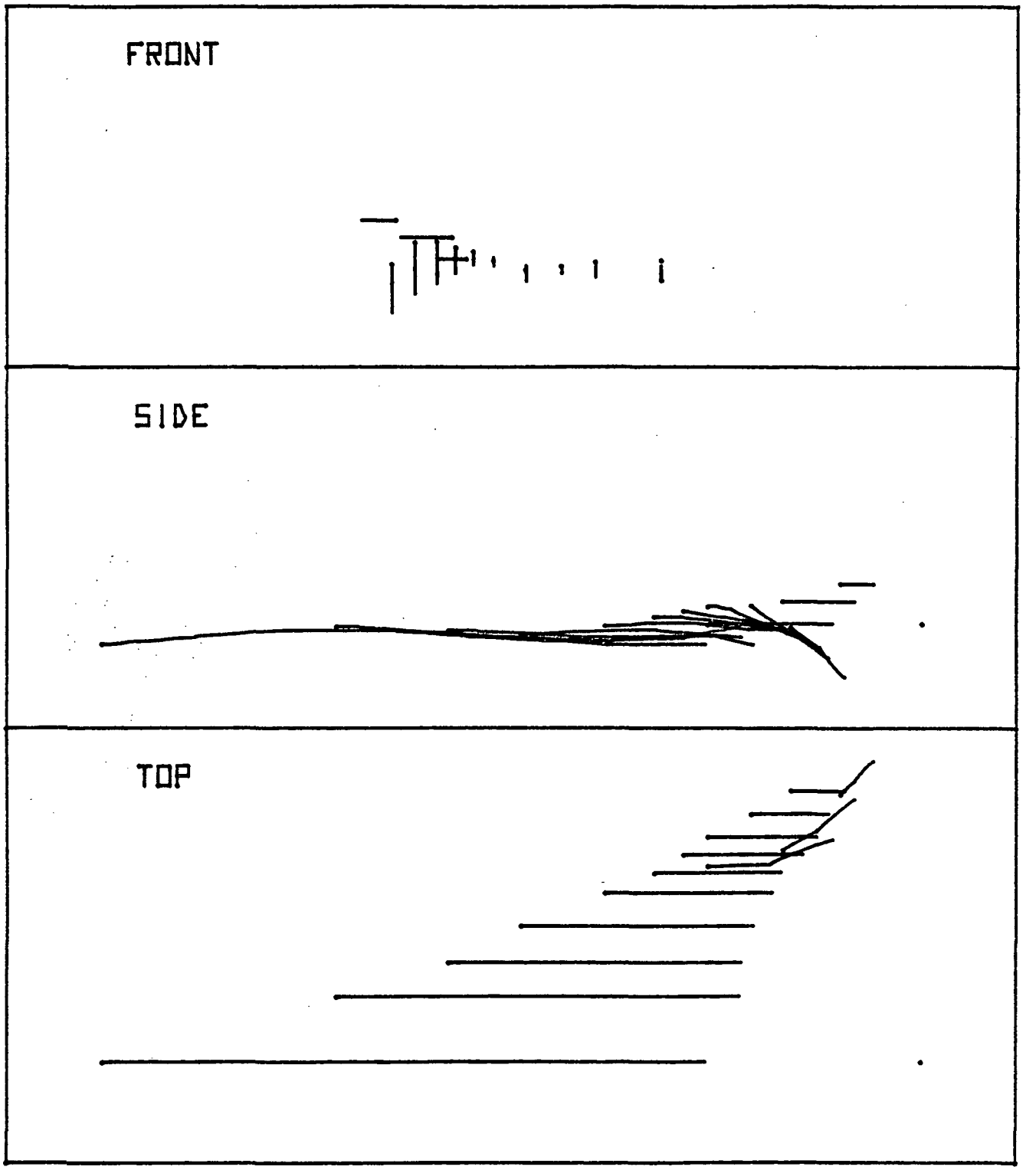

Figure A-9: 9th ELASTIC MODE SHAPE

Freq. = 4.85 Hz

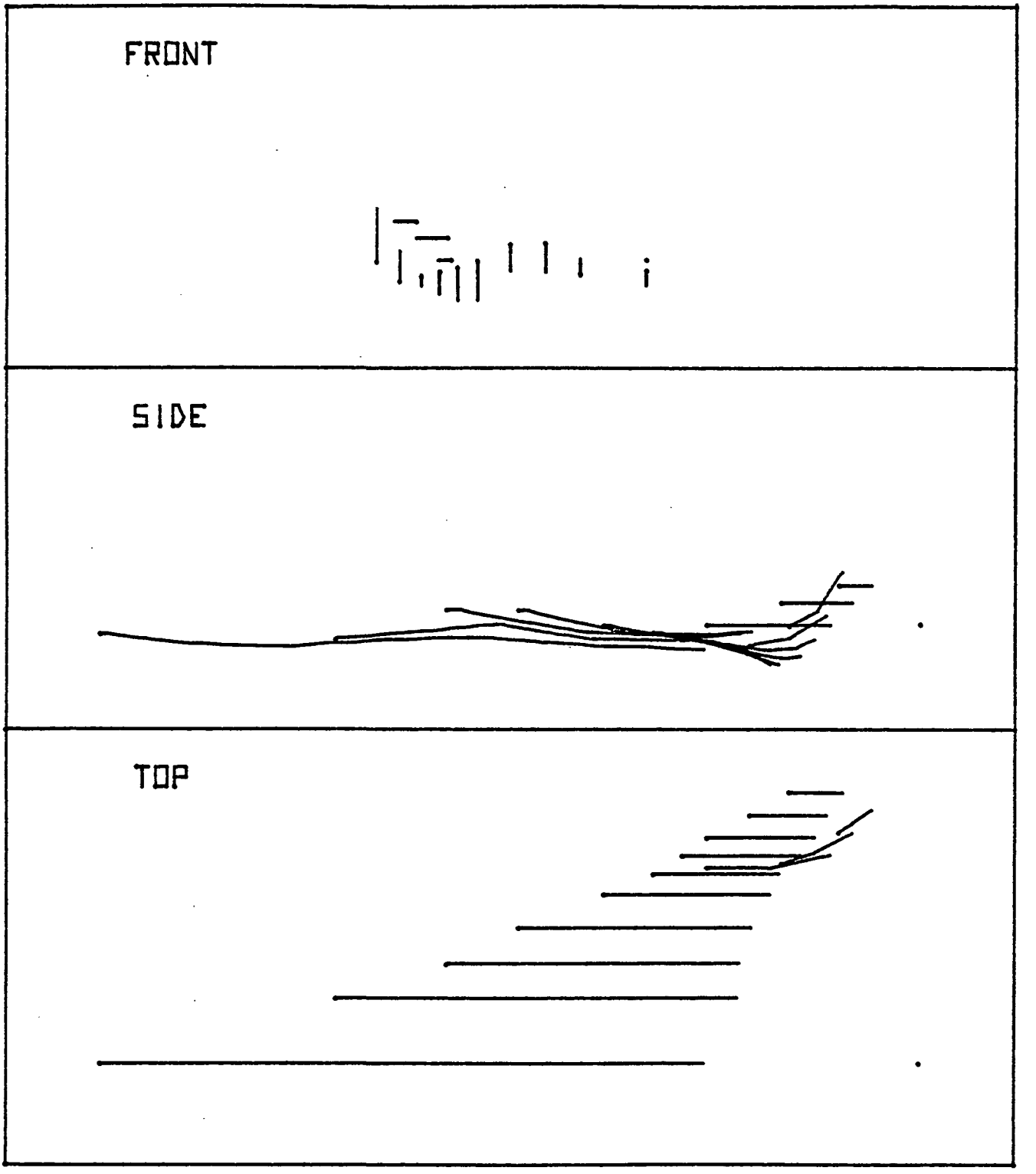

Figure A-10: 10^{th} ELASTIC MODE SHAPE

Freq. = 4.94 Hz

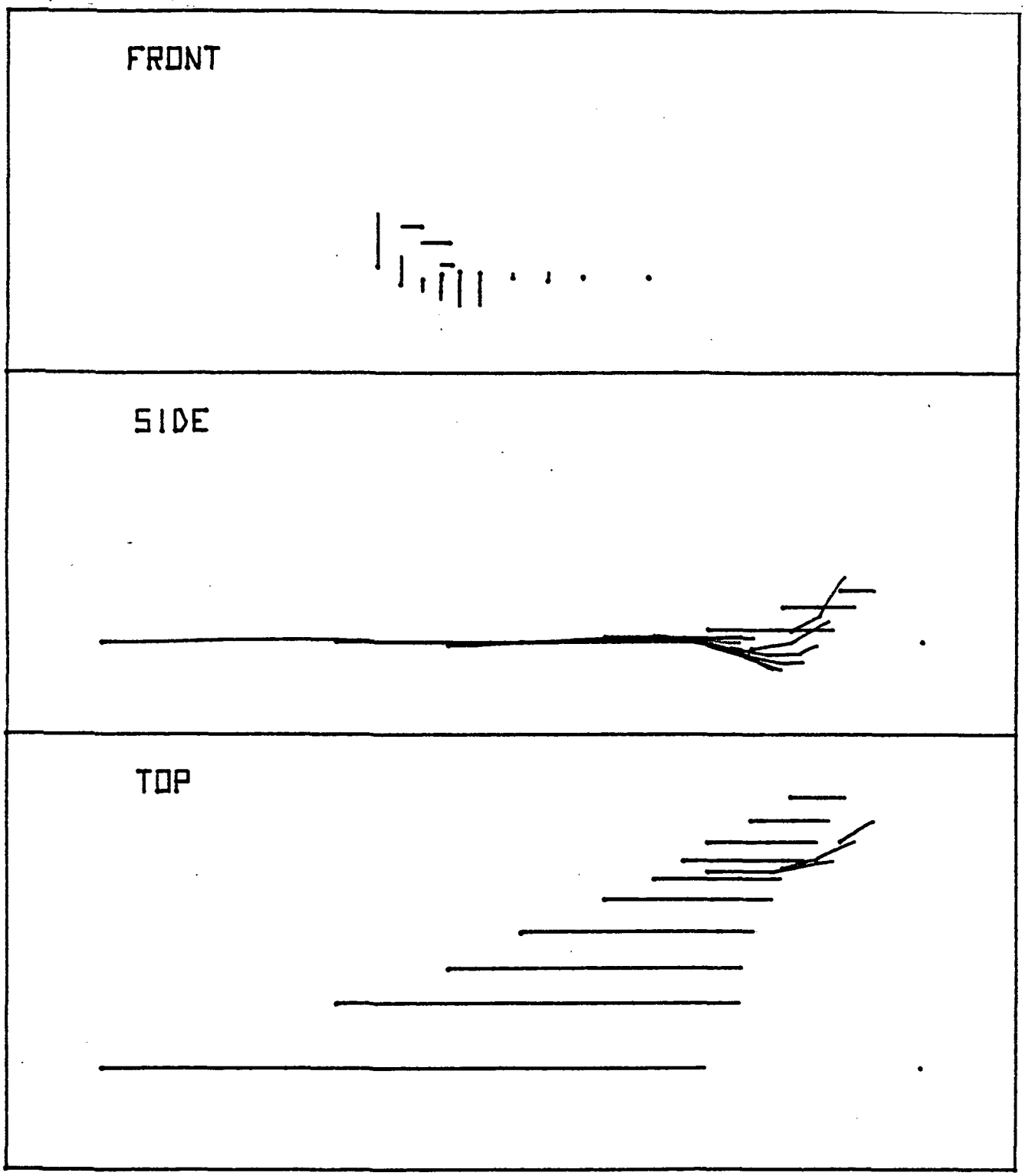

Figure A-11: 11th ELASTIC MODE SHAPE

Freq. = 5.77 Hz

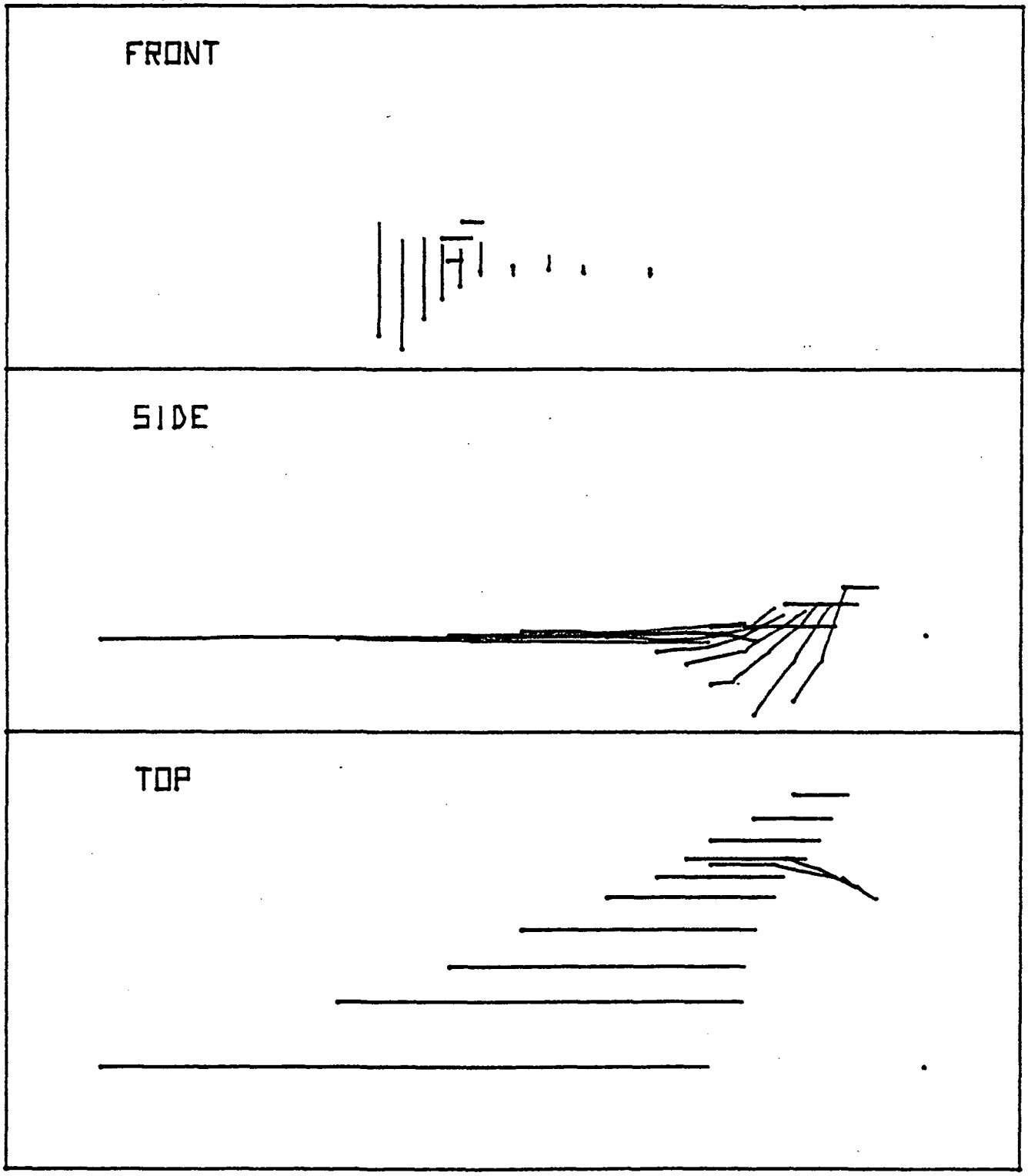

Figure A-12: 12th ELASTIC MODE SHAPE

Freq. = 6.23 Hz

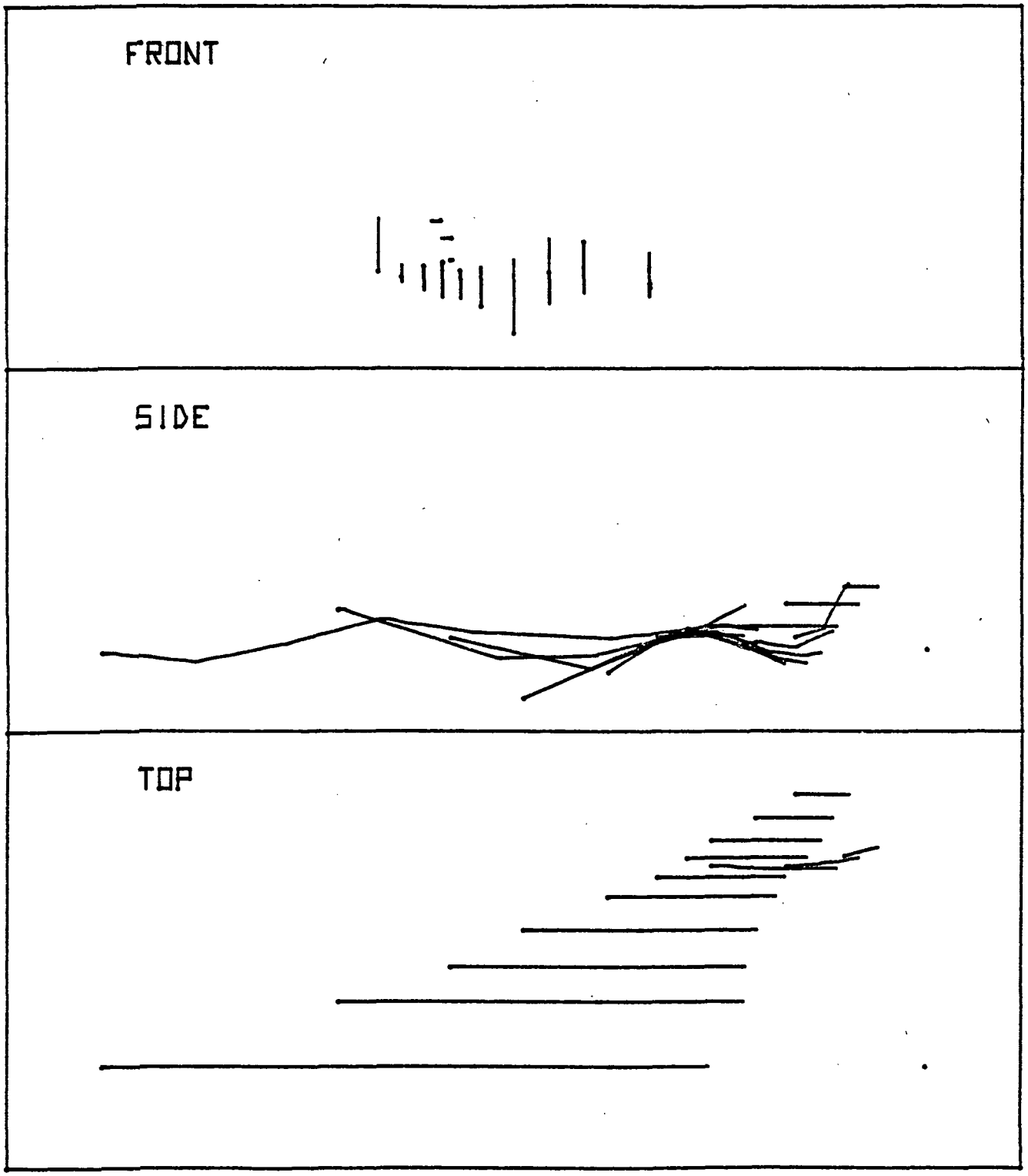

Figure A-13: 13th ELASTIC MODE SHAPE

Freq. = 6.62 Hz

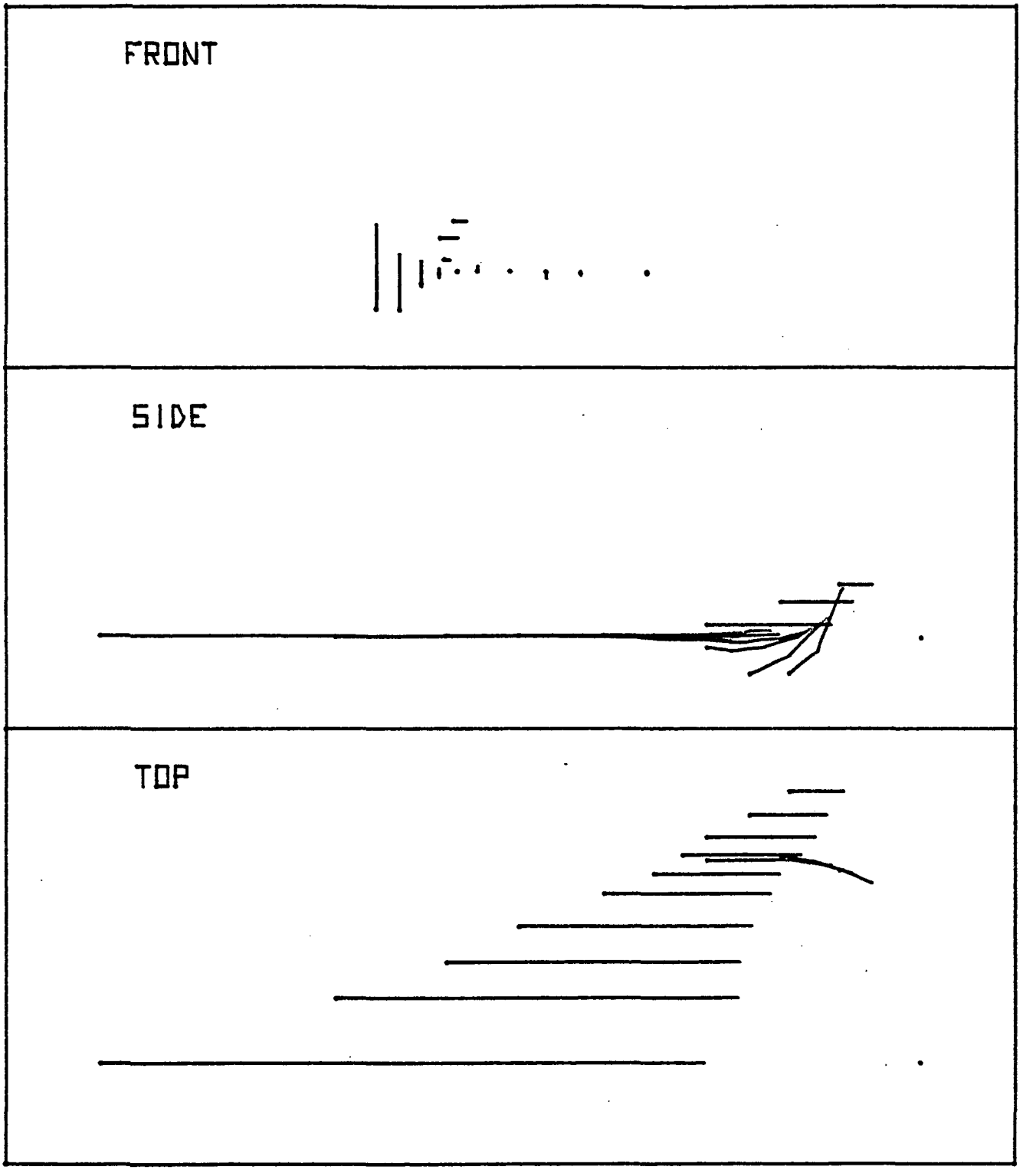

Figure A-14: 14^{th} ELASTIC MODE SHAPE

Freq. = 6.87 Hz

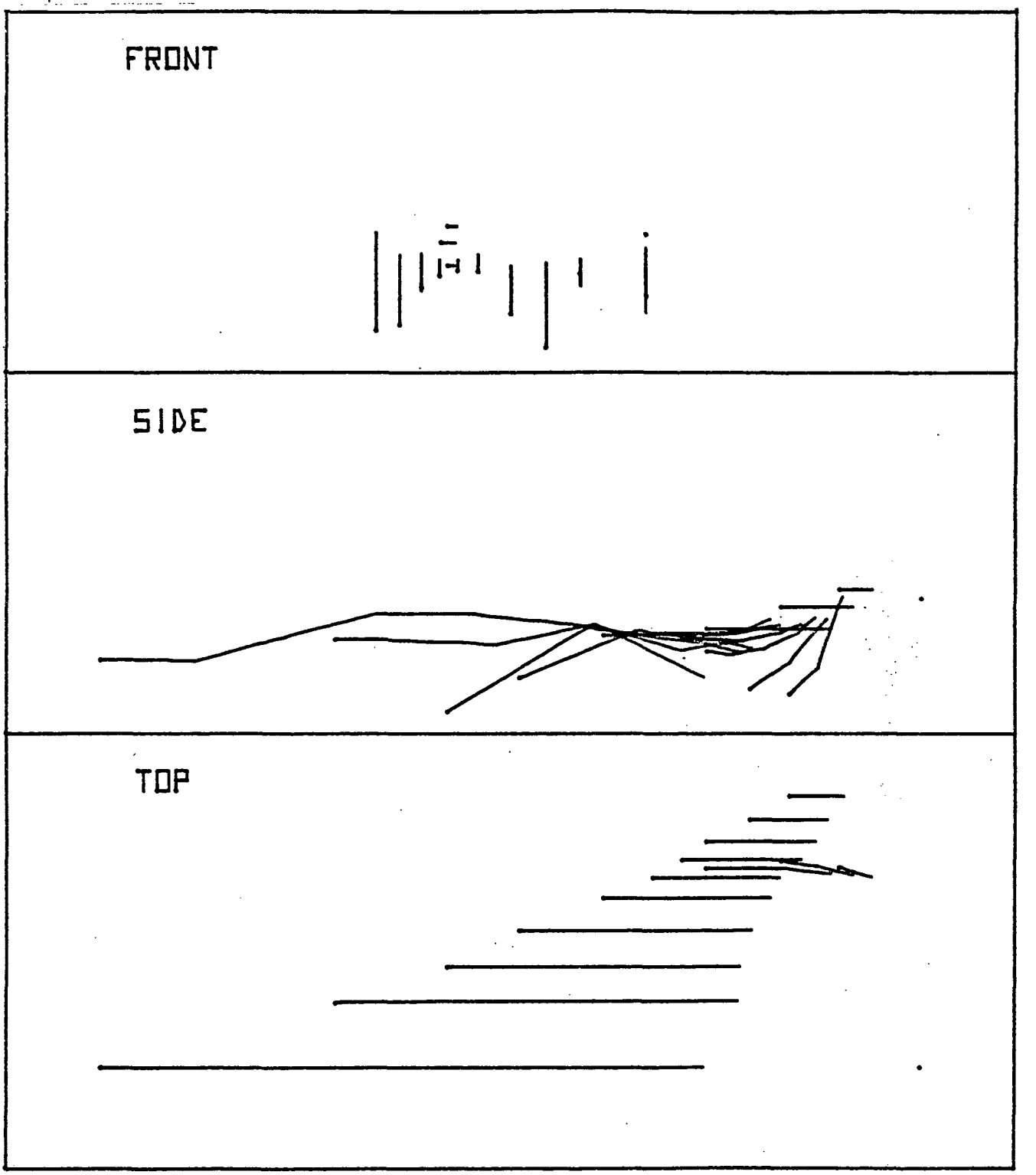

Figure A-15: 15th ELASTIC MODE SHAPE

Freq. = 7.64 Hz

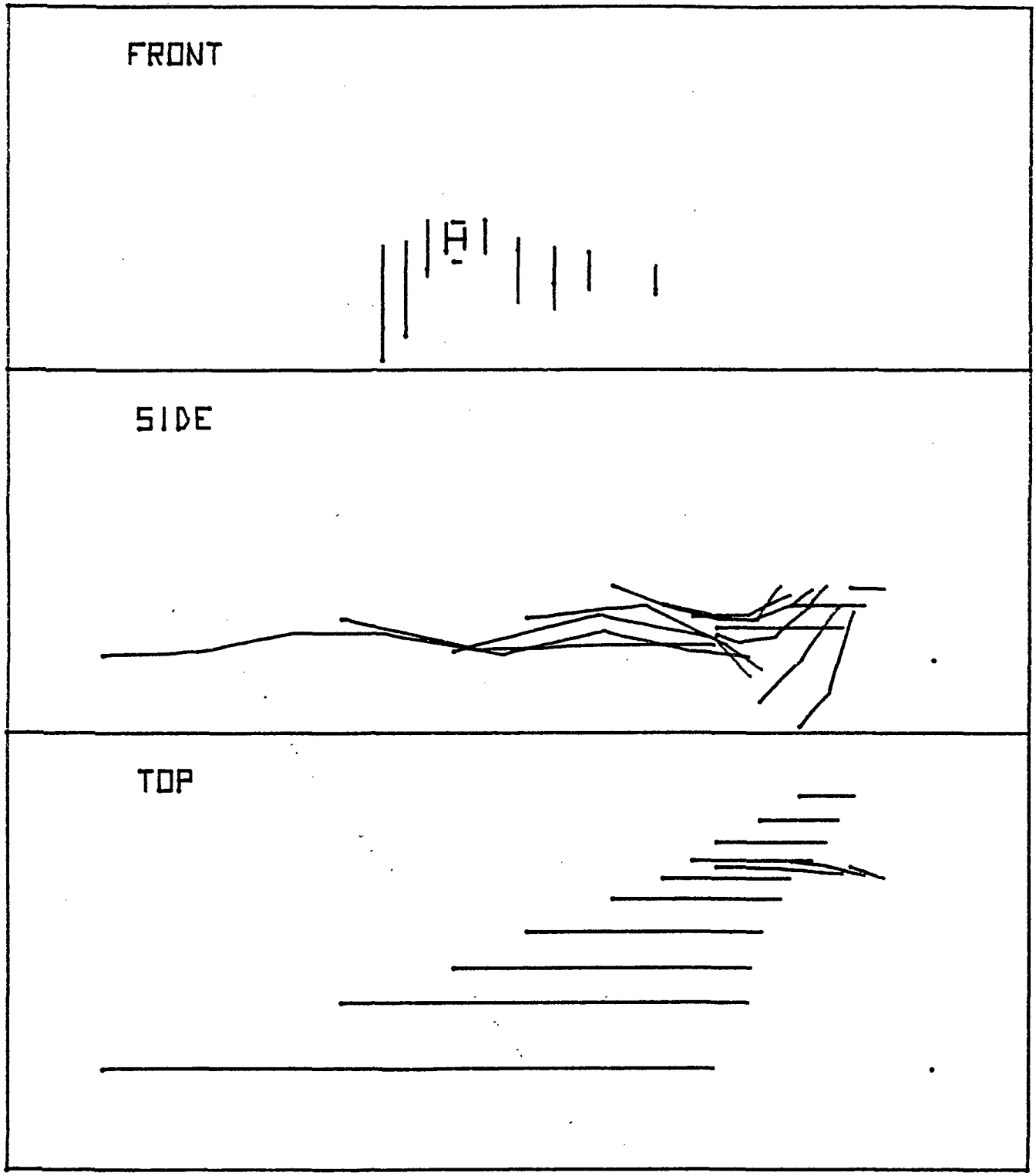

Figure A-16: 16th ELASTIC MODE SHAPE

Freq. = 7.84 Hz

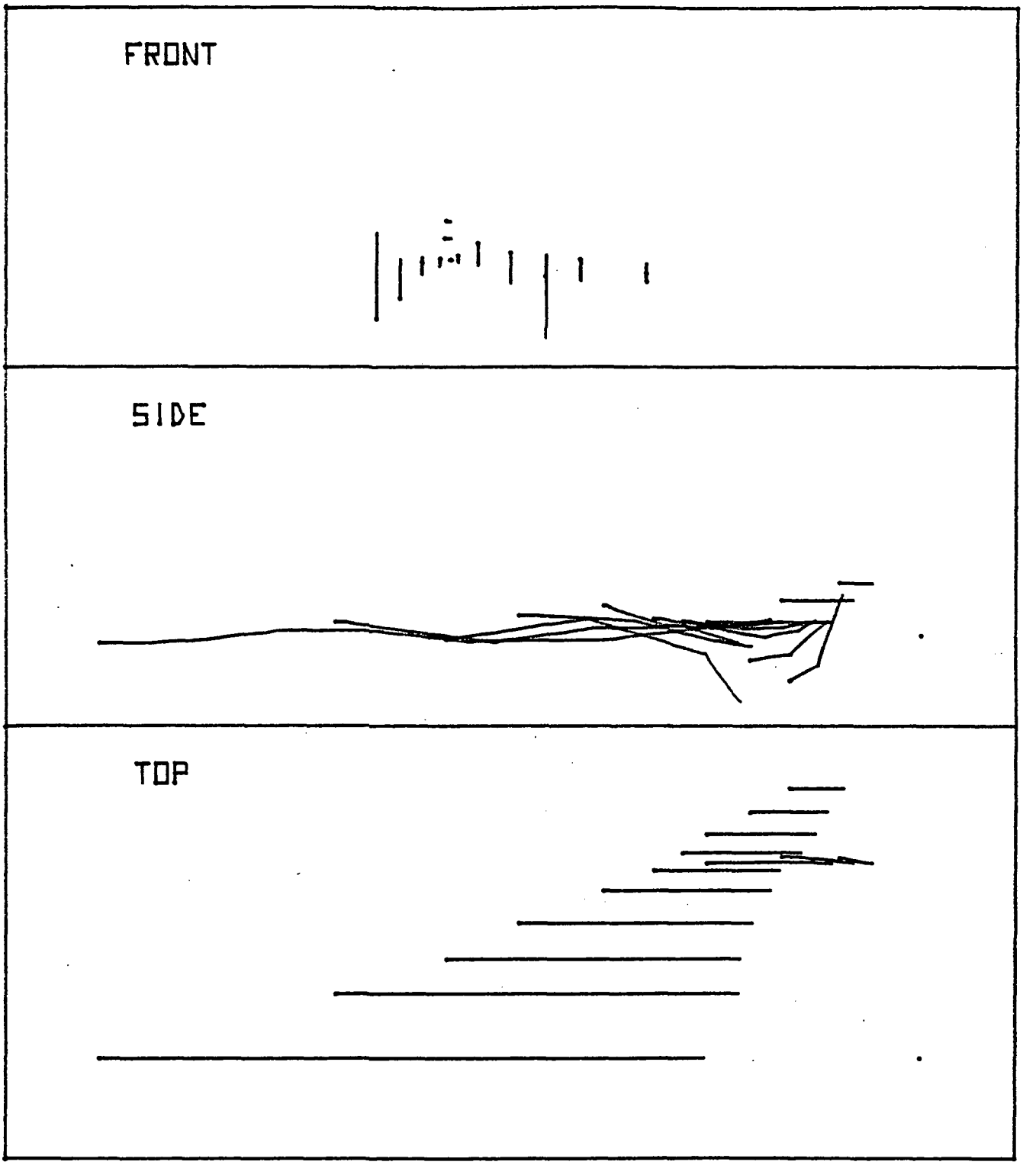

Figure A-17: 17th ELASTIC MODE SHAPE

Freq. = 8.39 Hz

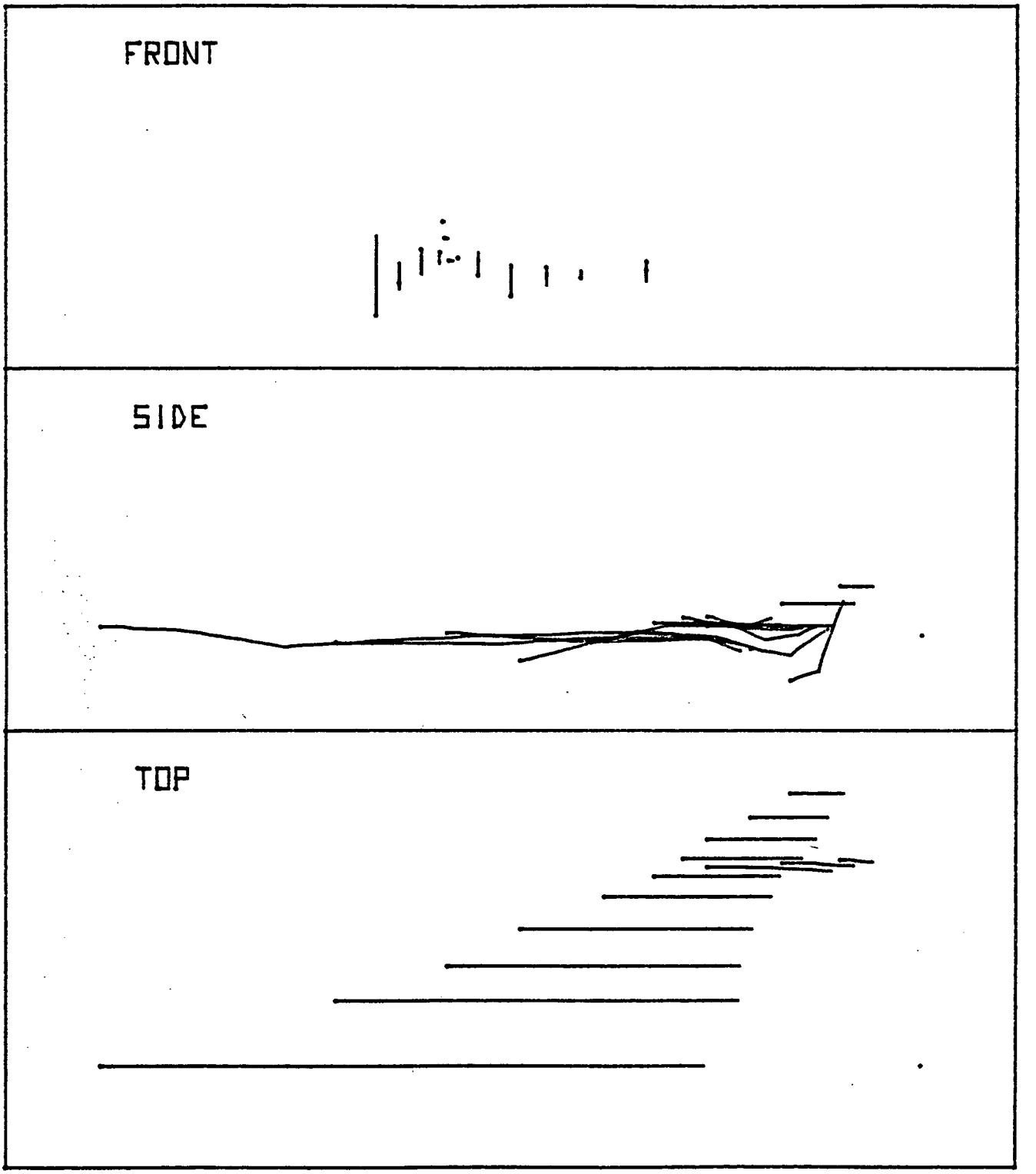

Figure A-18: 18th ELASTIC MODE SHAPE

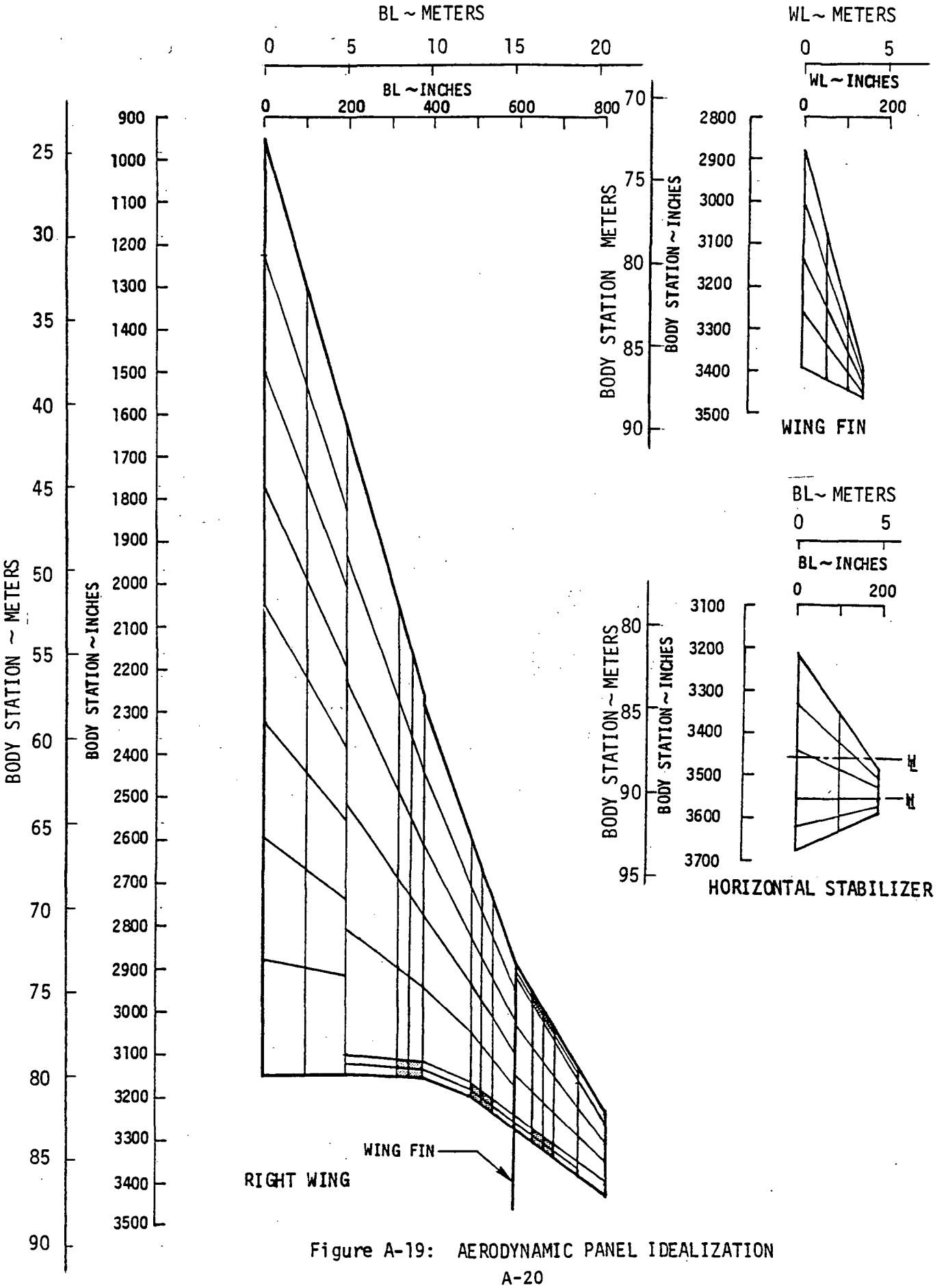

Figure A-19: AERODYNAMIC PANEL IDEALIZATION

APPENDIX "B"

FSS SYNTHESIS ROOT LOCI AND AIRPLANE CHARACTERISTIC FREQUENCIES AND DAMPING RATIOS

Root loci are shown for V_c, V_D and 1.2 V_D at Mach numbers of 0.9, 1.2 and 2.7 in Figures B-I through B-IX. Gain root loci for the nominal system only are shown for the 1.2 V_D analytical flutter clearance conditions. Gain loci for the nominal system and for $\pm$ .785 rad (45 deg) of phase added in the feedback are shown for V_c and V_D.

Damping and frequency of the airplane rigid body and structural modes with the FSS and HSAS are compared to damping and frequency of the airplane with HSAS only for V_c, V_D and 1.2 V_D at Mach numbers of 0.9, 1.2 and 2.7 in Tables B-I through B-IX. Damping and frequency of the airplane characteristic modes with the HSAS included in the mathematical model were generated subsequent to the FSS synthesis to verify FSS performance and compatibility with the airplane basic flight control system.

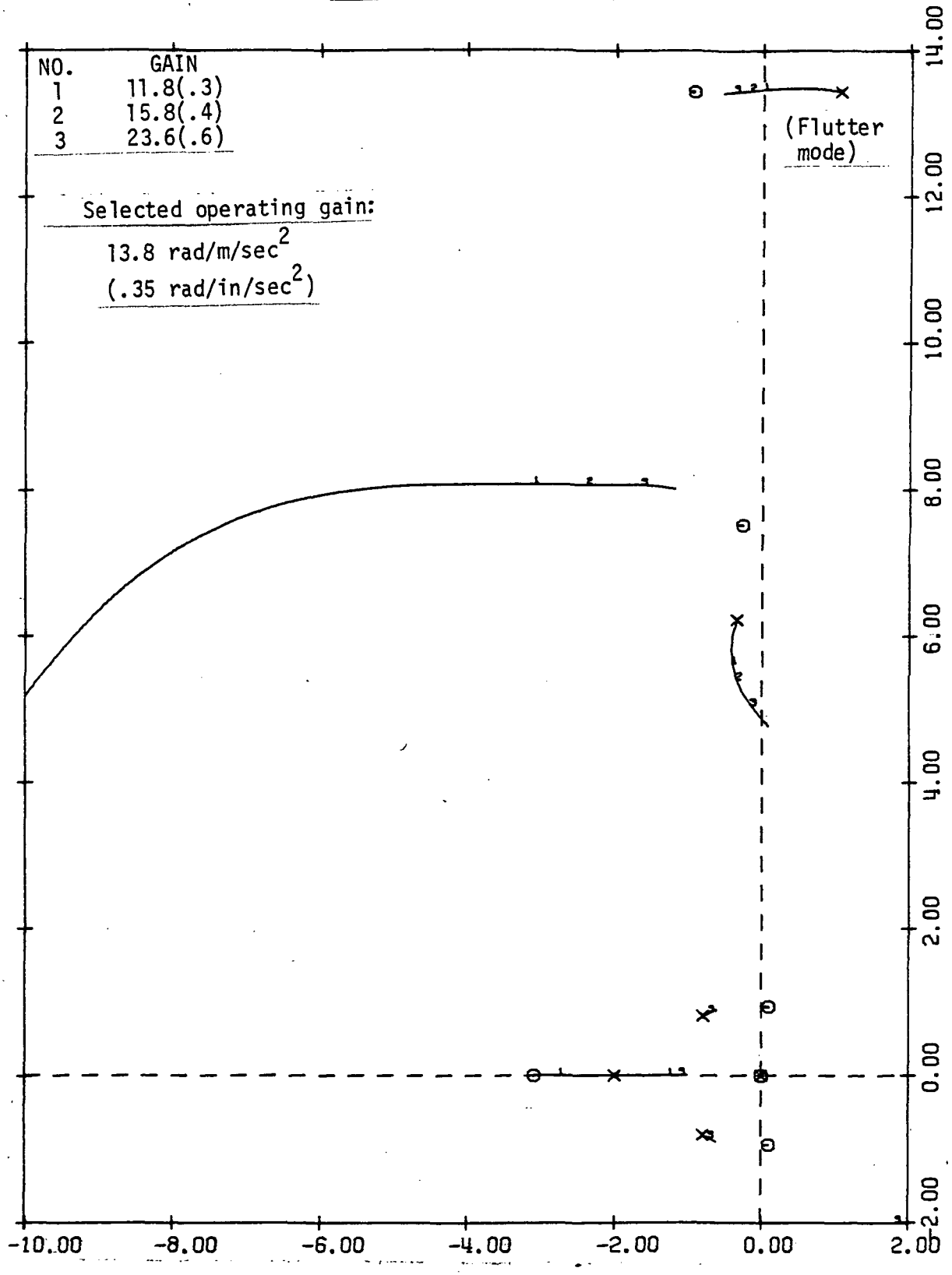

Figure B-1: GAIN ROOT LOCI FOR MACH 0.9, 1.2 V_D

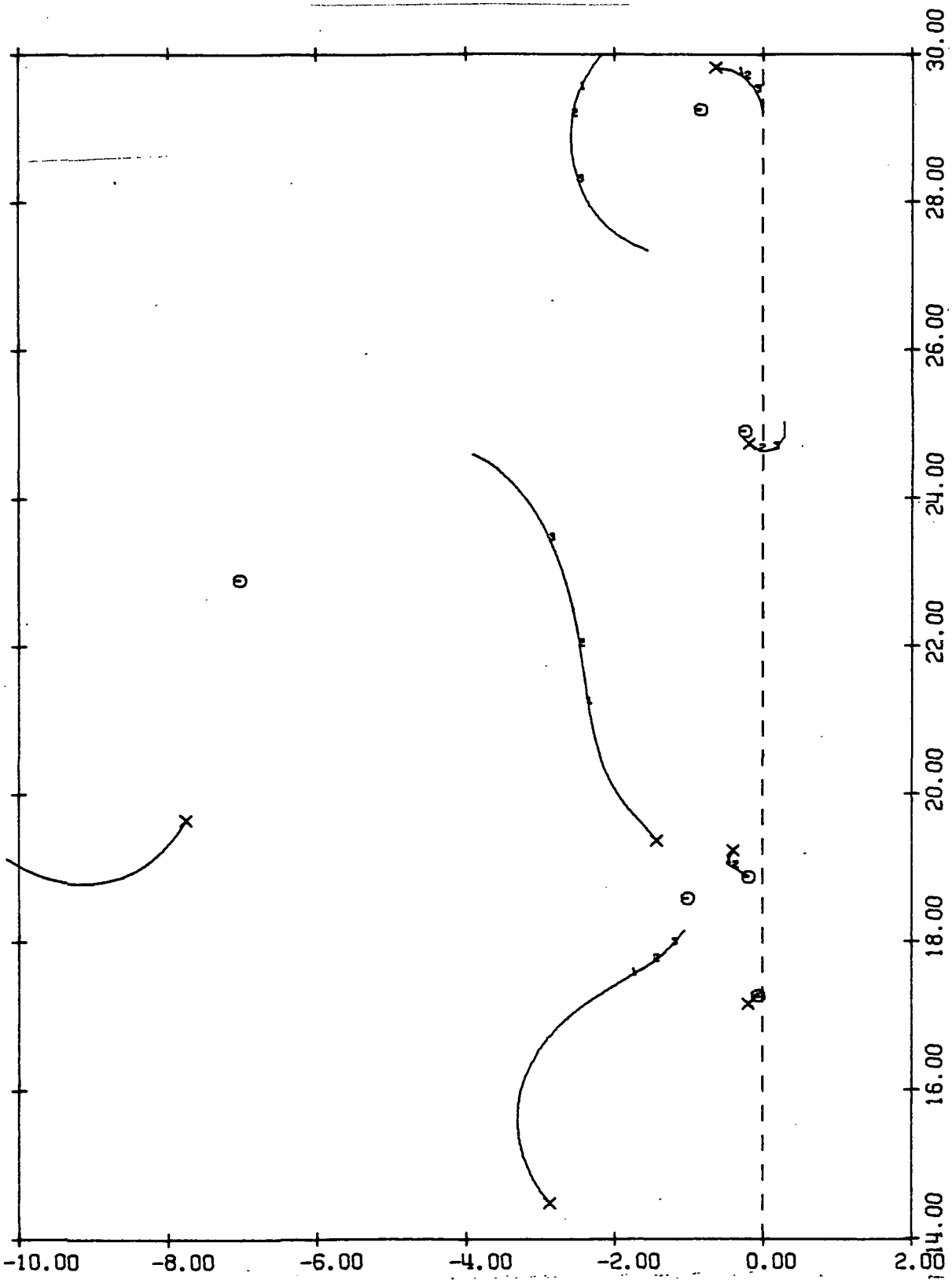

Figure B-1: CONTINUED

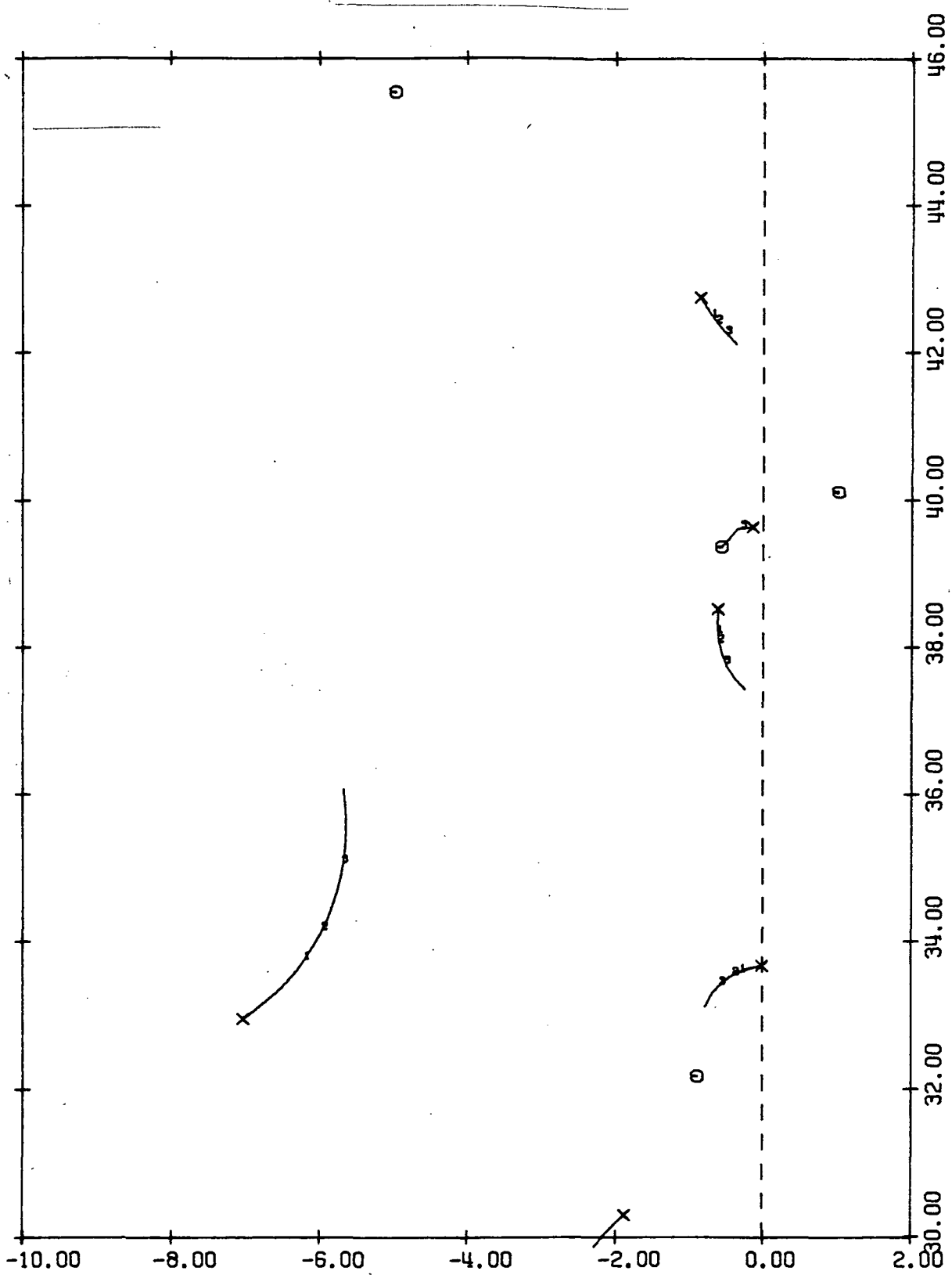

Figure B-1: CONTINUED

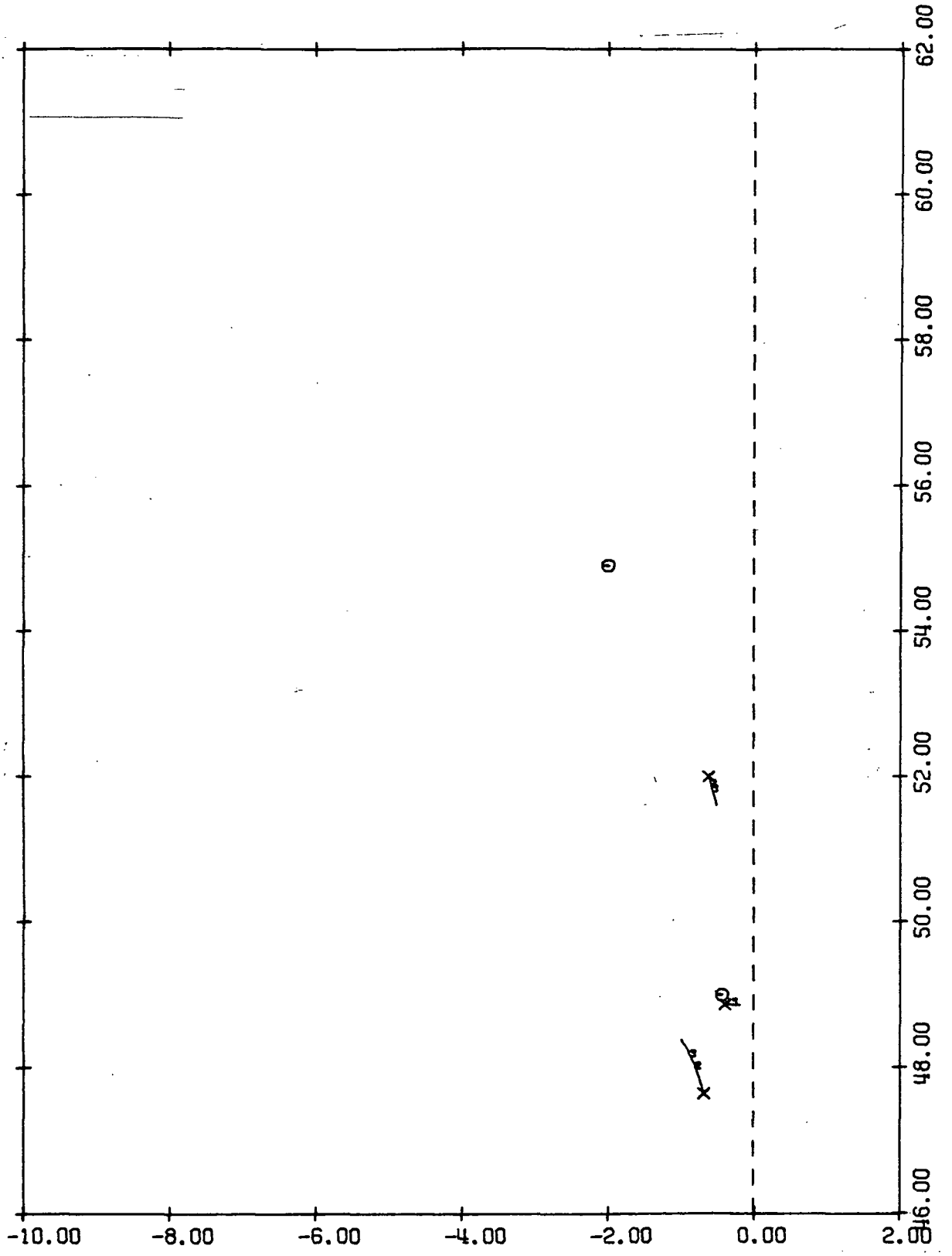

Figure B-1: CONCLUDED

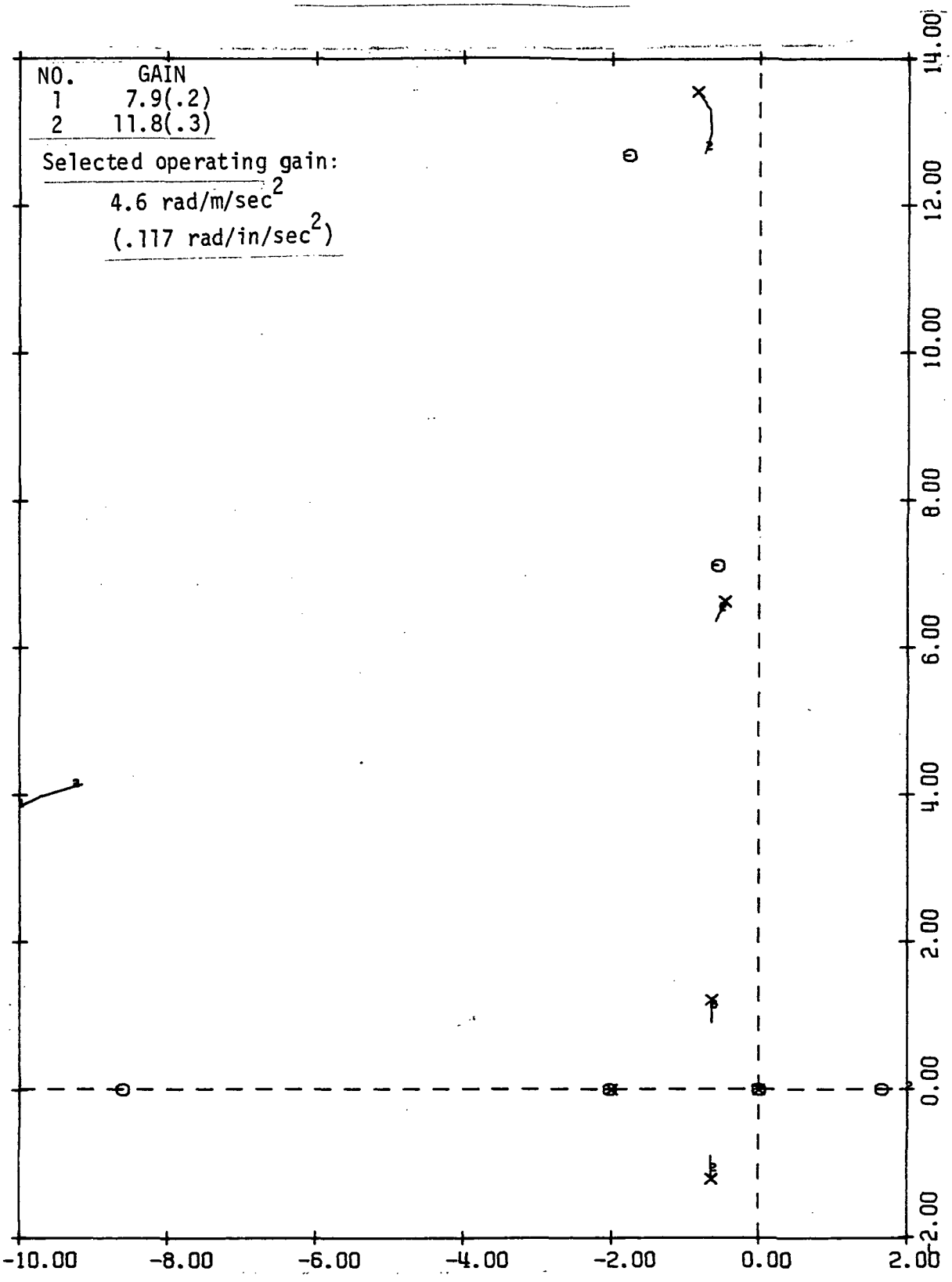

Figure B-2: GAIN ROOT LOCUS FOR MACH 1.2, 1.2V_D

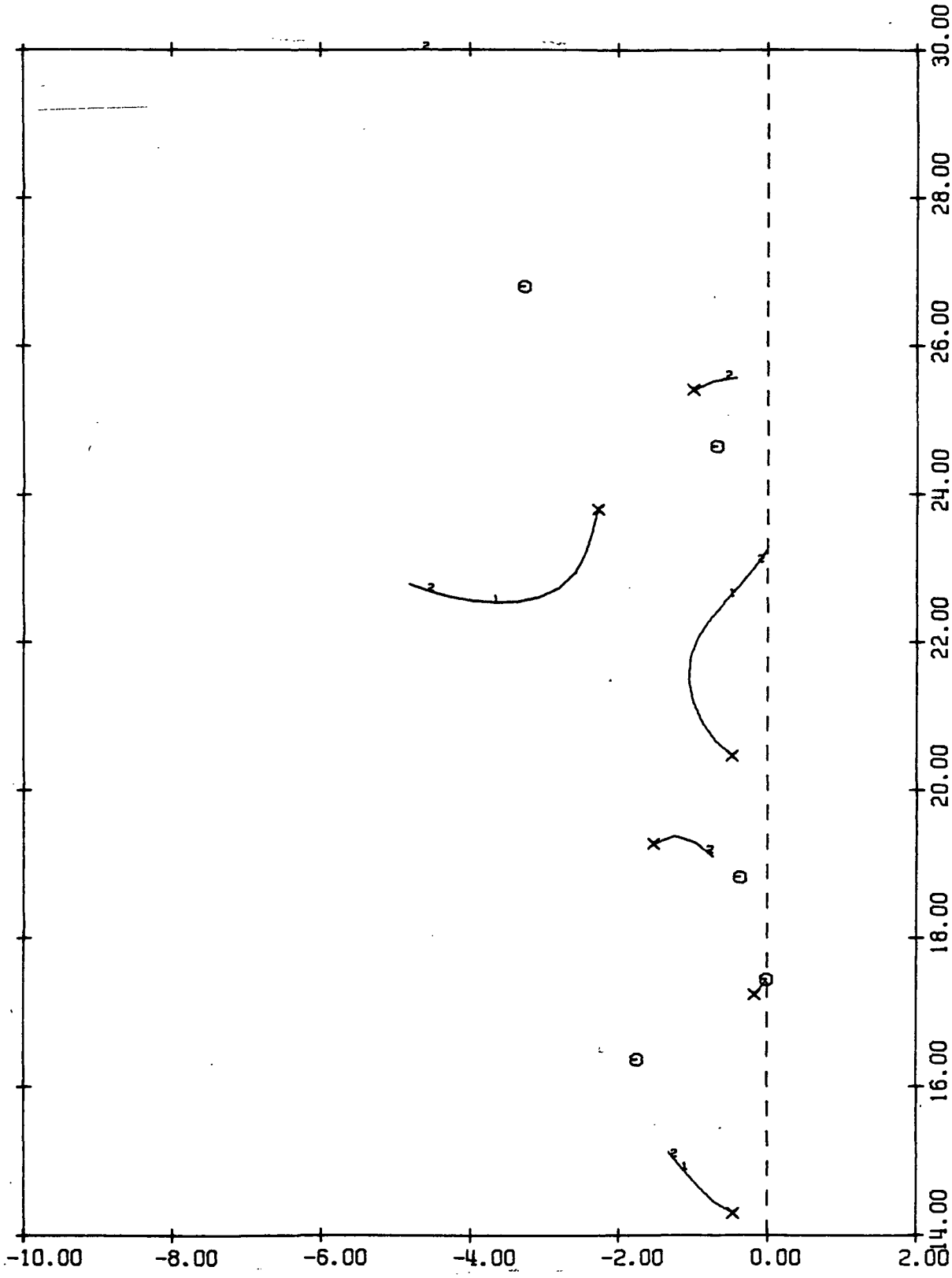

Figure B-2: CONTINUED

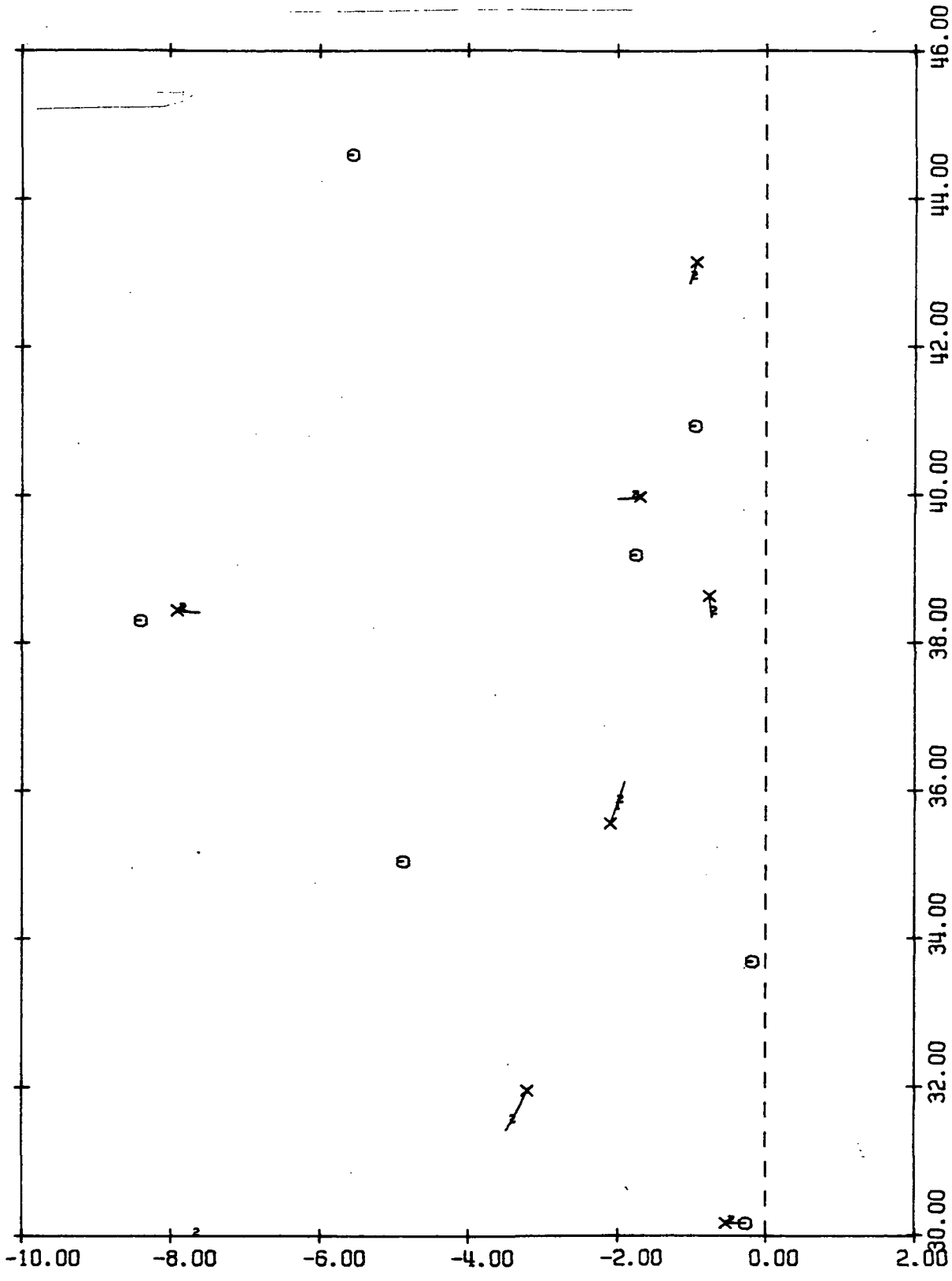

Figure B-2: CONTINUED

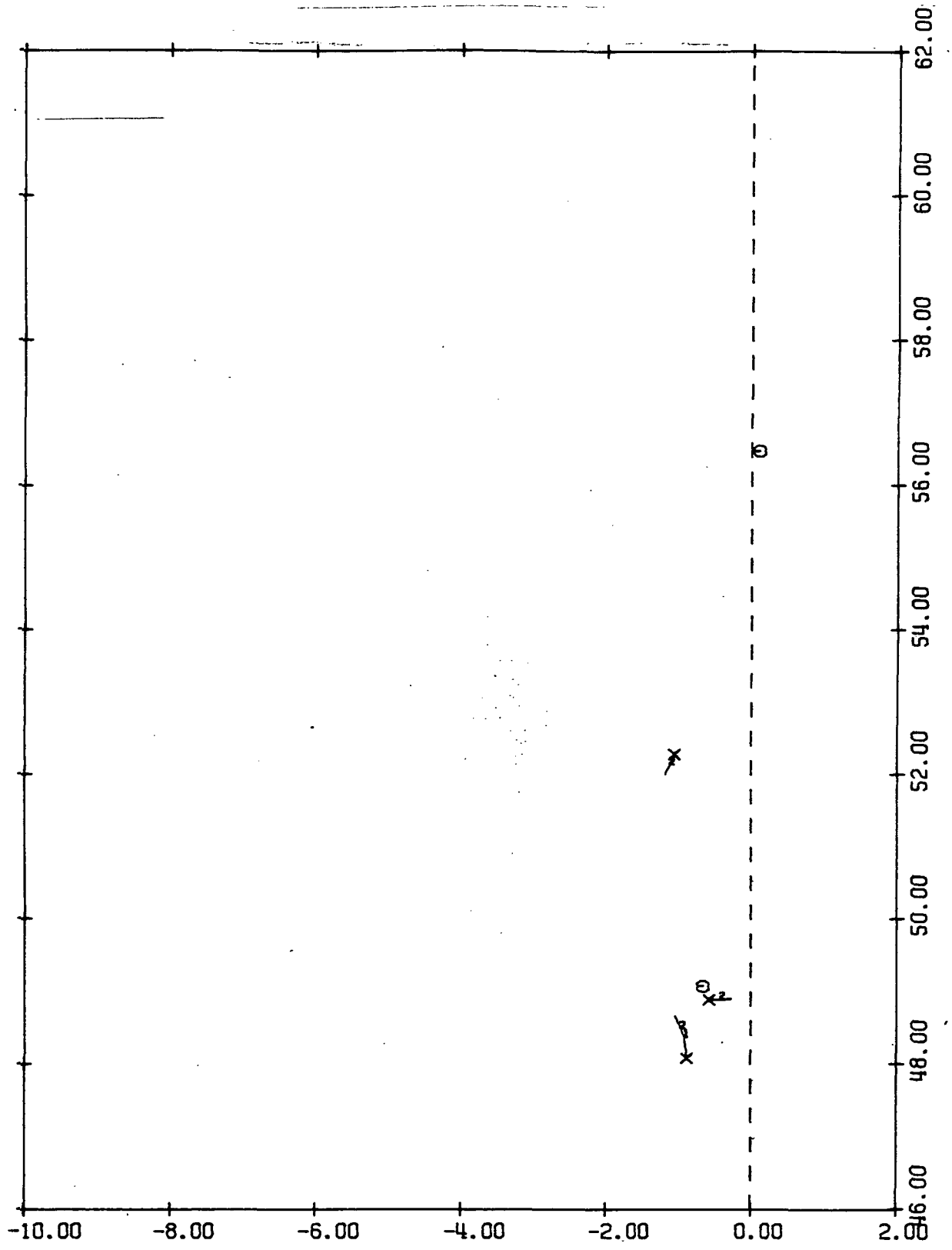

Figure B-2: CONCLUDED

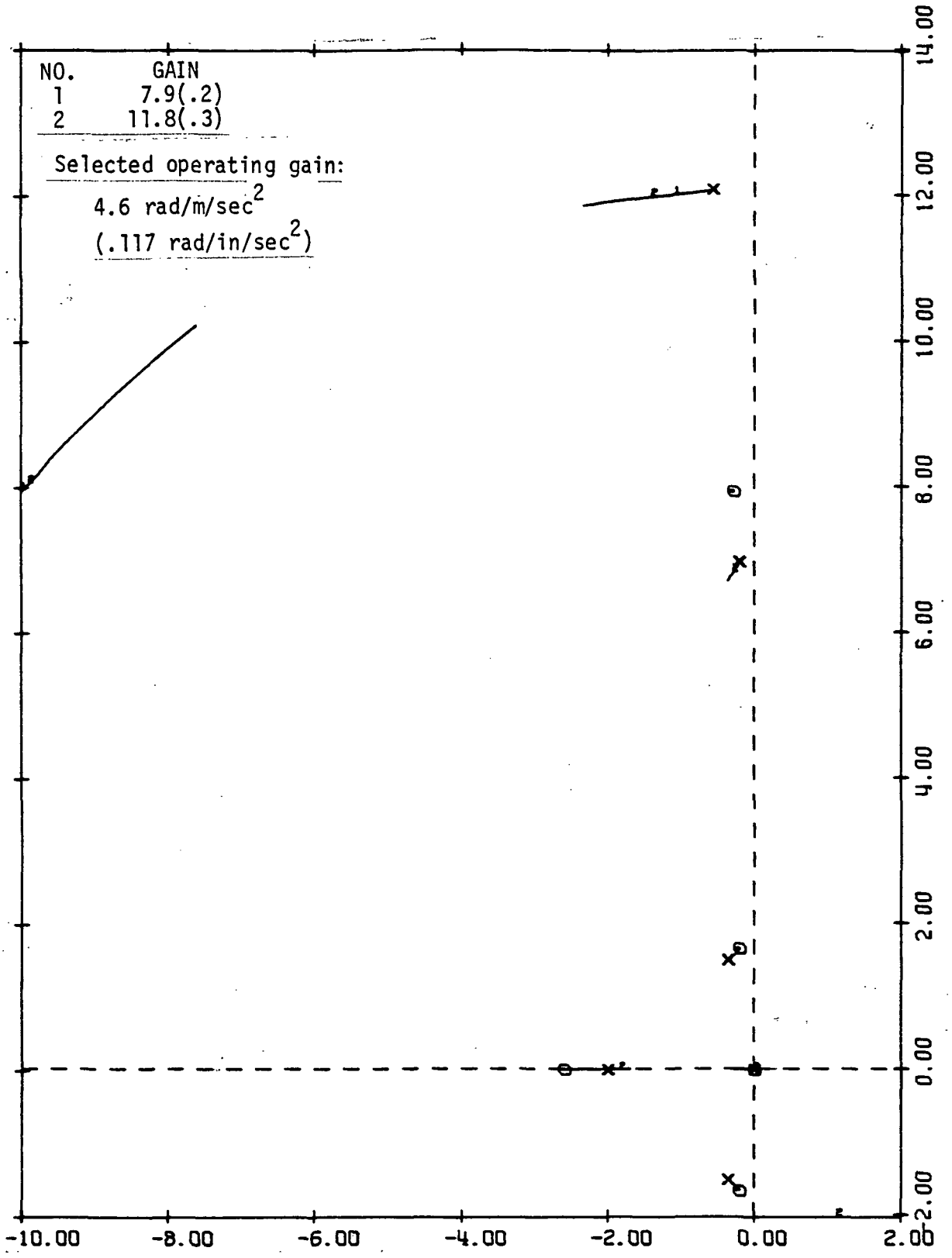

Figure B-3: GAIN ROOT LOCUS FOR MACH 2.7, $1.2V_D$

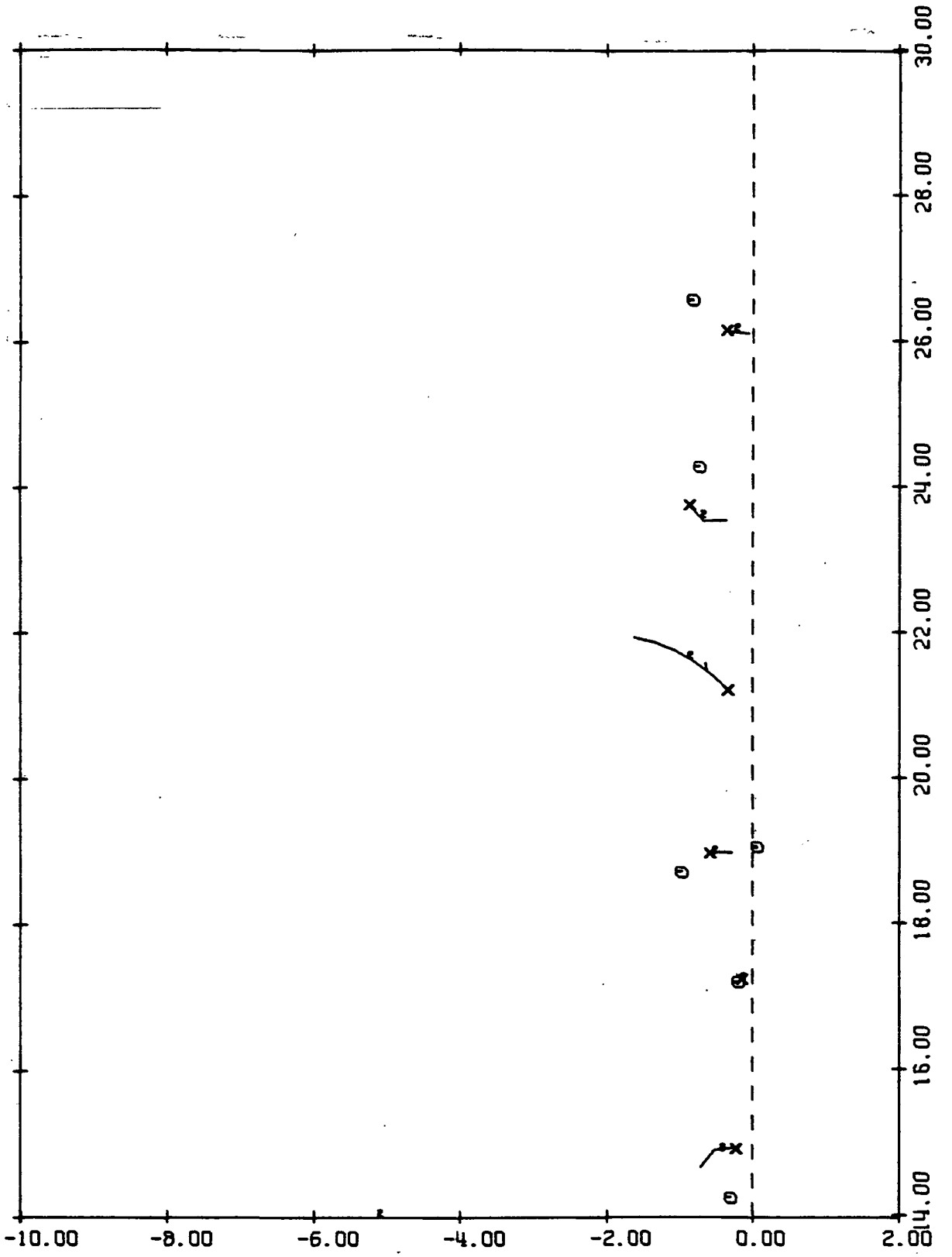

Figure B-3: CONTINUED

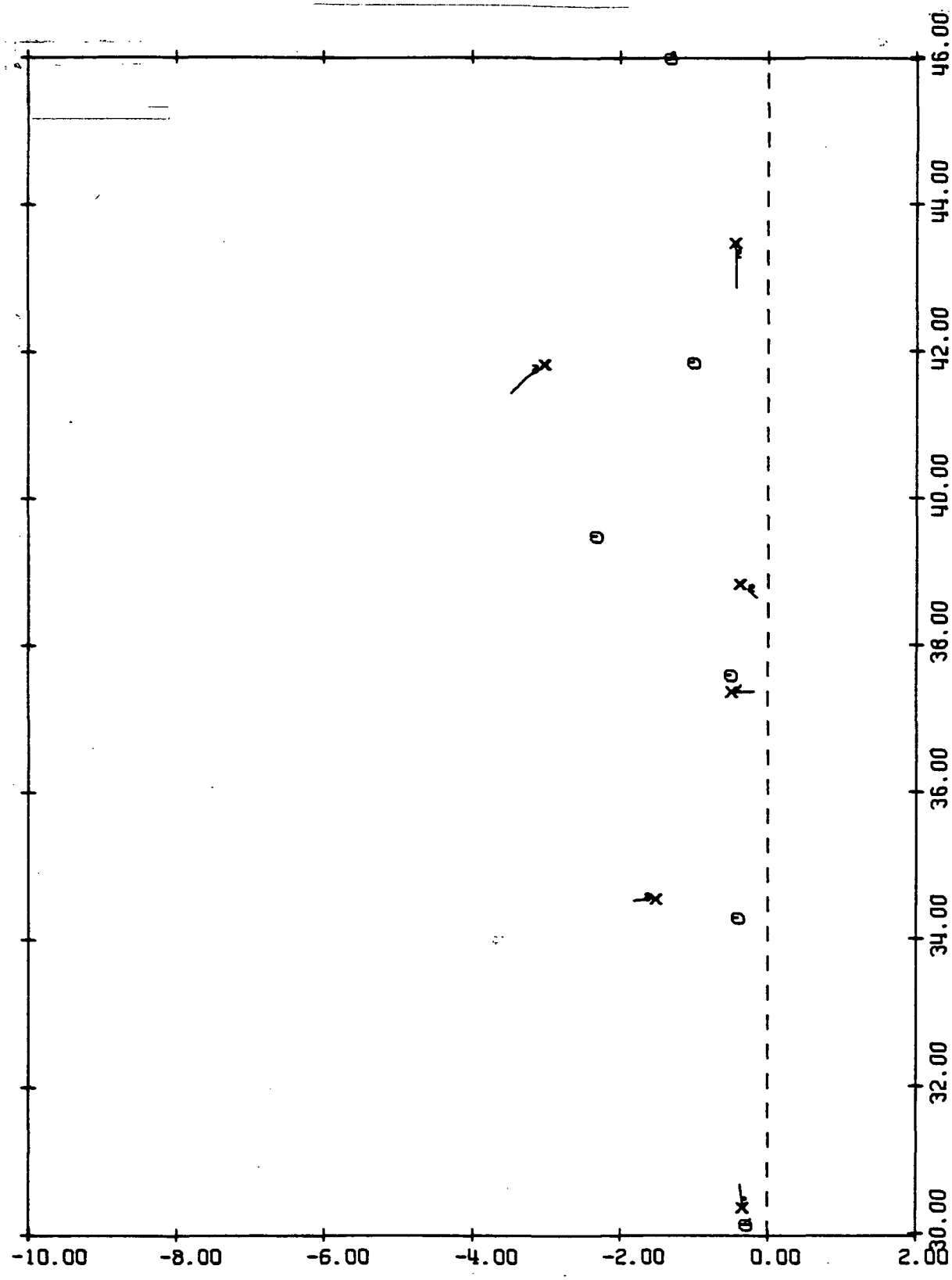

Figure B-3: CONTINUED

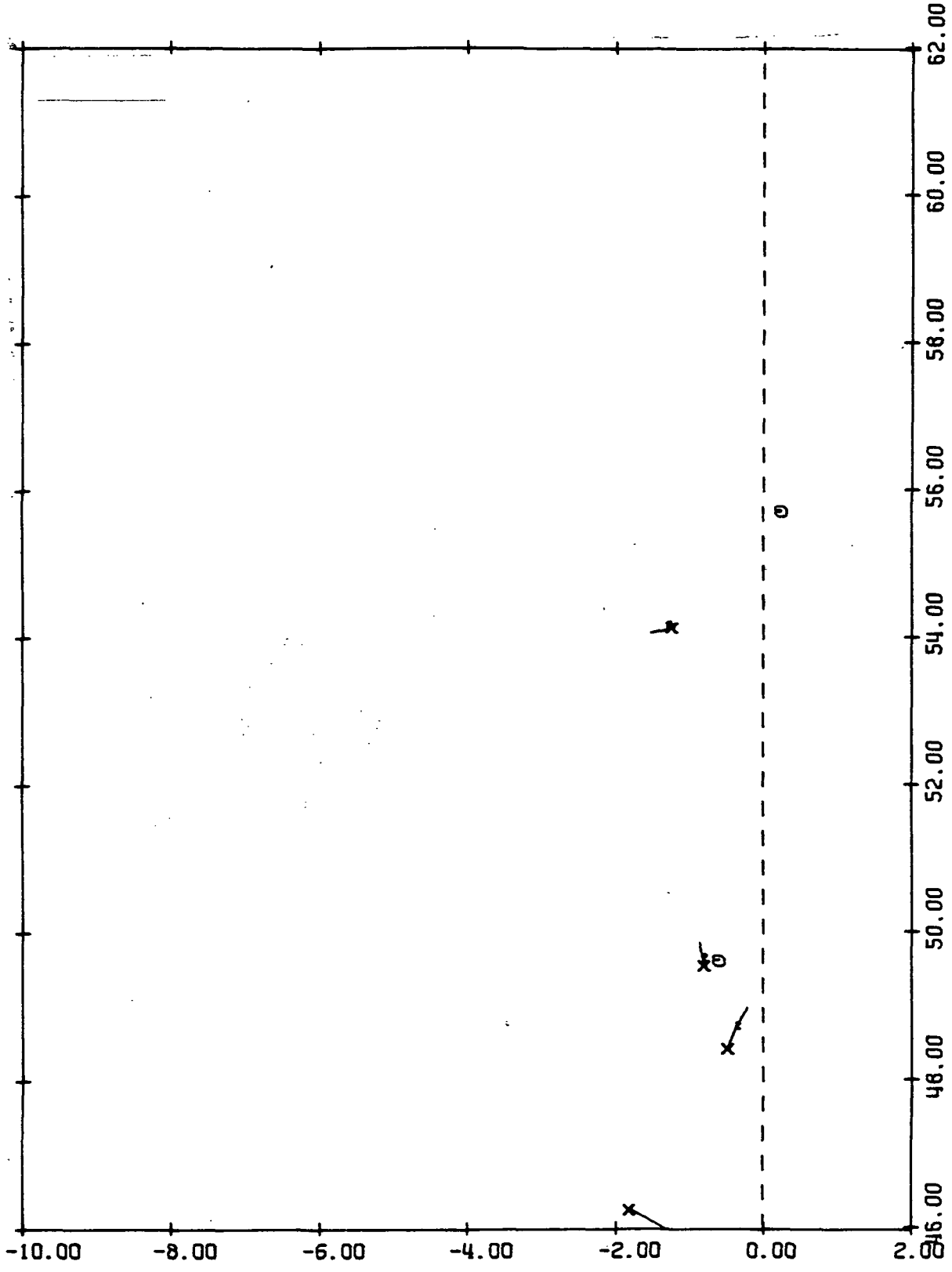

Figure B-3: CONCLUDED

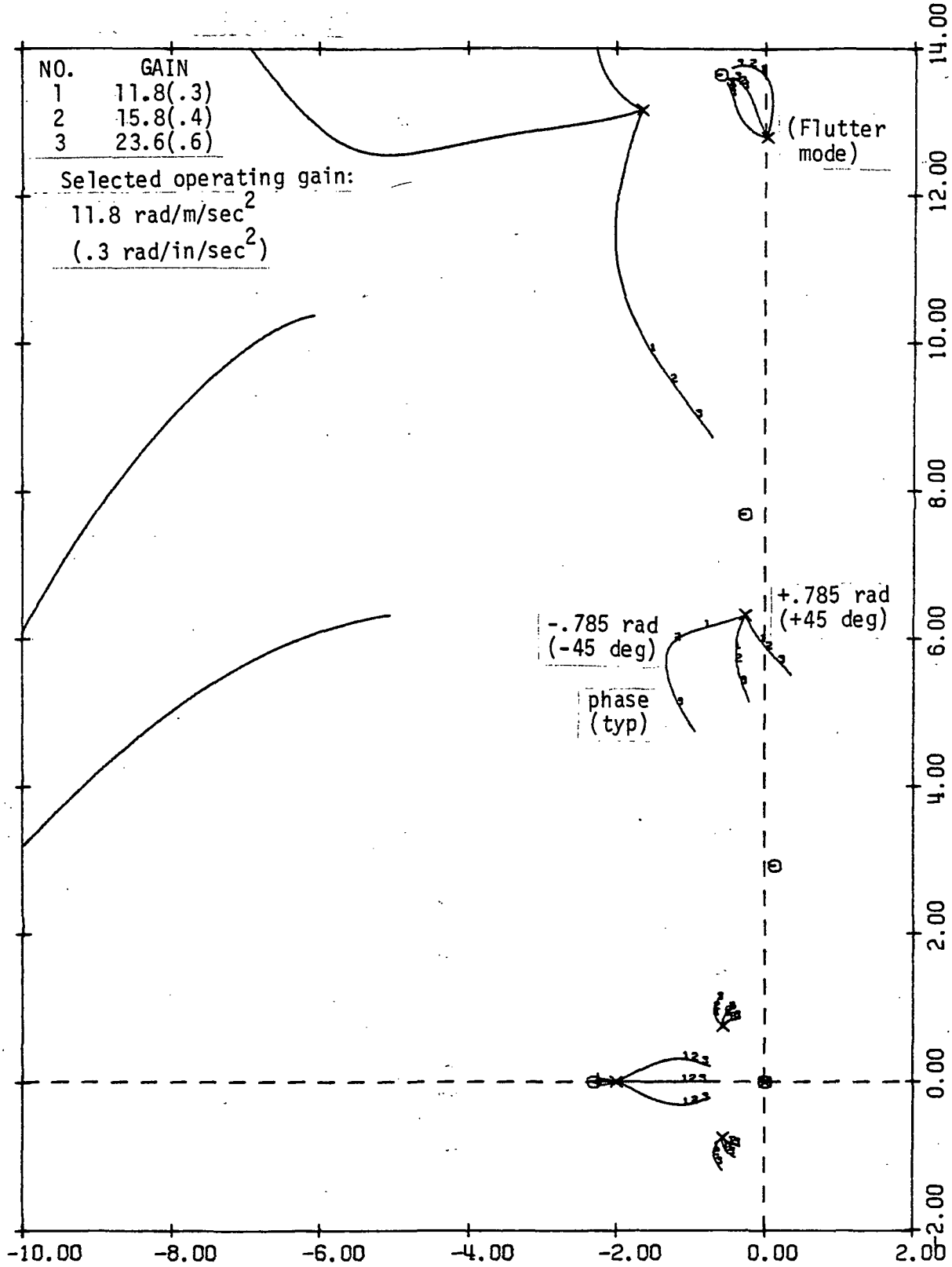

Figure B-4: PHASE-GAIN ROOT LOCUS FOR MACH 0.9, V_D

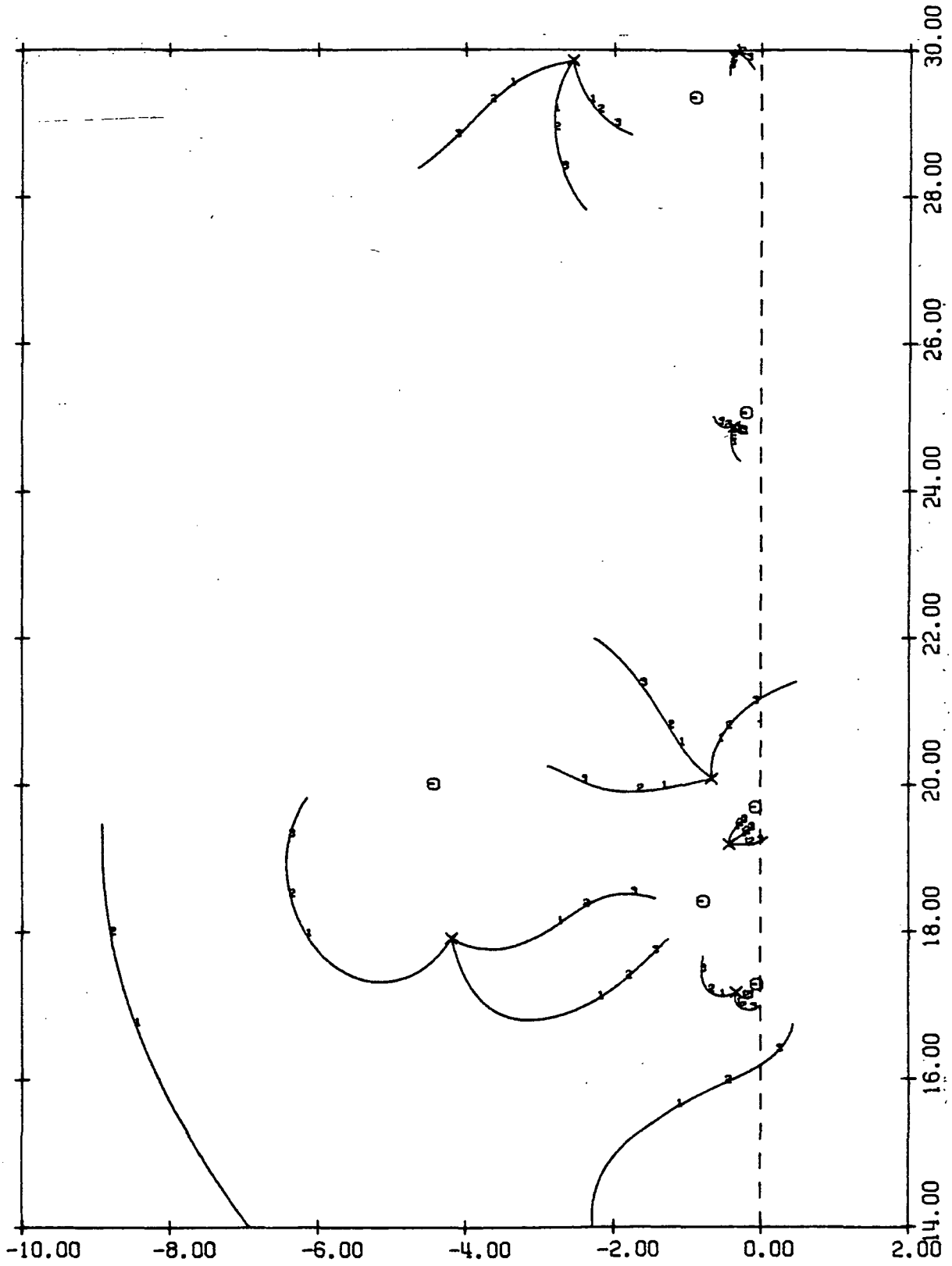

Figure B-4: CONTINUED

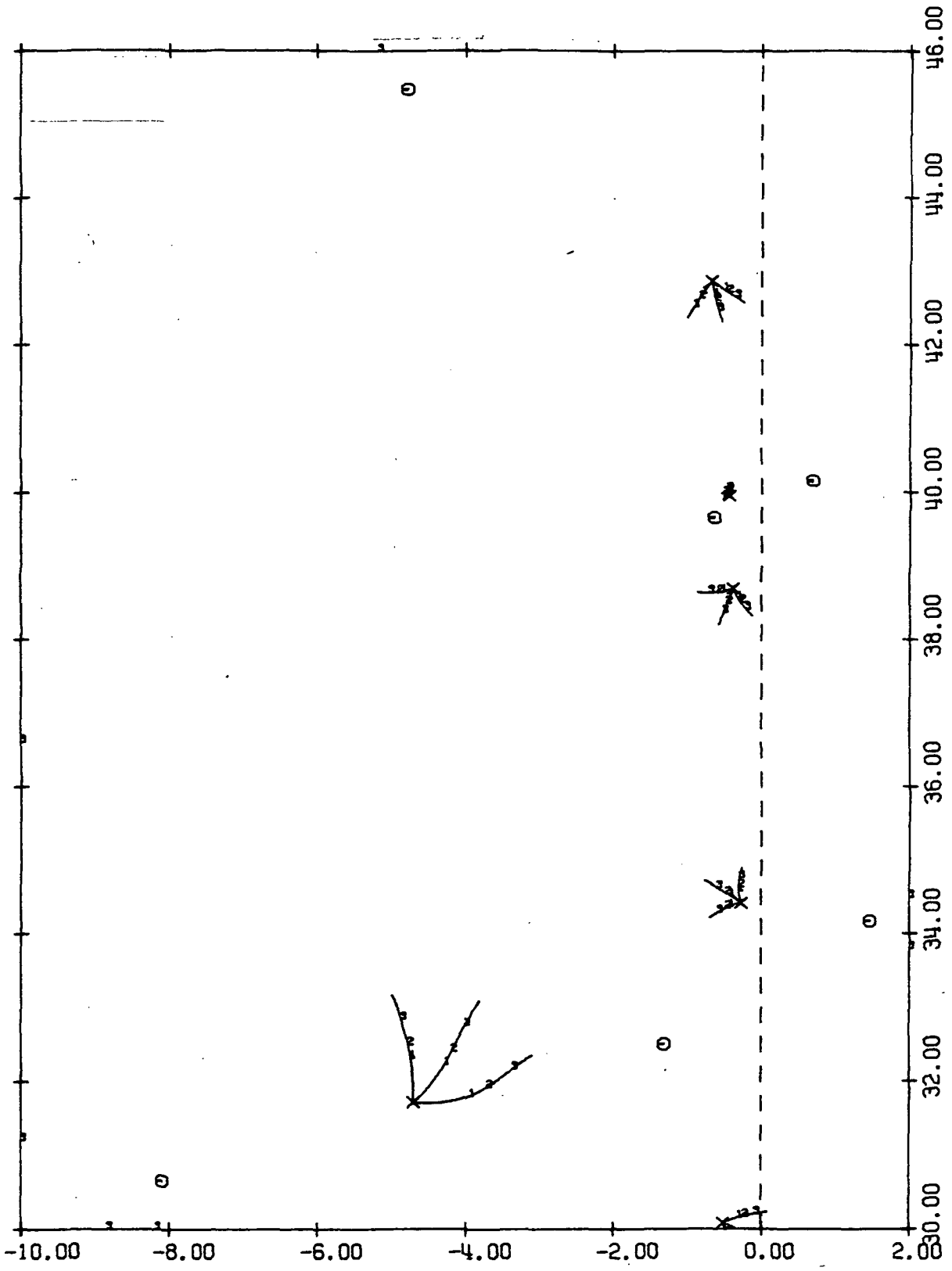

Figure B-4: CONTINUED

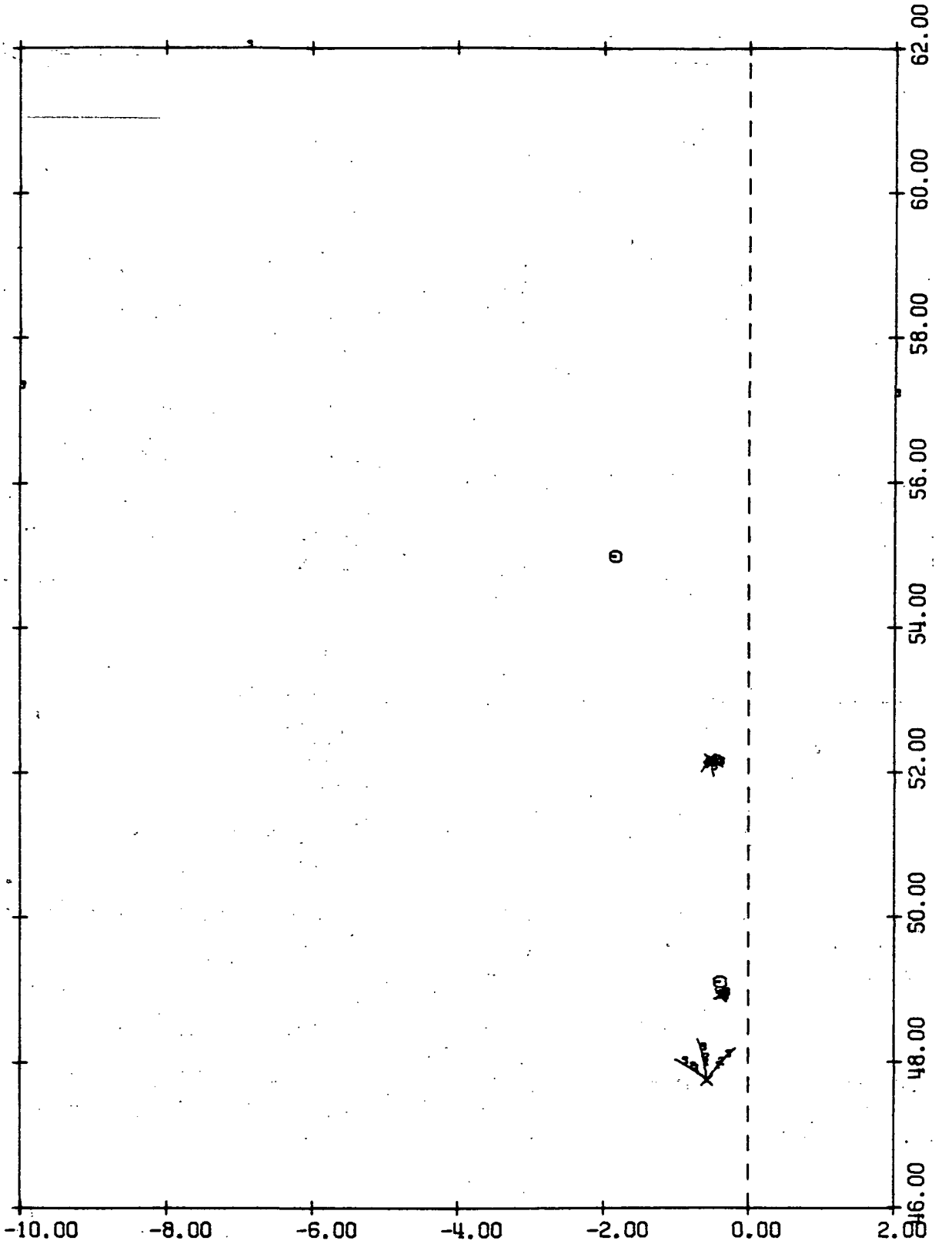

Figure B-4: CONCLUDED

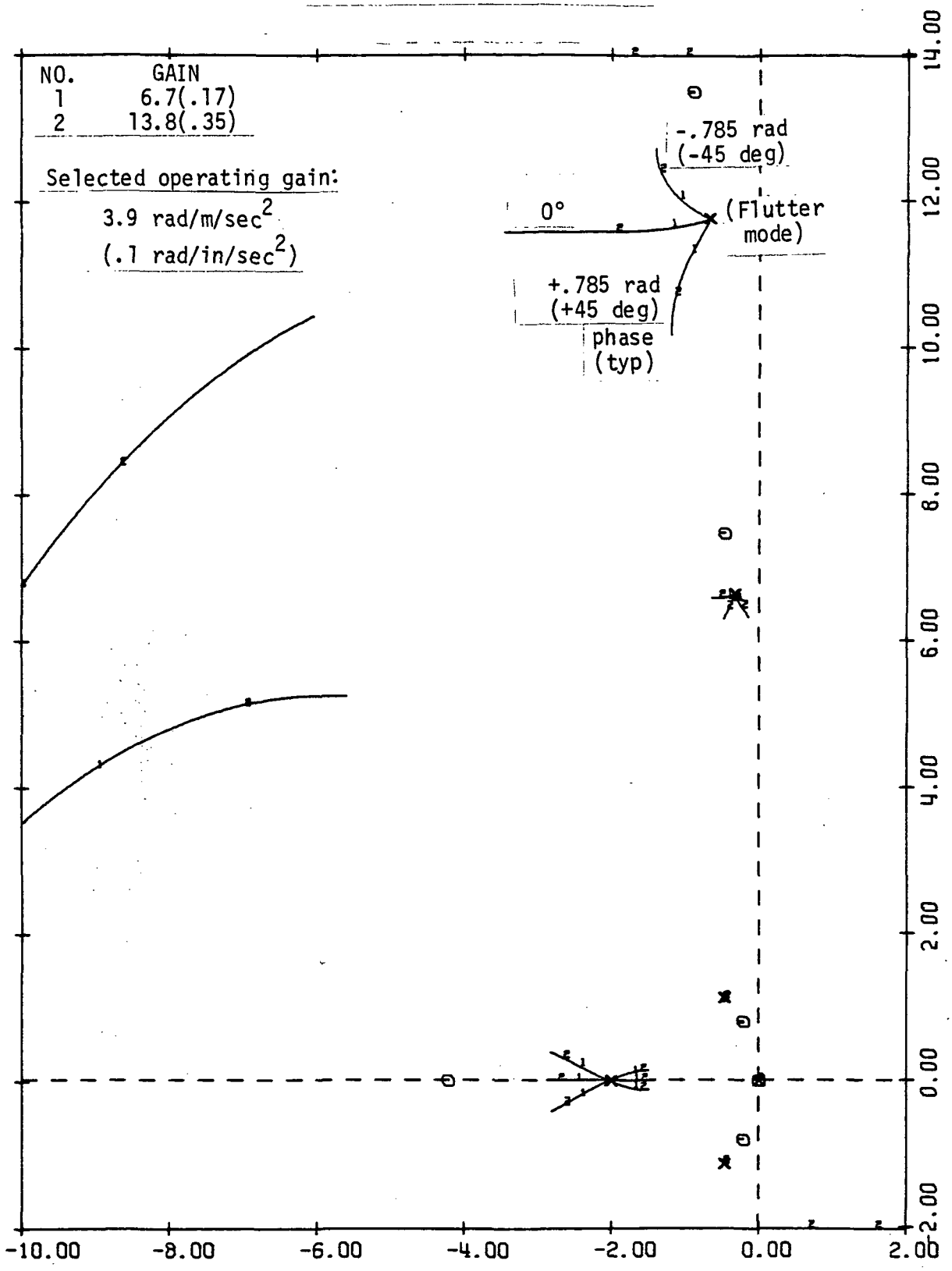

Figure B-5: PHASE-GAIN ROOT LOCUS FOR MACH 1.2, V_D

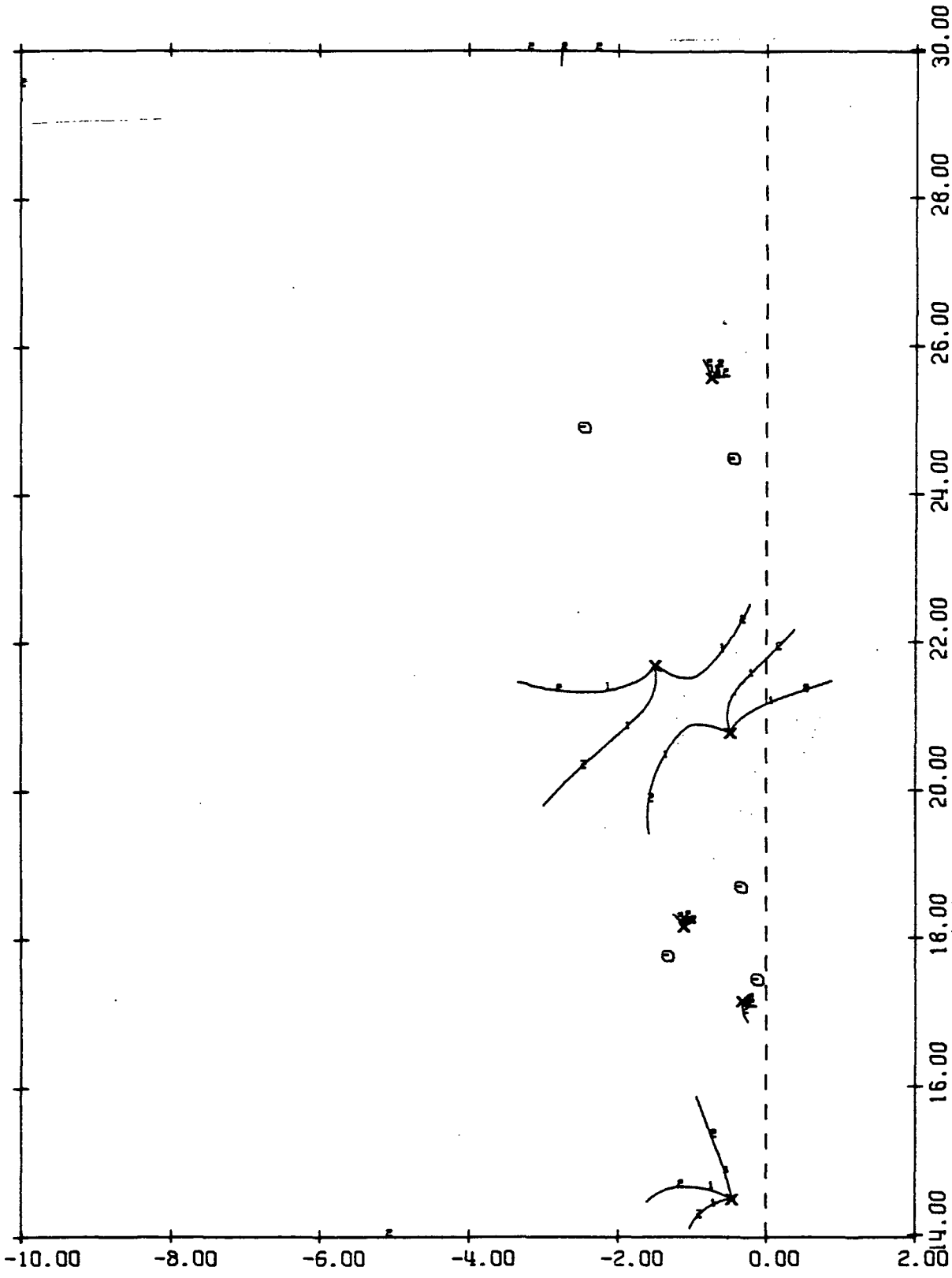

Figure B-5: CONTINUED

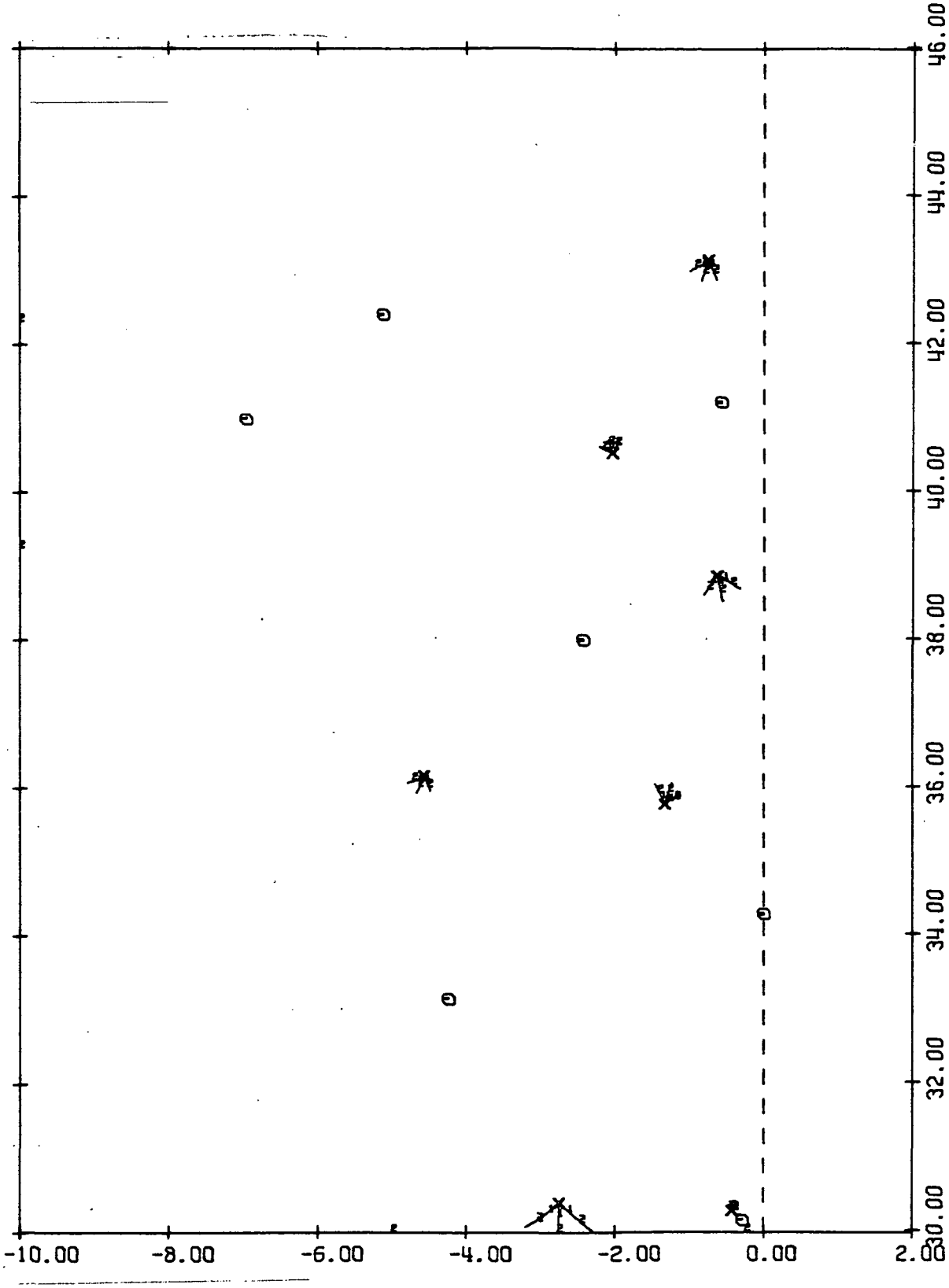

Figure B-5: CONTINUED

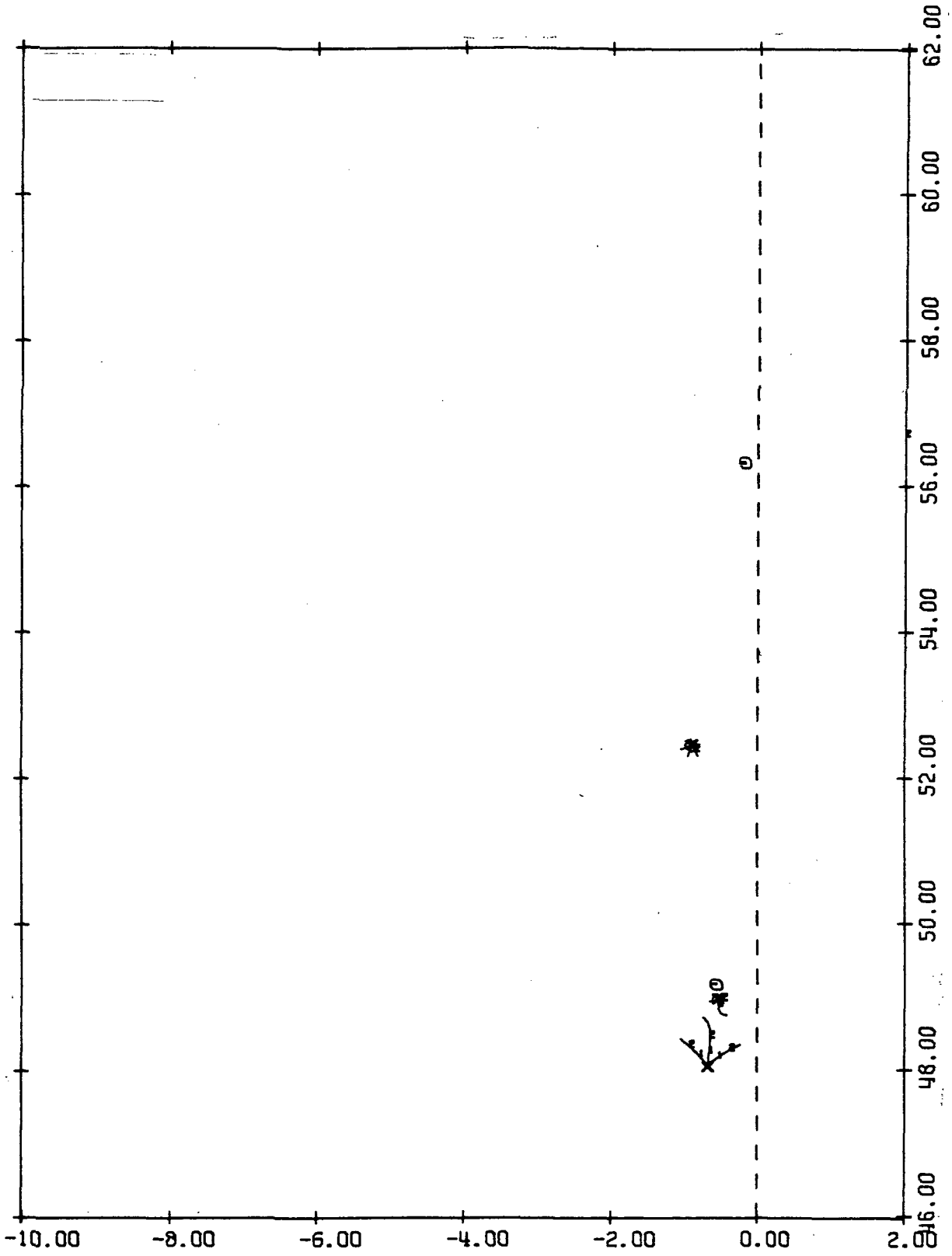

Figure B-5: CONCLUDED

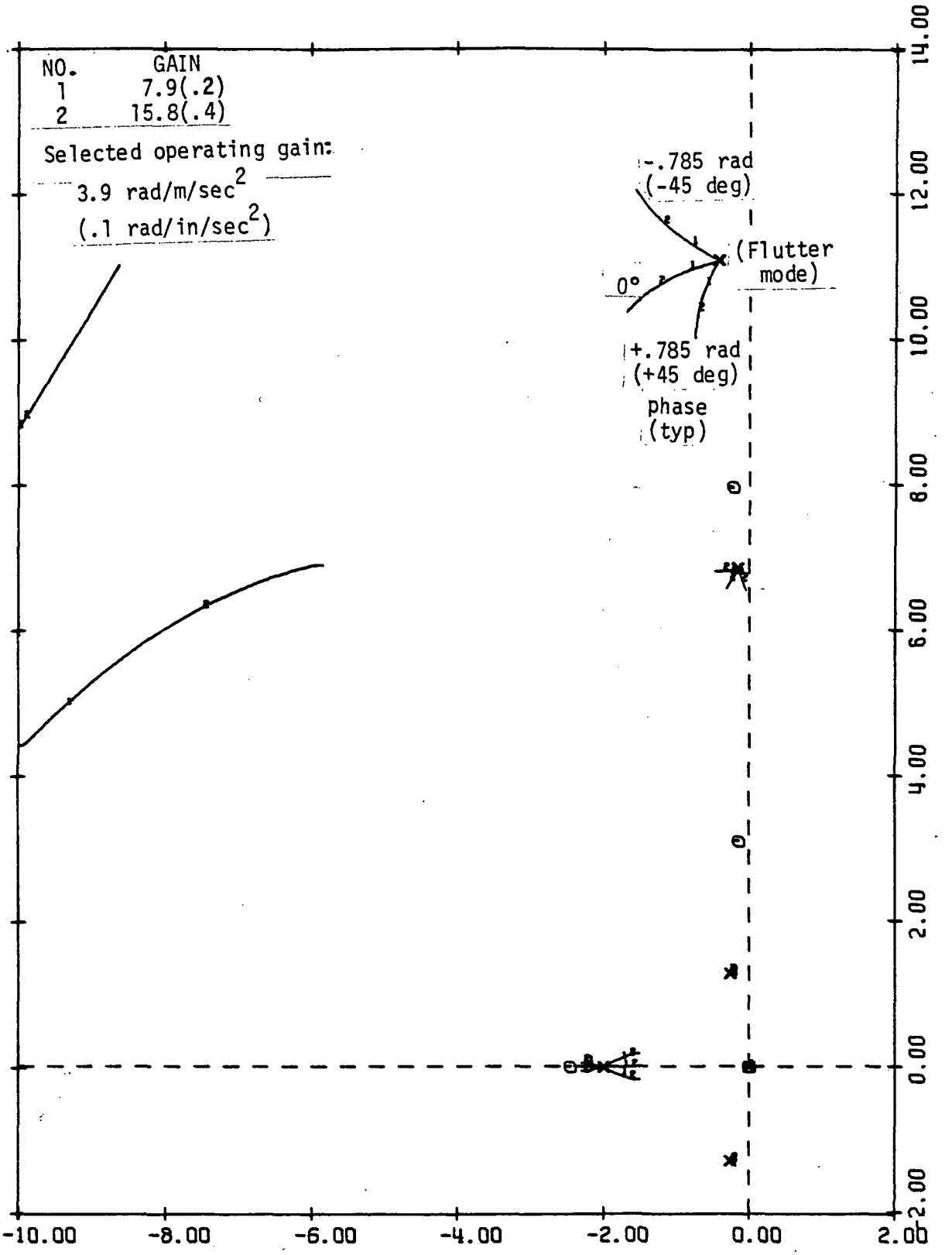

Figure B-6: PHASE-GAIN ROOT LOCUS FOR MACH 2.7, V_D

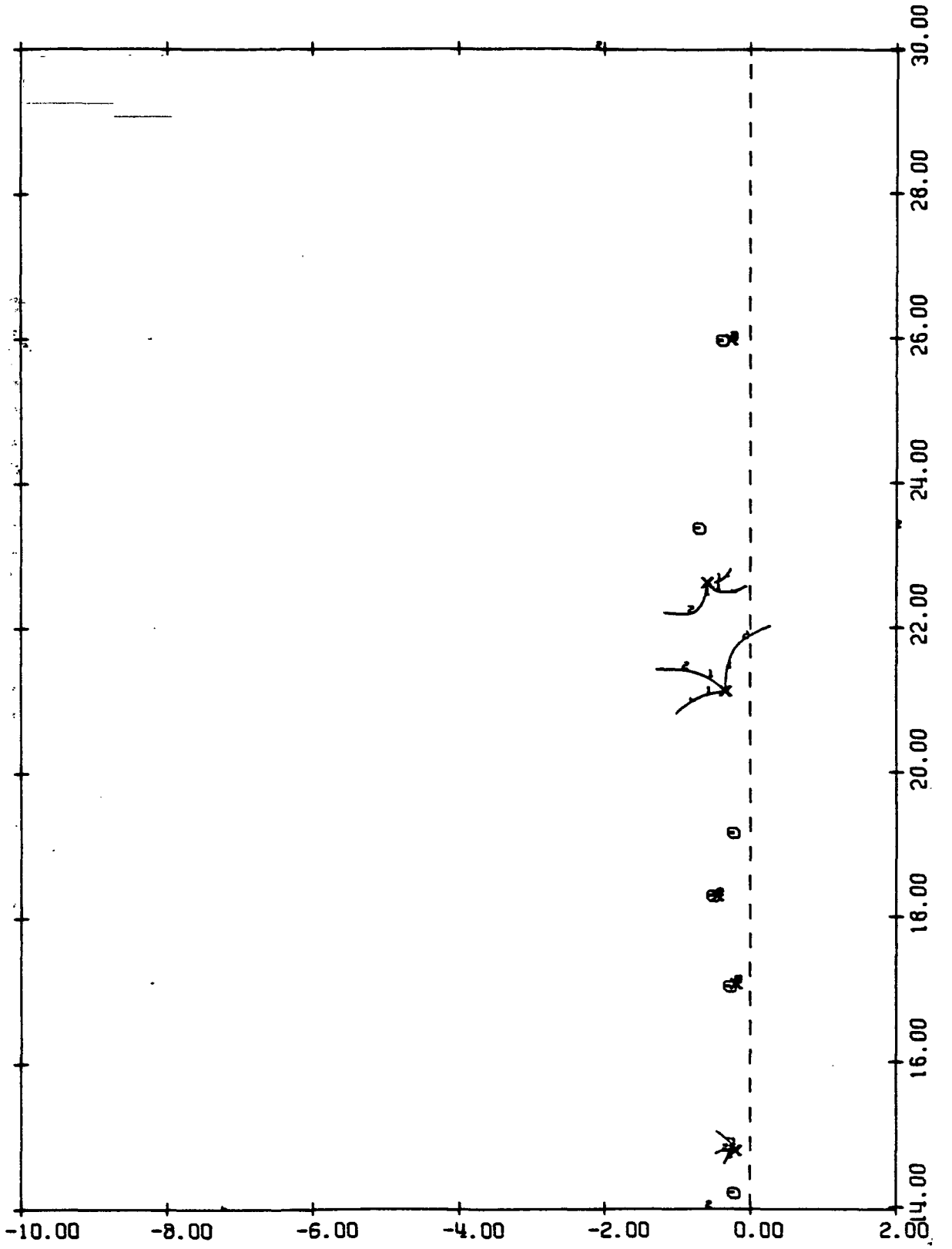

Figure B-6: CONTINUED

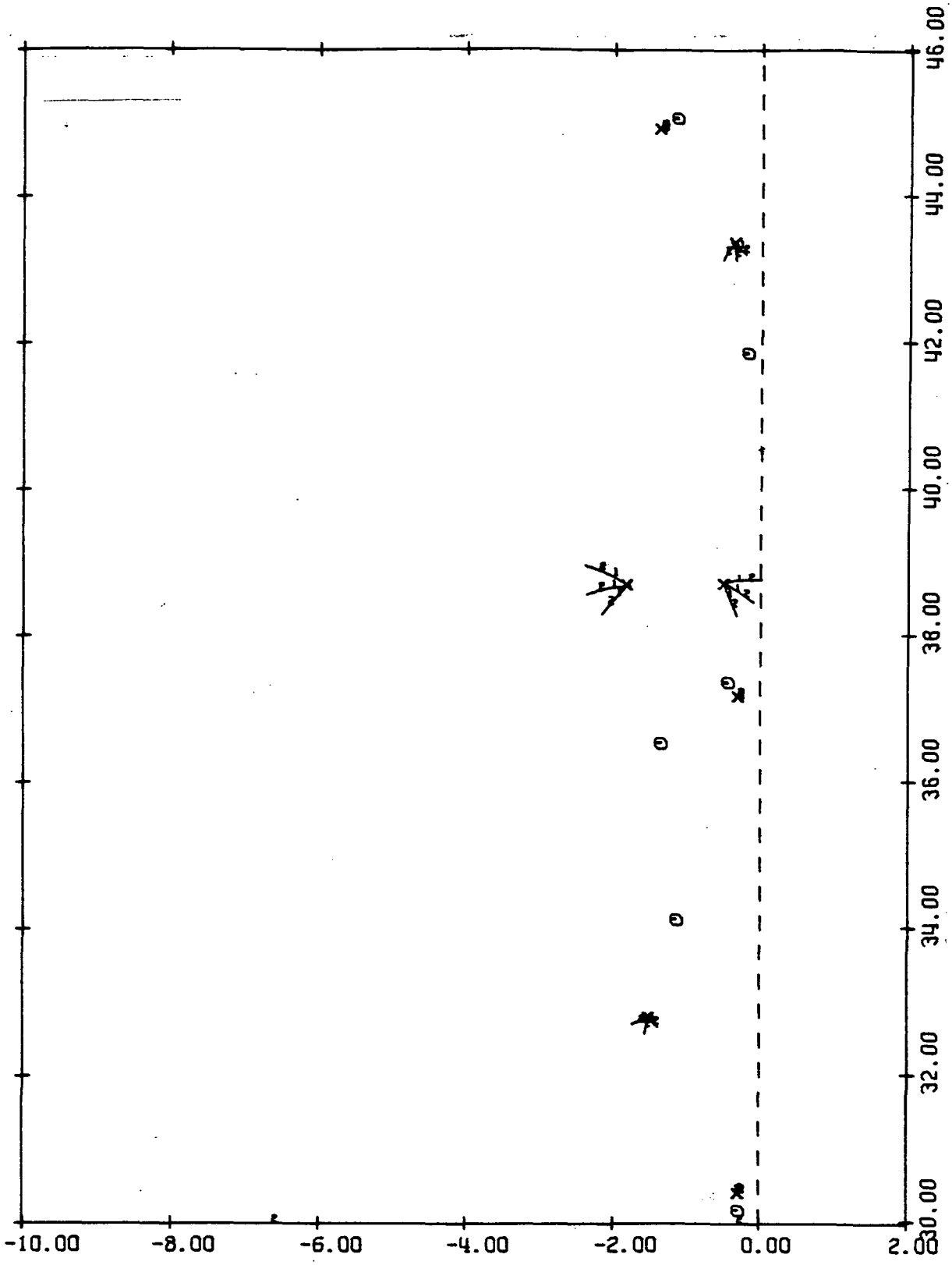

Figure B-6: CONTINUED

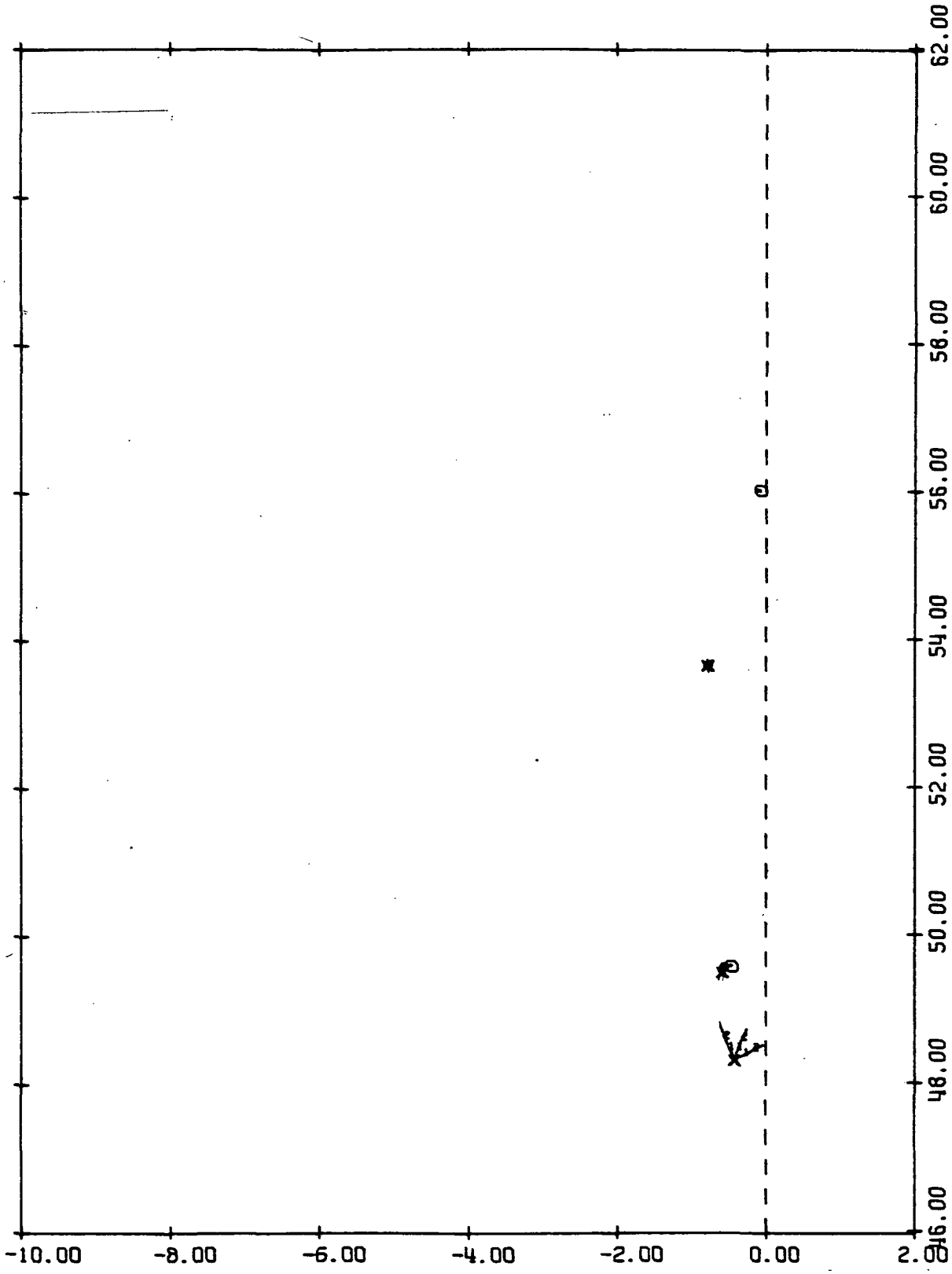

FIGURE B-6: CONCLUDED

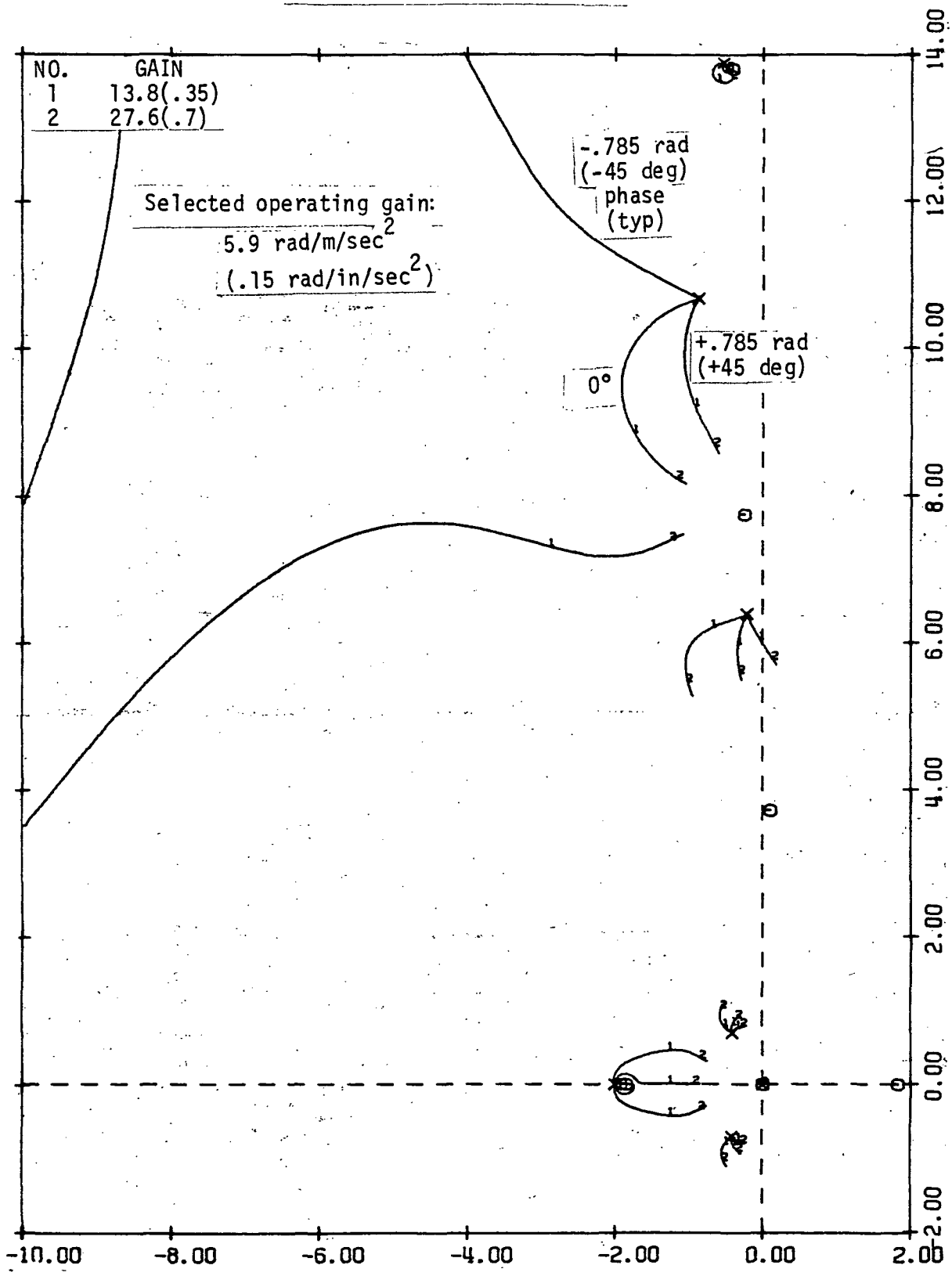

Figure B-7: PHASE-GAIN ROOT LOCUS FOR MACH 0.9, V_C

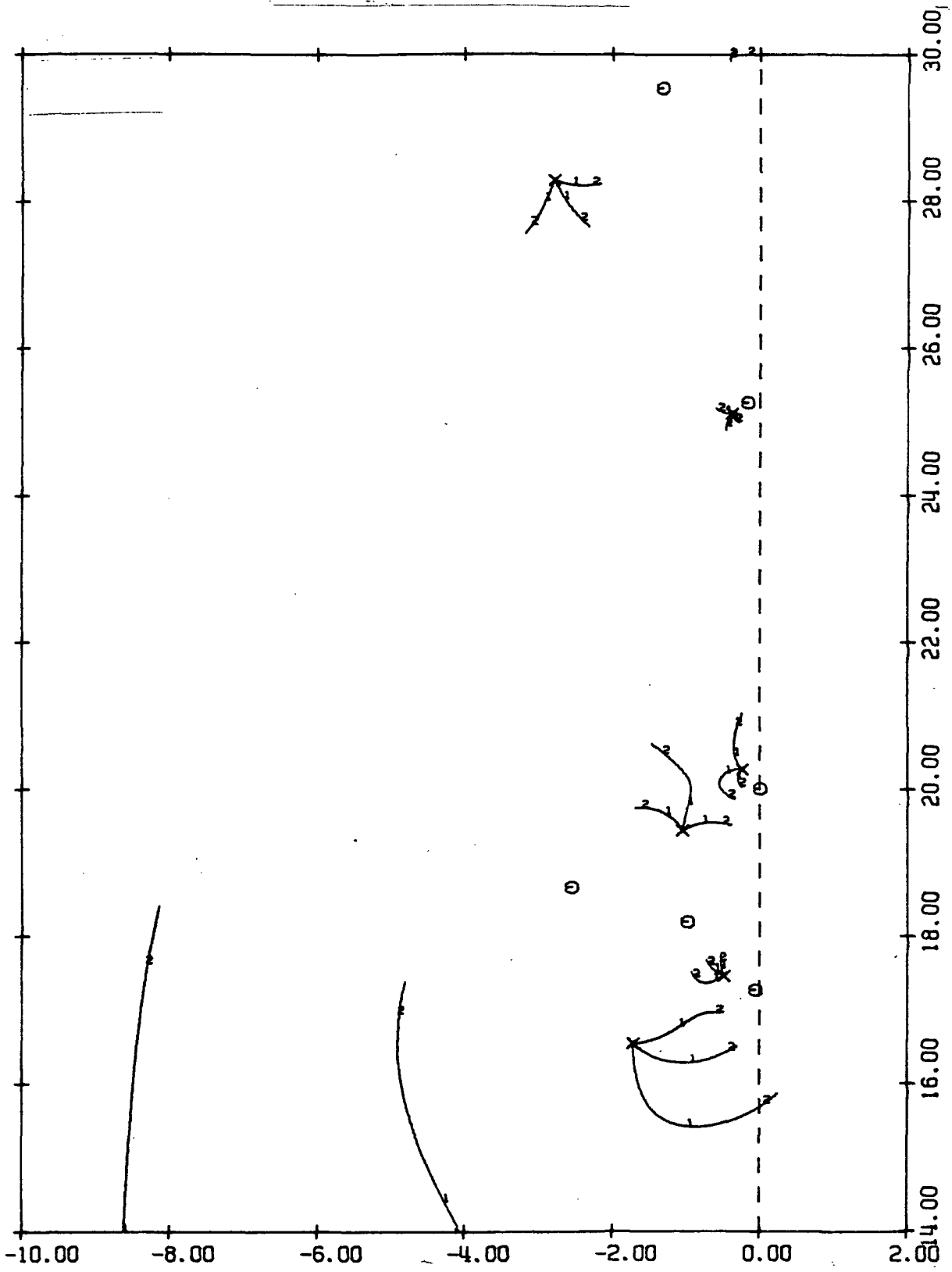

Figure B-7: CONTINUED

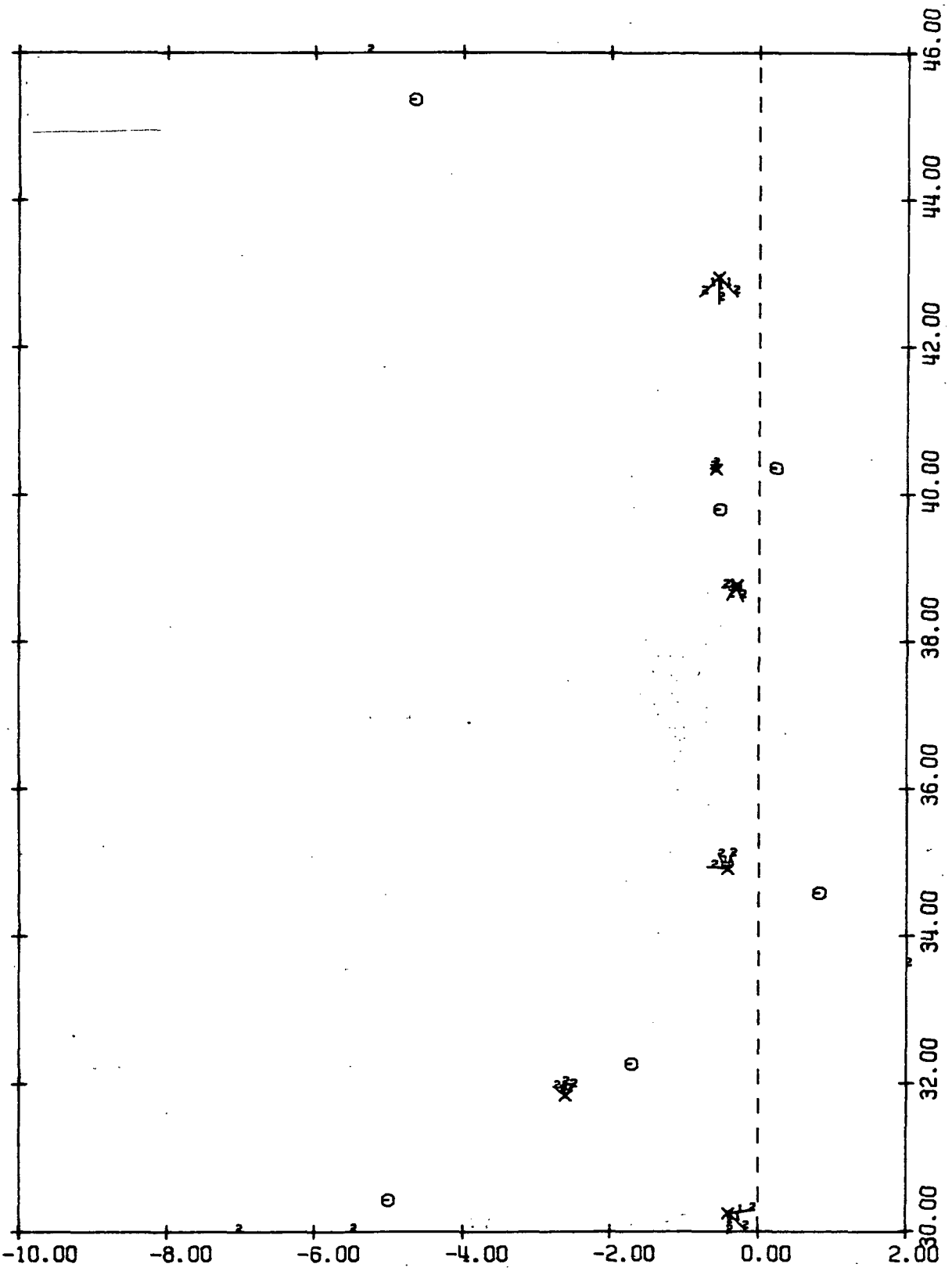

Figure B-7: CONTINUED

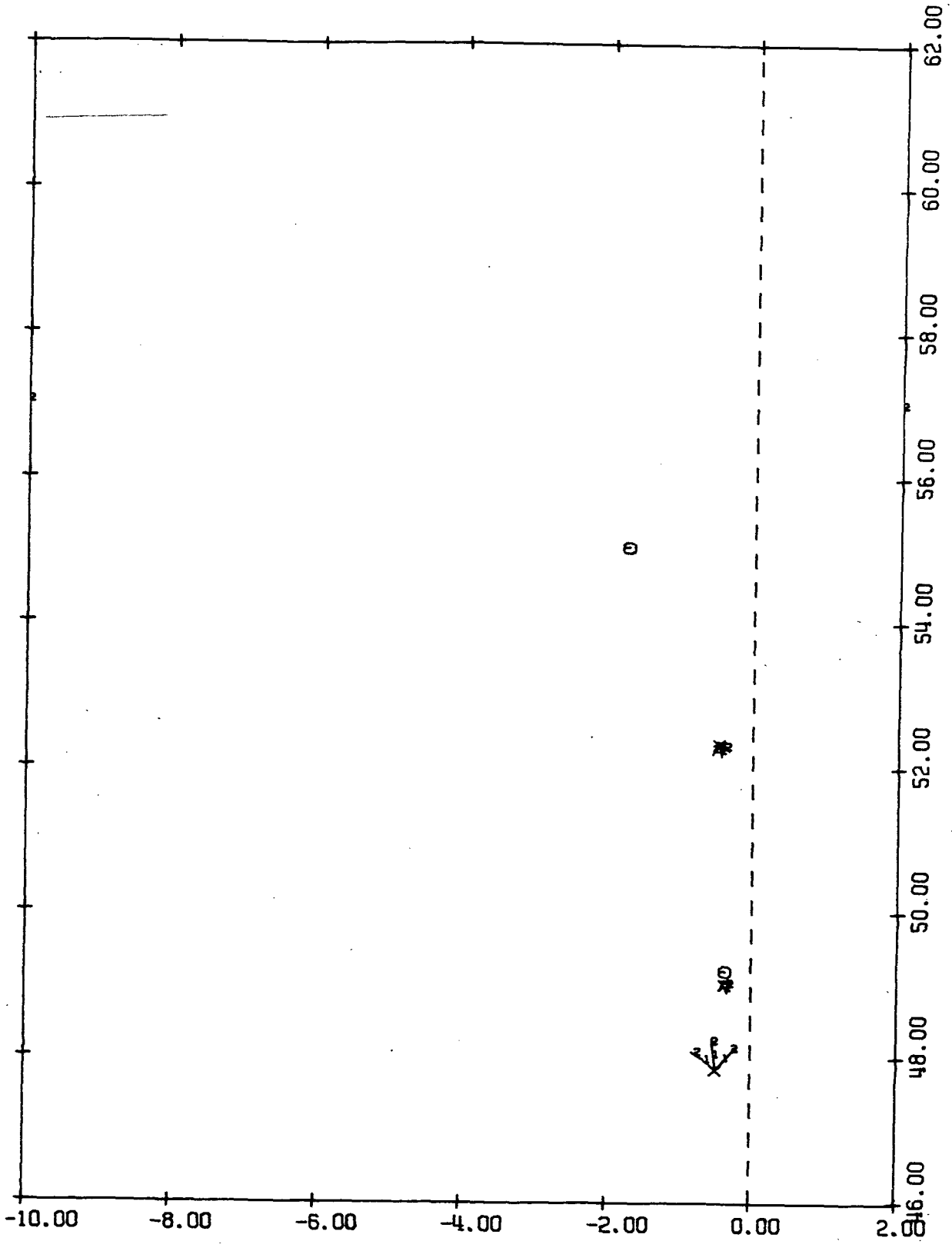

Figure B-7: CONCLUDED

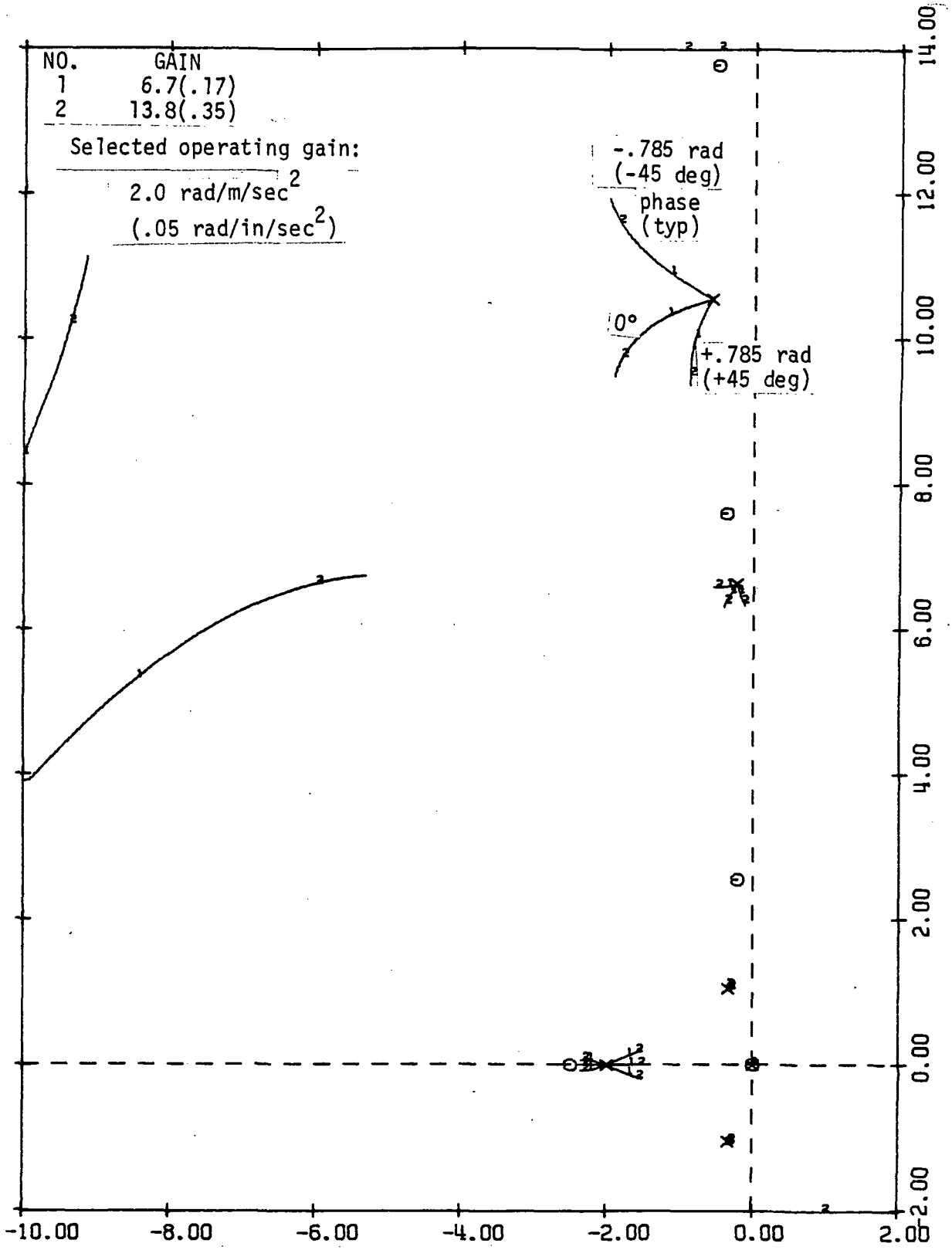

Figure B-8: PHASE-GAIN ROOT LOCUS FOR MACH 1.2, V_C

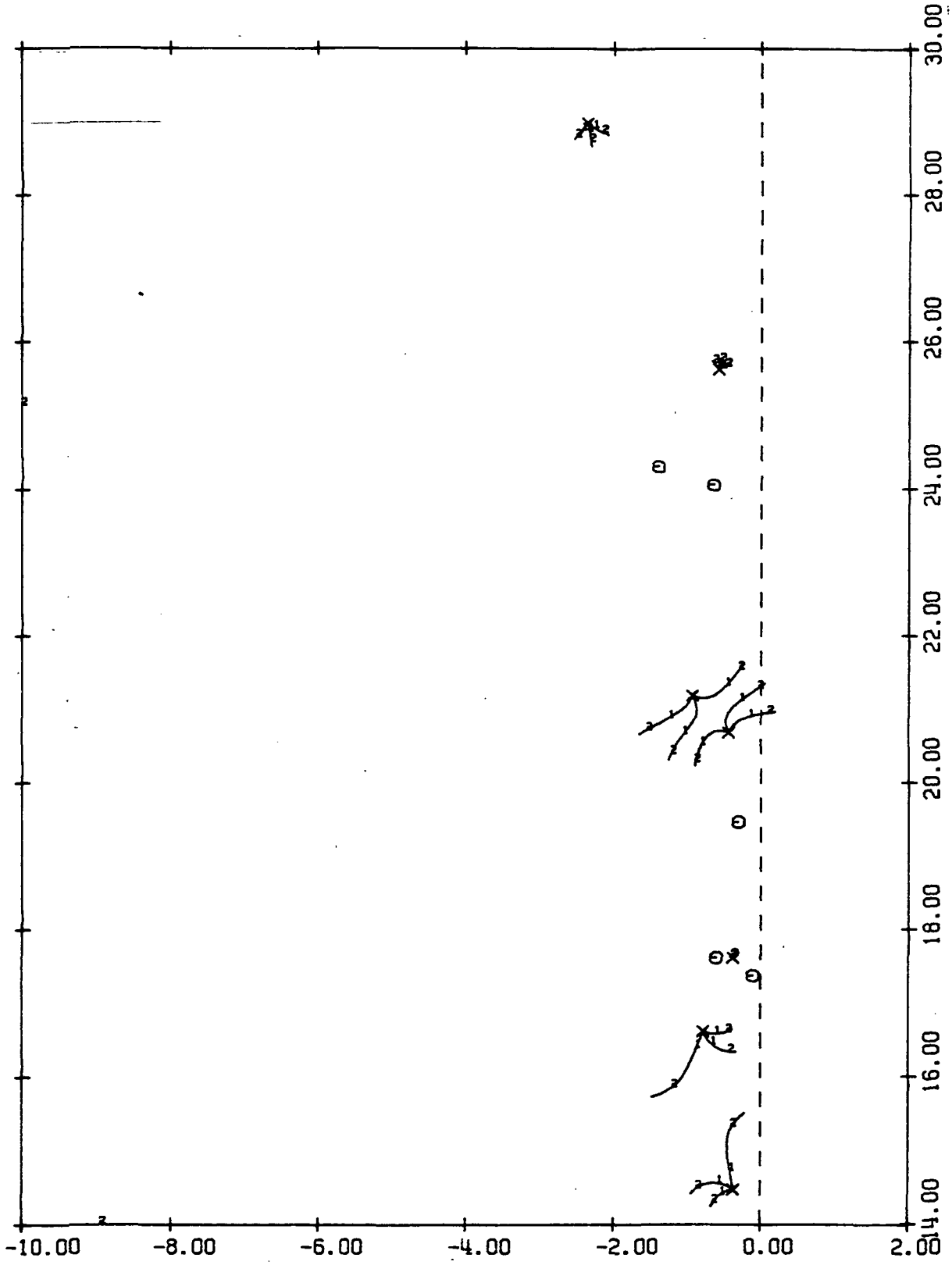

Figure B-8: CONTINUED

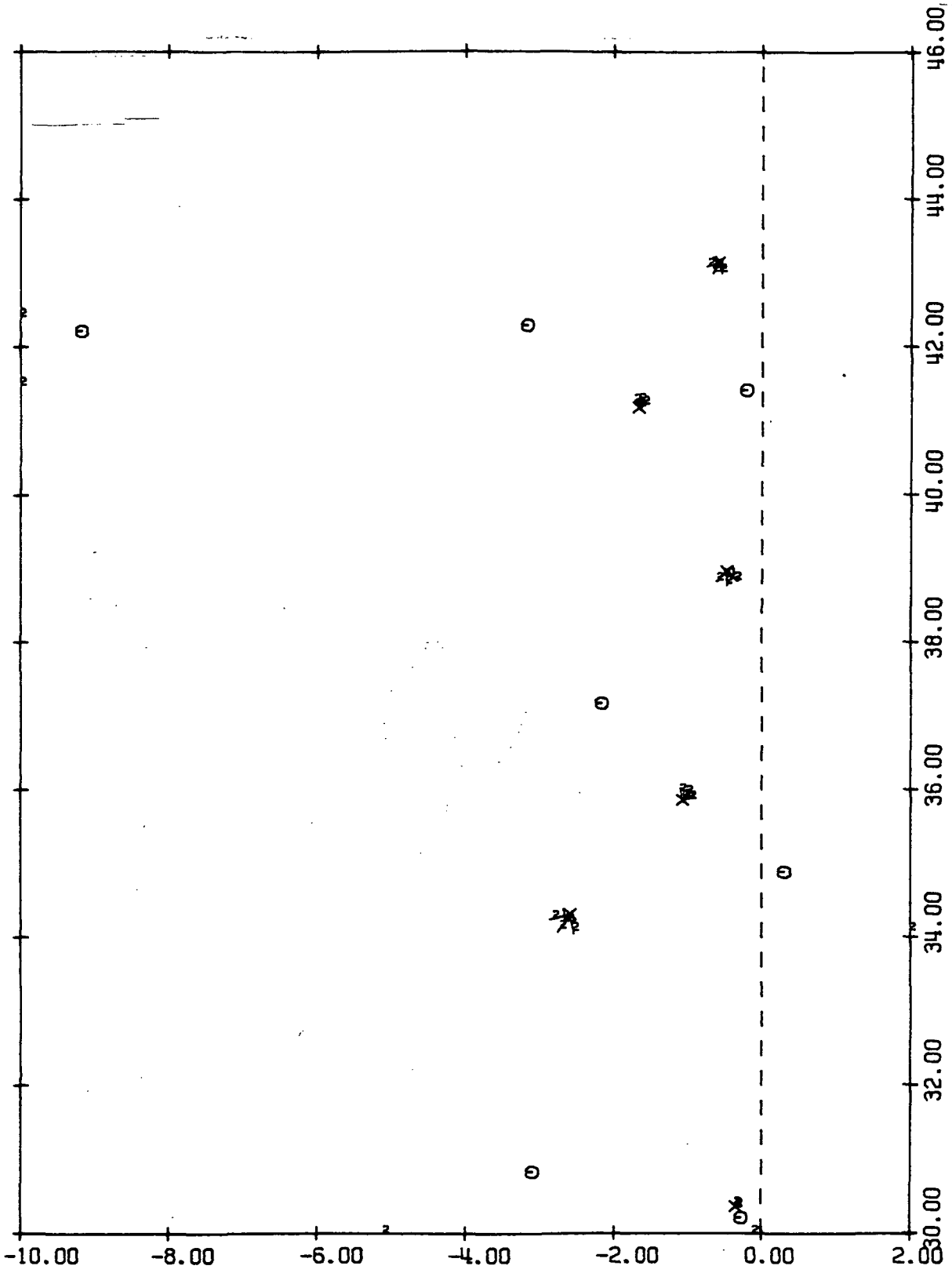

Figure B-8: CONTINUED

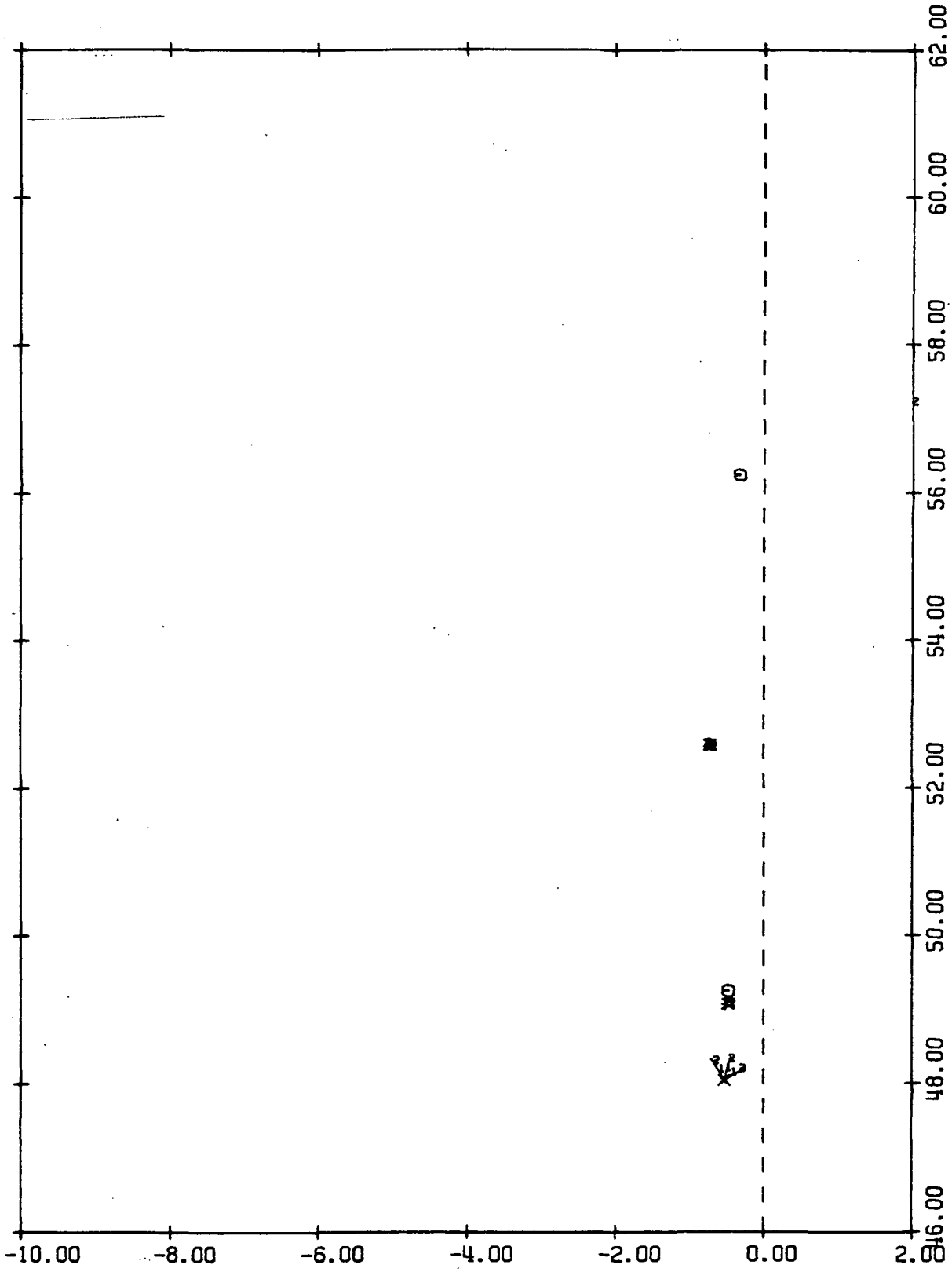

Figure B-8: CONCLUDED

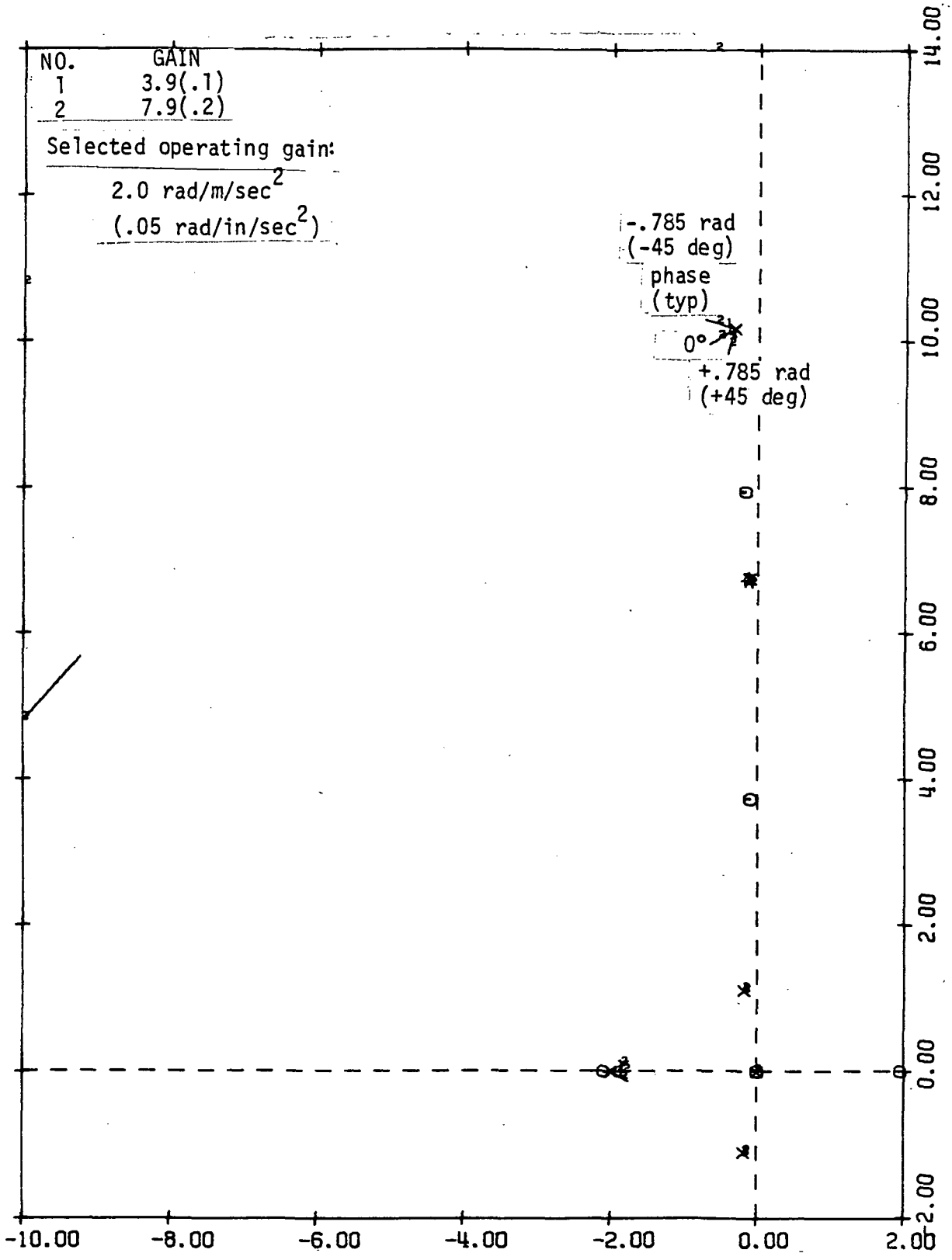

Figure B-9: PHASE-GAIN ROOT LOCUS FOR MACH 2.7, V_C

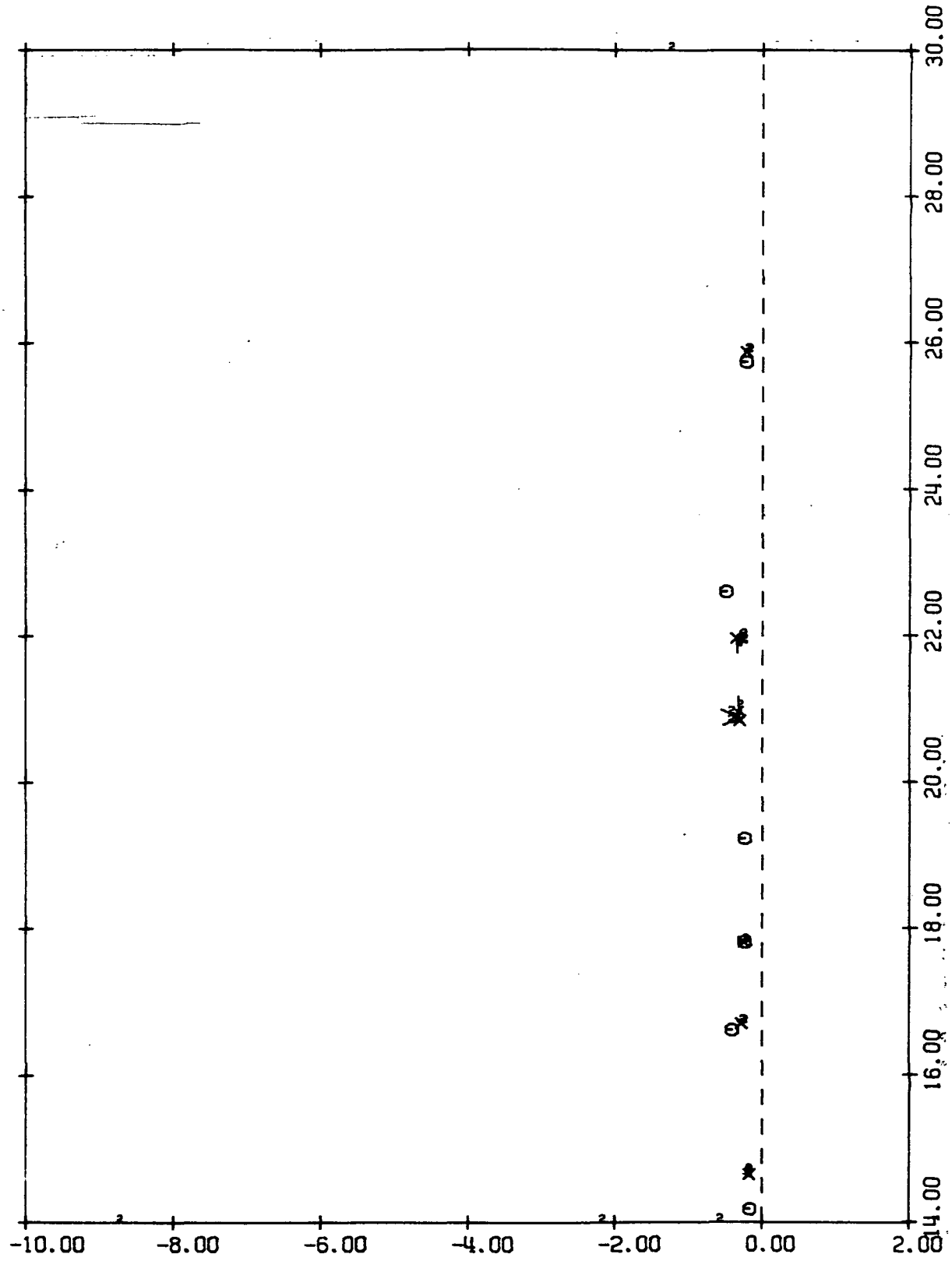

Figure B-9: CONTINUED

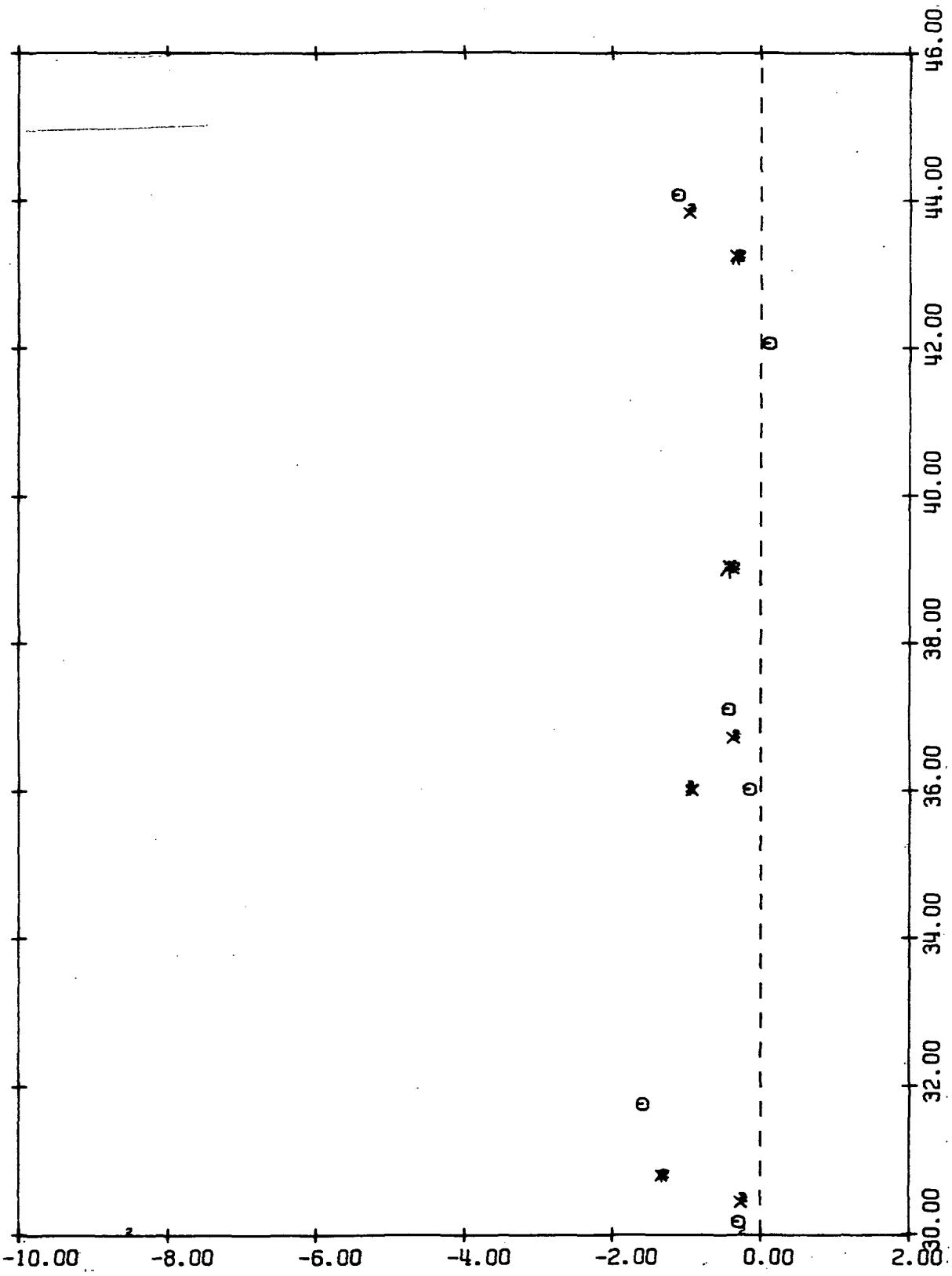

Figure B-9: CONTINUED

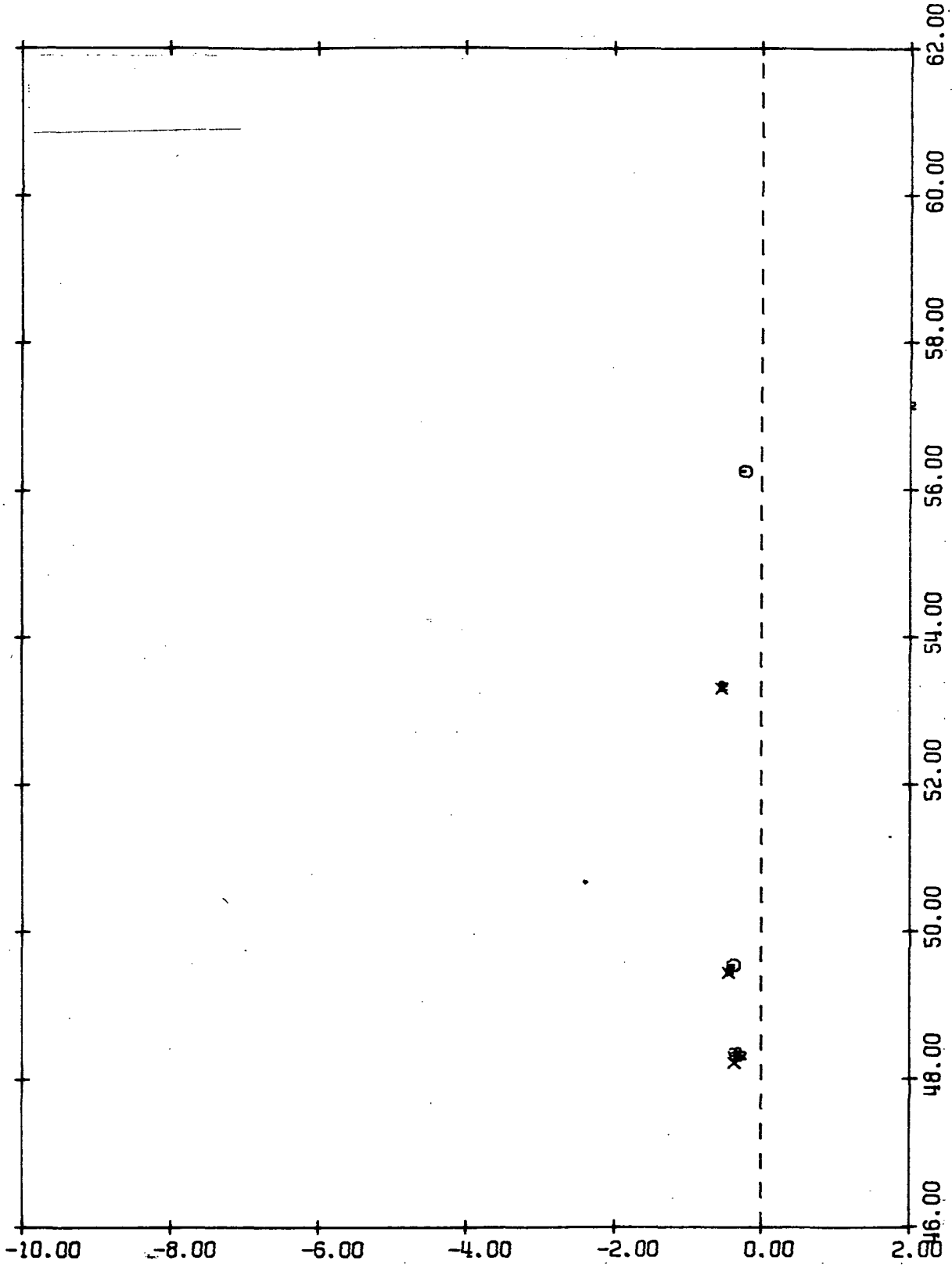

Figure B-9: CONCLUDED

TABLE B-I

AIRPLANE DAMPING AND FREQUENCY COMPARISON AT 1.2 V_D - MACH 0.9

	Airplane with HSAS		Airplane with HSAS & FSS	
	Damping ratio, ζ	Frequency rad/sec	Damping ratio, ζ	Frequency rad/sec
Short period	.587	1.15	.551	1.15
Structural modes	.057	6.30	.080	5.58
	-.075	13.45	.009	13.46
	.189	14.66	.104	17.53
	.011	17.16	.005	17.08
	.010	19.15	.017	19.05
	.072	19.74	.097	21.61
	.376	20.75	.482	23.60
	.008	24.71	.003	24.63
	.021	29.83	.085	29.57
	.062	30.47	.009	29.73
	.001	33.68	.011	33.60
	.209	33.70	.174	34.44
	.016	38.54	.016	38.15
	.004	39.67	.006	39.66
	.020	42.75	.016	42.44
	.014	47.78	.015	48.11

TABLE B-II

AIRPLANE DAMPING AND FREQUENCY COMPARISON AT 1.2 V_D - MACH 1.2

	Airplane with HSAS		Airplane with HSAS & FSS	
	Damping ratio, ζ	Frequency rad/sec	Damping ratio, ζ	Frequency rad/sec
Short period	.449	1.46	.447	1.42
Structural modes	.066	6.72	.066	6.70
	.066	13.57	.048	13.16
	.029	14.30	.063	14.68
	.010	17.24	.008	17.24
	.077	19.40	.050	19.32
	.024	29.44	.043	21.89
	.102	23.85	.127	22.96
	.039	25.37	.033	25.46
	.018	30.17	.018	30.18
	.098	32.02	.101	31.87
	.059	35.57	.058	35.68
	.019	38.66	.019	38.56
	.200	38.91	.200	38.90
	.040	40.04	.041	40.04
	.022	43.14	.022	43.04
	.015	48.04	.015	48.21

TABLE B-III

AIRPLANE DAMPING AND FREQUENCY COMPARISON AT 1.2 V_D - MACH 2.7

	Airplane with HSAS		Airplane with HSAS & FSS	
	Damping ratio, ζ	Frequency rad/sec	Damping ratio, ζ	Frequency rad/sec
Short period	.245	1.62	.244	1.62
Structural modes	.023	7.04	.027	6.70
	.048	12.08	.070	12.06
	.014	14.93	.020	14.94
	.009	17.25	.009	17.25
	.030	18.98	.030	18.99
	.016	21.22	.024	21.38
	.036	23.78	.035	23.71
	.014	26.16	.013	26.16
	.011	30.37	.011	30.38
	.044	34.56	.046	34.55
	.013	37.41	.012	37.40
	.010	38.83	.009	38.80
	.071	41.95	.073	41.91
	.010	43.47	.010	43.38
	.053	46.94	.051	46.94
	.015	48.31	.015	48.48

TABLE B-IV

AIRPLANE DAMPING AND FREQUENCY COMPARISON AT V_D - MACH 0.9

	Airplane with HSAS		Airplane with HSAS & FSS	
	Damping ratio, ζ	Frequency rad/sec	Damping ratio, ζ	Frequency rad/sec
Short period	.480	1.06	.426	1.13
Structural modes	.044	6.37	.069	5.94
	.001	12.83	.023	13.47
	.123	13.25	.463	18.57
	.019	12.17	.019	17.02
	.231	18.25	.135	17.11
	.018	19.19	.011	19.30
	.032	20.12	.049	20.53
	.014	24.88	.015	24.80
	.085	30.04	.095	29.38
	.017	30.08	.011	30.00
	.145	32.02	.130	32.45
	008	34.43	.012	34.51
	.010	38.71	.011	38.56
	.011	39.99	.012	40.00
	.016	42.87	.015	42.68
	.011	47.83	.012	48.04

TABLE B-V

AIRPLANE DAMPING AND FREQUENCY COMPARISON AT V_D - MACH 1.2

	Airplane with HSAS		Airplane with HSAS & FSS	
	Damping ratio, ζ	Frequency rad/sec	Damping Ratio, ζ	Frequency rad/sec
Short period	.367	1.33	.369	1.33
Structural modes	.049	6.69	.052	6.65
	.059	11.78	.082	11.74
	.031	14.50	.042	14.60
	.019	17.16	.018	17.14
	.061	18.20	.060	18.23
	.023	20.79	.080	21.14
	.071	21.69	.019	21.30
	.029	25.58	.029	25.62
	.014	30.28	.014	30.29
	.089	30.51	.089	30.40
	.037	35.78	.037	35.83
	.128	36.30	.128	36.27
	.016	38.87	.016	38.81
	.047	40.53	.048	40.56
	.017	43.14	.017	43.08
	.012	48.03	.012	48.13

TABLE B-VI

AIRPLANE DAMPING AND FREQUENCY COMPARISON AT V_D - MACH 2.7

	Airplane with HSAS		Airplane with HSAS & FSS	
	Damping ratio, ζ	Frequency rad/sec	Damping ratio, ζ	Frequency rad/sec
Short period	.213	1.40	.210	1.40
Structural modes	.019	6.90	.022	6.86
	.040	11.10	.055	11.05
	.013	14.80	.016	14.80
	.011	17.09	.011	17.09
	.025	18.31	.024	18.31
	.016	21.14	.021	21.23
	.026	22.65	.024	22.59
	.010	25.99	.010	25.99
	.010	30.41	.010	30.41
	.047	32.81	.047	32.78
	.008	37.21	.008	37.21
	.047	38.72	.011	38.69
	.013	38.73	.050	38.71
	.008	43.37	.008	43.32
	.037	45.22	.036	45.24
	.011	48.31	.011	48.41

TABLE B-VII

AIRPLANE DAMPING AND FREQUENCY COMPARISON AT V_c - MACH 0.9

	Airplane with HSAS		Airplane with HSAS & FSS	
	Damping ratio, ζ	Frequency rad/sec	Damping ratio, ζ	Frequency rad/sec
Short period	.407	.96	.386	.99
Structural modes	.034	6.41	.046	6.26
	.083	10.71	.166	10.30
	.038	13.90	.040	13.85
	.103	16.57	.086	16.35
	.028	17.47	.030	17.49
	.053	19.46	.051	19.57
	.011	20.27	.015	20.28
	.015	25.12	.016	25.10
	.099	28.44	.097	28.33
	.013	30.24	.012	30.21
	.080	31.93	.080	31.96
	.012	34.92	.013	34.96
	.008	38.78	.008	38.75
	.014	40.37	.014	40.38
	.013	42.95	.013	42.89
	.010	47.88	.010	47.95

TABLE B-VIII

AIRPLANE DAMPING AND FREQUENCY COMPARISON AT V_C - MACH 1.2

	Airplane with HSAS		Airplane with HSAS & FSS	
	Damping ratio, ζ	Frequency rad/sec	Damping ratio, ζ	Frequency rad/sec
Short period	.299	1.21	.296	1.21
Structural modes	.035	6.66	.037	6.63
	.056	10.56	.070	10.53
	.025	14.48	.028	14.50
	.047	16.62	.046	16.57
	.021	17.62	.021	17.62
	.021	20.69	.023	20.81
	.044	21.19	.042	21.05
	.023	25.63	.022	25.64
	.081	29.08	.081	29.05
	.011	30.36	.011	30.36
	.076	34.36	.076	34.34
	.030	35.86	.030	35.87
	.012	38.97	.012	38.95
	.040	41.16	.040	41.18
	.014	43.15	.014	43.13
	.010	48.02	.010	48.06

TABLE B-IX

AIRPLANE DAMPING AND FREQUENCY COMPARISON AT V_c - MACH 2.7

	Airplane with HSAS		Airplane with HSAS & FSS	
	Damping ratio, ζ	Frequench rad/sec	Damping ratio, ζ	Frequency rad/sec
Short period	.176	1.20	.173	1.20
Structural modes	.015	6.77	.016	6.76
	.033	10.18	.038	10.15
	.012	14.65	.013	14.65
	.017	16.70	.017	16.70
	.014	17.81	.014	17.81
	.015	20.84	.016	20.86
	.016	21.97	.016	21.96
	.008	25.87	.009	25.88
	.009	30.44	.009	30.45
	.043	30.81	.043	30.80
	.026	36.03	.026	36.02
	.010	36.74	.010	36.74
	.011	39.06	.011	39.04
	.008	43.26	.007	43.25
	.024	43.97	.025	43.98
	.008	48.23	.008	48.26